https://ntrs.nasa.gov/search.jsp?R=20180005195 2019-04-30T04:35:18+00:00Z

# Using observations and source specific model tracers to characterize pollutant transport during FRAPPÉ and DISCOVER-AQ

**G. G. Pfister[1], P. Reddy[1,2], M.C. Barth[1], F.F. Flocke[1], A. Fried [3], S.C. Herndon[4], B.C. Sive [5], J.T. Sullivan [6], A.M. Thompson[6], T.I. Yacovitch[4], A.J. Weinheimer[1], A. Wisthaler[7]**

[1] Atmospheric Chemistry Observations and Modeling, National Center for Atmospheric Research, Boulder, Colorado, USA
[2] formerly Air Pollution Control Division, Colorado Department of Public Health and Environment, Boulder, Colorado, USA
[3] Institute of Arctic and Alpine Research, University of Colorado Boulder, Boulder, Colorado, USA
[4] Aerodyne Research Inc., Billerica, Massachusetts, USA.
[5] Air Resources Division, National Park Service, Denver, Colorado, USA
[6] Earth Sciences Division, NASA Goddard Space Flight Center, Greenbelt, Maryland, USA
[7] Department of Chemistry, University of Oslo, Oslo, Norway

**Key Points**:

- Upslope flows are a frequent occurrence on high ozone days in the NFRMA thereby impacting remote mountain sites.
- Aircraft measurements and model tracers confirm transport of pollution to the mountains and spill-over into the valleys to the West of the Continental Divide
- The northern Foothills are frequently impacted by oil and gas sources, while the southern Foothills more frequently experience impact from urban sources.

# Abstract

Transport is a key parameter in air quality research and plays a dominant role in the Colorado Northern Front Range Metropolitan Area (NFRMA), where terrain induced flows and recirculation patterns can lead to vigorous mixing of different emission sources. To assess different transport processes and their connection to air quality in the NFRMA during the FRAPPÉ and DISCOVER-AQ campaigns in summer 2014, we use the Weather Research and Forecasting Model with inert tracers. Overall, the model represents well the measured winds and the inert tracers are in good agreement with observations of comparable trace gas concentrations. The model tracers support the analysis of surface wind and ozone measurements and allow for the analysis of transport patterns and interactions of emissions. A main focus of this study is on characterizing pollution transport from the NFRMA to the mountains by mountain-valley flows and the potential for recirculating pollution back into the NFRMA. One such event on 12 August 2014 was well captured by the aircraft and is studied in more detail. The model represents the flow conditions and demonstrates that during upslope events, frequently there is a separation of air masses that are heavily influenced by oil and gas emissions to the North and dominated by urban emissions to the South. This case study provides evidence that NFRMA pollution not only can impact the nearby Foothills and mountain areas to the East of the Continental Divide, but that pollution can "spill over" into the valleys to the West of the Continental Divide.


# 1. Introduction

Two major field campaigns – the National Science Foundation (NSF)/National Center for Atmospheric Research (NCAR) and State of Colorado Front Range Air Pollution and Photochemistry Éxperiment (FRAPPÉ) and the 4$^{th}$ deployment of the National Aeronautics and Space Administration (NASA) Deriving Information on Surface conditions from Column and Vertically Resolved Observations Relevant to Air Quality (DISCOVER-AQ) – were conducted jointly in summer 2014 to study summertime ozone pollution in the Colorado Northern Front Range Metropolitan Area (NFRMA), an area that is in non-attainment of the current ozone standards. Characterizing and modeling air quality in the NFRMA poses large challenges due to the complex terrain and meteorology as well as the mix of diverse pollution sources including

urban sources, power plants, large industrial sources, agricultural activities, oil and gas exploration and natural sources like wildfires, biogenic VOCs or windblown dust.

The NFRMA is located at an elevation of roughly 1600-1800 m, on the plains just east of the Central Rocky Mountains. To the West of the NFRMA, the terrain becomes mountainous, mostly wooded, with scattered smaller communities up to elevations below 3000 m, and then transitions into the mostly uninhabited alpine region along the Continental Divide, reaching up to 4300 m altitude. Several major river canyons extend from the high terrain down into the NFRMA, which in parts are less than 1 km wide, i.e. of sub-grid scale in most chemical transport models, adding to the complexity of the terrain and transport.

In the summer months, particularly during weak synoptic conditions, the local meteorology is mainly controlled by thermally driven, terrain-induced, diurnal flow patterns, often also referred to as upslope/downslope or mountain-valley winds (Johnson and Toth, 1982; Toth and Johnson, 1985, Arritt et al., 1992; and references therein). This has unique consequences for the transport, mixing and photochemical processing of local emissions (Haagenson, 1978; Greenland, 1980; Doran, 1996; Baumann et al., 1997; Olson et al., 1997) including the potential of bringing NFRMA pollution into the pristine mountains (Parrish et al., 1986; Brodin et al., 2010; Brodin et al., 2011; Benedict et al., 2011; Darrouzet-Nardi et al. 2012). Conversely, stronger frontal passages can induce outflow of NFRMA pollution to the East, impacting downwind agricultural areas in the central Great Plains. Such export events, as well as thunderstorms, are the major mechanisms for cleaning out accumulated pollution in the NFRMA. The characteristics and variability of mountain-valley winds are the main focus of this paper, but we also assess the general distribution and mixing of different emission sources.

Transport is a key driver in air quality research and plays a dominant role in determining pollution levels, specifically in the Front Range, where terrain induced flow and recirculation patterns can lead to vigorous mixing of different emission sources. As a result, the analysis of wind roses does not necessarily provide sufficient information on the origin of air masses arriving at a certain location. A more appropriate method in this regard might be back-trajectories, but these do not provide information on the dilution and spatial distribution of different emissions unless methods such as a Lagrangian particle dispersion model (LPDM) is

used (e.g. Stohl et al., 2005; Angevine et al., 2013; Briode et al., 2013; Hegarty et al., 2013). In this work, to assess different transport processes and their connection to air quality in the NFRMA during the campaign period, we use a chemical transport model, the Weather Research and Forecasting Model (WRF) with inert tracers. During the campaign, we conducted a real-time WRF forecast which included tracers from different emission sectors and regions. This product showed high value as a planning tool during the campaign and is used in this study. The model tracers support the analysis of surface wind and ozone measurements and allow for the analysis of how emissions from different source types are transported and where and when we find efficient mixing of different emission sources. The analysis of the tracers can point towards conditions that should be investigated further using chemical measurements and modeling and is valuable in support of the field observations analysis.

Here, we provide an evaluation of the model and use the average spatial distribution of tracers to assess which regions are on average most impacted by which source sector and how these emissions typically are mixed. We use the WRF tracers to look in more detail at a day where the NCAR/NSF C-130 aircraft captured well an upslope event (12 August 2014) and compare this case study to other upslope events during the campaign period.

## 2. Field Campaign Observations

During summer 2014 two major field campaigns took place in the NFRMA with the objective to study the drivers of ozone pollution. The FRAPPÉ field experiment was carried out jointly with the 4$^{th}$ deployment of the NASA DISCOVER-AQ between 15 July – 20 August 2014 with most DISCOVER-AQ platforms ending on about 10 August. For simplicity, we refer to the joint campaigns as FRAPPÉ/DAQ.

Chemical and meteorological observations were conducted in total from five aircraft, multiple mobile vans, ozonesondes, lidars, tethered balloons, and numerous operational and additional surface sites. In this paper, we use measurements from two of the aircraft, the NASA P-3B and the NSF/NCAR C130. The NASA P-3 conducted flights on 16 days starting on 17 July and ending on 8 August 2014 following a repetitive pattern over the NFRMA. The flight pattern included spirals over 6 surface sites to assess the diurnal and small scale variability in pollutants.

For the NCAR/NSF C130, in contrast, flight patterns were designed to target specific objectives dictated by atmospheric conditions. The 15 flights from 26 July to 18 August 2014 were focused on emissions in the NFRMA, followed upslope transport of NFRMA pollution into the mountains, and measured Colorado Western slope emissions and outflow from the NFRMA. Our focus in this paper is on flights in the NFRMA and the nearby mountains. Aircraft data focused in here include NOx, ethane and ammonia data on the NCAR/NSF C-130 and NASA P-3. For more details on the data and measurement techniques the reader is referred to Weinheimer et al., [1994] for $NO_x$ measurements, Yacovitch et al. [2014] for NASA P-3 ethane measurements, Sun et al. [2014] for NASA P-3 ammonia measurements, Richter et al. [2015] for NCAR/NSF C-130 ethane measurements and Herndon et al. [2005] for NCAR/NSF C-130 ammonia measurements.

In Table 1 we list the surface sites that are included in this study with their location. The area topography is shown in Figure 1. In addition to sites in the NFRMA, we include four high altitude sites to the West of the NFRMA. The area of the NFRMA is rather small; the distance from Chatfield to Fort Collins is about 110 km and from RF North to Platteville about 70 km. Yet, as will be shown, the variability in emissions and dynamics is very high, posing significant challenges to characterizing the drivers behind high concentrations of air pollution.

# 3. Model Description

During the campaigns, the Weather Research and Forecasting Model (WRF) V3.3.1 was run in forecast mode to support flight design and forecasting. National Center for Environmental (NCEP) Global System Forecast (GSF) analysis fields at 0.5°x0.5° were used to initialize WRF at 00UTC and 12UTC and 48-hour forecasts were constrained by lateral boundary conditions from GFS forecasts. A 2-domain setup was used with a 15 km outer domain covering the Western U.S. (not shown) and an inner 3 km domain covering Colorado and parts of neighboring States. Only results of the inner domain are considered here. The vertical resolution was set to 36 levels between the surface and 10 hPa. Other model configuration settings include the Yonsei University (YSU) boundary layer scheme [Hong et al., 2006; Hong 2010, Hu et al., 2013], Thompson microphysics [Thompson et al., 2008], the Rapid Radiative TransferModel for GCMs (RRTMG) radiation schemes [Iacono et al., 2008], the Kain-Fritsch cumulus scheme for the

outer domain [Kain, 2004], Noah land surface model [Tewari et al., 2004], and the Monin-Obukov surface layer scheme [Janjic, 1994]. Instantaneous model output is saved at each simulation hour. For comparison and integration with the observations, the hourly gridded model output has been interpolated to the time and location of the measurements.

We added a set of chemically inert tracers to WRF to track the transport of different source sectors. The tracers are only emitted from their respective sources and there are no other production mechanisms. These tracers are an addition to the scheme described by Barth et al. (2012). The tracers included in the current study are an oil and gas tracer ($TR^{OG}$) representative of emissions from oil and natural gas (OG) activities in Colorado; an area tracer ($TR^{Area}$) and a mobile tracer ($TR^{Mobile}$) representative of Colorado area and mobile emissions, respectively; and an agricultural tracer ($TR^{Agr}$) representative of agricultural emissions in Colorado. To define the tracer emissions, we chose surrogate chemical species that are characteristic for the specified emissions, but note that the tracers do not represent the chemical nature of the chemical surrogates. We use nitrogen oxide ($NO_x$) for $TR^{AREA}$ and $TR^{Mobile}$, ethane for $TR^{OG}$ and ammonia ($NH_3$) for $TR^{Agr}$. $TR^{Area}$ and $TR^{Mobile}$ are combined in our analysis ($TR^{AreaMobile}$) and for simplicity also referred to as "urban". Each tracer was given a 2-day lifetime, which allows to follow the transport but avoids that the tracers accumulate in the NFRMA.

Base emission inventories were chosen based on availability and representativeness for 2014 sources. OG emissions are based on the Western Regional Air Partnership 2008 inventory. Comparison to more recent emission inventories now available to us (EPA NEI 2011 and an inventory based on 2014 activity data) shows that the 2008 inventory reasonably well represents the 2014 spatial distribution (not shown). Area and mobile sources are from a Colorado Department of Public Health and Environment inventory projected for 2018, and agricultural emissions are from the Environmental Pollution Agency (EPA) National Emission Inventory (NEI) 2011. An average diurnal cycle was superimposed on $TR^{Area}$, $TR^{Mobile}$ and $TR^{Ag}$. Other tracers not used in this analysis include a tracer from $NO_x$ sources from neighboring states within the WRF inner domain, a lightning $NO_x$ tracer, a stratospheric tracer, and a lateral boundary conditions tracer.

In Figure S1 we plot maps of the model emission tracers together with the same sites shown in Figure 1. In Figure S2 we show the diurnal cycle in $TR^{Area}$ and $TR^{Mobile}$. The majority of the tracer emissions are within the NFRMA and there are no major emission sources for 100 km and more to the West. To create a continuous time series from the individual forecast cycles we extracted forecast hours 6-18 from each 00 and 12 UTC cycle, i.e. we allow for a 6 hour spinup. Only when specifically noted, we use the results from a single forecast cycle only. We do note that model simulations might vary substantially between different forecast cycles, however, this study is not about evaluating the performance of individual forecast lead times.

# 4. Model Evaluation – Meteorology

We provide an evaluation of the modeled meteorology and transport during the FRAPPÉ/DAQ period. We focus on the performance of model winds given that the focus of this study is on NFRMA transport patterns, and assess the general model performance over the period of the campaign. Individual case studies are presented later in the paper. We select only surface sites for which both ozone and wind observations are available.

We begin with an evaluation of modeled 10 m winds to surface observations taken at selected sites in the NFRMA. In Figure 2, we compare the vector average wind direction and average wind speed at six locations, which are used later in the analysis. Statistics are shown over the FRAPPÉ time period (15 July – 20 August). These include two sites in the NFRMA near the Foothills (RF North and the NASA P-3 spiral location NREL Golden), and two locations in the Colorado Eastern plains (WC Tower and Aurora East). In addition, we include two high elevation sites, Longs Peak and Trail Ridge Road, for which wind and ozone measurements are available. The Longs Peak station is located just to the West of the Peak to Peak Highway, and Trail Ridge Road is situated just below the Continental Divide on the east side near Trail Ridge Road. Evaluations for additional surface sites are shown in Figure S3 and include the remaining NASA P-3 spiral locations. Except for Trail Ridge Road, where hourly averages are provided, observations are available as 1-minute averages. For direct comparison to the surface sites, the observations are hourly averaged and then compared to the instantaneous hourly model output. We expect that most of the surface sites are impacted by local effects that likely will not get

resolved by the model despite a 3 km grid resolution. We also note that the definition of a "vector averaged" wind direction can be misleading given the high variability, but nevertheless allows insight into general flow regimes.

For NFRMA sites, the model represents well the average wind speed at 10 m above ground level (agl) with the exception of Fort Collins CSU (Figure S3), where the model is biased high. Both observations and model show a tendency for highest wind speeds in the afternoon. The model captures the average wind direction at most sites with a dominance of easterly (upslope) winds in the morning/early afternoon. Winds take on a more westerly component (downslope) in the late afternoon and during nighttime, but the wind direction varies more strongly amongst the sites as local topography and large scale flow patterns influence the buildup of the downsloping winds. Sites in the Northern NFRMA (Fort Collins CSU and WC Tower) show a dominance of winds from the NW at night. Both Fort Collins CSU and the Weld County Tower site are in the Cache la Poudre drainage, which might explain the northwesterly flow at night. The WC Tower site might also be under the influence of northwesterly flow coming from the western corner of the Cheyenne Ridge which has a steeper slope than the Platte Valley to the South. Sites from Denver up to Greely (e.g. La Casa, BAO, Platteville), however, show winds mostly from the SW, representing the drainage flows along the Platte River Valley, the region stretching from Denver to about Greeley (Toth et al., 1995)

The two sites near the Foothills (NREL Golden and RF North) show westerly downsloping winds taking over late afternoon/early evening and while the model performs well during the periods of pronounced slope winds, it has slight difficulty representing the switch from upslope to downslope winds. These two sites specifically are impacted by sub-grid local topographic features as they are nestled near the Foothills at or near the mouth of canyons. The model with a 3 km resolution has difficulties fully representing these conditions. The winds during this transition period are also more variable compared to periods of established slope winds adding, additional challenge.

Even though we can identify general flow patterns across the NFRMA region, there are notable differences amongst the different sites representing complex mixing and circulation patterns. Wind direction can vary across even neighboring sites such as Platteville and WC Tower, which

are both located in the Colorado Eastern plains and only 22 km apart. While at WC Tower winds after midnight are mostly from the North, Platteville (Figure S3) shows drainage flows from the South-West during nighttime. The drainage flows are not very prominent in the observations, because the site is situated in a shallow topographical depression which leads to localized disturbances in the wind fields. The model does not resolve the small scale topographical influence and more clearly shows the drainage flows. Drainage flows are also evident at the nearby BAO site and at the downtown Denver La Casa site. Upslope flows dominate at both sites during the day but are more variable at Platteville compared to WC Tower. This demonstrates that wind direction alone, albeit helpful, cannot necessarily be used to identify the origin of plumes measured at any of the surface sites. This is important to keep in mind in the analysis of the data and warrants the integration of different data sets and models to assess transport flows and source impacts.

The two high altitude sites Longs Peak and Trail Ridge Road, which are considered as being representative of remote conditions and strongly influenced by the higher-level Westerlies, show an overall dominance of winds from the NW in the measurements. The model, in contrast, simulates at both sites winds more strongly from the W as is typical for free-tropospheric winds in the northern mid-latitudes. The Longs Peak site is located in the valley of Cub Creek, which has a NW to SE orientation and likely channels the local winds. The model cannot resolve this and the model elevation interpolated to this site is higher compared to the actual elevation (2854 m versus 2743 m). A similar influence of topography might cause the NW wind direction at Trail Ridge Road. Winds show a higher deviation from the north-westerly (westerly in the model) direction in the afternoon indicating that occasional upslope flows interrupt the typical Westerly flow. This is true specifically at Longs Peak, which is closer to the NFRMA. The model overestimates the wind speed at both sites which is likely related to the model not simulating the influence of small scale topography and unresolved surface roughness.

To provide further evaluation of the model performance regarding the vertical structure of key meteorological parameters, we compare wind observations taken by ozone sondes launched at Platteville and Fort Collins West (Figures 3 a and b). At Platteville, where data from 40 ozone sonde launches are available (13 July – 10 Aug, daytime only) the model represents well the

average profiles of wind speed, relative humidity and temperature throughout the atmosphere. Note that what appears like a shallow inversion layer in temperature is due to only four data points at the lowermost altitude bin and cannot be regarded as representative for the entire time period. The model picks up the overall profile shape in wind direction, except at the lowermost altitude bins, where the model simulates easterly winds while the average wind direction in the observations is from the S. This is in line with the surface data. As can be seen from windroses (Figure 3 c) and from Figure S3, the average wind direction at the surface is dominated by Easterlies in the model throughout the day, while the measurements are much more variable in the morning and from mostly the ESE sector in the afternoon indicating that the model presents more the regional flow and has difficulties picking up the local variability.

The model shows a good agreement in wind direction for Fort Collins-West, where data from 12 launches are available (20 July-6 August). WRF simulates the mean SSE winds near the surface, but transitions faster to Westerlies above compared to the observations. Wind speed, which compared well at Platteville, is overestimated at the lowermost altitude bin, which is in agreement with the comparison of wind speed data at the nearby Fort Collins CSU site. The modeled relative humidity and temperature profiles agree well with the observations.

Finally, we also provide a brief evaluation of the modeled boundary layer height (PBLH) for selected time periods. Figure 4 compares the model to the PBLH derived from Micropulse Lidar (MPL) data at FC West, Platteville and NREL Golden. This is not a true direct comparison given the different definitions of the modeled and retrieved PBLH, but shown here to give an indication of the model's ability to represent the typical PBLH and day-to-day variability. The YSU PBL scheme used in the model is a first-order nonlocal scheme, with a countergradient term and an explicit entrainment term in the turbulence flux equation for heat or momentum [Hu et al., 2013]. In YSU, the PBLH is defined as the level in which minimum flux exists at the inversion level. The MPL retrieved PBLH, in contrast, have been obtained from gradients or variance in the backscatter profile, wavelet covariance, and fits to idealized profiles [Compton et al., 2013].

Despite the noise in the data, some unreasonable looking MPL retrievals (e.g. the first four days at Platteville) and the different definitions of PBLH, we can see that the model overall represents

the PBLH and the day-to-day variability fairly well, specifically for NREL Golden and FC West whereas the model underestimates more often the PBLH at Platteville. This is in line with the model also showing higher uncertainty in representing the wind direction at Platteville, thus performing less well for this site than for some others. Comparing PBLH amongst the three sites it is interesting to note that the PBLH can vary notably reflecting the local nature of sites and, in general, the variability in meteorological and dynamical conditions across the NFRMA.

# 5. Relationship between model tracers and chemical tracers

The modeled tracers are not directly comparable to any specific chemical measurements, but indirectly can be evaluated by assessing the correlation with their respective surrogate chemical tracer, i.e. the chemical species used to define the inert emission tracers. Such an analysis also gives insight to what degree the inert tracers can assist in the analysis of chemical measurements. We assess the average tracer distribution and provide a statistical analysis to determine how well the model tracers relate to one-minute averaged measurements of $NO_x$, $C_2H_6$ and $NH_3$, i.e. the species the tracer emissions were scaled to, on both aircraft (NASA P-3 and NCAR/NSF C-130). Similar to before, hourly output of the model tracers was interpolated to the time, location and altitude of the aircraft. The interpolation from hourly output is expected to lead to errors in representing the observed variability, but these errors are partly smoothed by investigating larger spatial and temporal averages.

In Figure 5 we show NCAR/NSF C-130 measurements of $NO_x$ and $C_2H_6$ mixing ratios together with mixing ratios of $TR^{AreaMobile}$ and $TR^{OG}$ (Results for $TR^{Agr}$ and $NH_3$ are shown in Figure S4). Only flight data within the NFRMA and below 3 km agl have been selected. Similar plots for the NASA P-3 aircraft data are shown in Figure 6 and Figure S5. For these graphs, the aircraft measurements have been averaged on a 0.1 degree x 0.1 degree grid for the NCAR/NSF C-130 flights and on a 0.05 degree x 0.05 degree grid for the NASA P-3 flights to ensure a reasonable number of points feeding into the analysis. The NCAR/NSF C-130 flight patterns are more variable and less repetitive; hence a larger averaging grid is used compared to NASA P-3, which used a repetitive flight pattern. For the NCAR/NSF C-130 analysis we also select a slightly larger region compared to the NASA P-3, including flight legs over the Foothills. However, the

general conclusions remain the same independent of grid size or region. The spatial correlation coefficient R is listed in the graphs as well as in Table 2 and has been calculated when applying different filtering in altitude. Grid averages are only calculated for grids where at least 3 data points are available

We find that the spatial pattern of the tracers is overall representative of the spatial pattern derived for the measured chemical tracers. We do not expect a perfect agreement between the tracers and their surrogate chemical species given that our inert tracers have a different lifetime than their chemical surrogates and that we are comparing hourly instantaneous model output to 1-minute average aircraft measurements. Uncertainties in modeled winds, PBLH and vertical mixing or the underlying emissions also impact the comparison. In line with the source regions (Figure S1), highest $NO_x$ and $TR^{AreaMobile}$ concentrations are found near the Denver urban area. In contrast. $C_2H_6$ and $TR^{OG}$, and $NH_3$ and $TR^{Agr}$ are highest NE of the urban area, but elevated values extend all the way into the northern part of the Denver urban area. Spatial correlations are in the range ~0.7-0.9 between the inert tracers and their respective surrogates. However, given that OG and agricultural sources both originate from similar regions, higher R values are also calculated for $TR^{Agr}$ with $C_2H_6$ and for $TR^{OG}$ with $NH_3$.

Filtering for lower altitudes, in general, reduces slightly the correlations given that the number of available data points is reduced and that near-surface concentrations are expected to be more impacted by small scale variability and local effects. Significant R values, however, are also calculated when a more stringent filtering for altitudes below 1 km agl is applied. In the case of the NCAR/NSF C-130, where flights in the selected NFRMA region were focused on measuring emissions and mostly conducted at low altitudes, 98% of the selected NFRMA data are below 3 km ag, and 63% are below 1 km agl. For the NASA P-3, the corresponding values are 77% and 48%, respectively.

In Figure 7 we look at the spatial correlations of the model tracers $TR^{AreaMobile}$ and $TR^{OG}$ with different chemical tracers. For the analysis, gridded averages of all model and observational data are derived and these are used to calculate the spatial correlation. We show the correlations when all flights are considered as well as correlations for individual flights so as to represent the variability encountered on individual days. This analysis helps to identify which chemical tracers

are suited for fingerprinting air masses and, in turn, can be used for evaluating the model tracer sources and transport. A larger number of VOC species was measured on the NCAR/NSF C-130 compared to the NASA P-3, but for those chemical tracers that were measured on both aircraft the findings are similar. The correlations can be highly variable between flights and reflect variations in the model performance and also the species lifetime. The fresher the emissions that were sampled and the simpler the chemistry for a chemical species, the better we expect the model tracers to represent the chemical observations.

$NO_x$, Ethanol and Toluene as well as Ethylbenzene and o-Xylene, the latter two only measured on the NCAR/NSF C-130, show a high correlation with $TR^{AreaMobile}$ and a rather low correlation with $TR^{OG}$ indicating these to be valuable tracers for urban emissions. In turn, ethane, propane and methane show a consistently good correlation with $TR^{OG}$ and low correlation with $TR^{AreaMobile}$ and can be considered as indicators for emissions from OG sources. High correlations with $TR^{OG}$ are found for $NH_3$ due to the colocation of agricultural and OG sources. Benzene is emitted by both urban and OG sources and the mean correlation is high with both model tracers on the NCAR/NSF C-130, while on the NASA P-3 it has good correlation with $TR^{OG}$ but low R with $TR^{AreaMobile}$. In part, this might be attributed to the NASA P-3 flight pattern where high benzene values during spirals over Platteville in the OG source region (Halliday et al., 2016) dominate the signal. Both aircraft, however, show a large spread in R values across the individual flights pointing out the dependence of the derived correlation on the flight patterns and specific meteorological conditions on any given flight day.

Correlations of $TR^{AreaMobile}$ with CO are high for the NASA P-3 but much lower (~0.5) for the NCAR/NSF C-130. This is due to a much smaller number of data points available for the NCAR/NSF C-130. The CO instrument on this aircraft experienced problems during the first part of the campaign and data are only available for August flights. On either aircraft, CO does not show any correlation with the OG source tracer, yet CO commonly is used to normalize emissions and measured concentrations for a variety of airmasses. This analysis, however, suggests that it is more appropriate to identify source specific tracers when analyzing emission ratios, conduct inverse modeling studies or look at species ratios to account for dilution effects, specifically in regions of diverse sources.

# 6. Average Tracer Distributions

The comparison with observations shows that the model captures the general flow regimes and source regions well. Here we now use just the model tracers to visualize the transport and distribution of different source types. Note that we only focus on surface data and do not have information on entrainment from higher altitudes from the measurements. In Figure 8, we plot the average spatial distribution of $TR^{AreaMobile}$ and $TR^{OG}$ for different times of the day to demonstrate where, on average, the strongest impact from the different emission sectors is found. We calculate the average mixing ratio within the planetary boundary layer (PBL) to reduce the influence of diurnal changes in vertical mixing and dilution. As noted by Zhang et al. [2016] and Kaser et al. [2017] and as was also observed during the campaign from measurements of $NO_x$ that were taken during the P-3 spirals, concentrations are not necessarily well mixed within the PBL. However, we believe that the PBL average tracer concentrations are a more suited quantity to analyze and the general findings and conclusions do not change if instead surface concentrations were considered. In addition to showing the average spatial tracer distribution, we denote the average surface ozone concentrations at all locations, where during FRAPPÉ/DAQ surface ozone monitors were placed. This also includes sites not listed in Table 1. In support of the analysis we further show in Figure S6 the average daytime ventilation index for the same times shown in Figure 8. The Ventilation Index is the mathematical product of the mixing height and the average horizontal transport wind throughout the depth of the PBL and provides an estimate of how high and how far pollutants will disperse.

During nighttime (0-6LT), when the urban emissions are at their diurnal minimum, the distribution of $TR^{AreaMobile}$ reveals a pooling of emissions from the Denver Metro area into the Platte River Valley, i.e. towards the region with strongest OG sources. Lowest ozone mixing ratios are found in the Denver Metro area, WC Tower (located in Greeley) and Fort Collins (FTC) CSU, where high $NO_x$ from urban sources (Figure S1) causes ozone titration, and at Platteville, likely due to transport of high $NO_x$ and low ozone from the Denver area.

In the morning (6-12 LT) flow reversal transports aged emissions back into the NFRMA mixing with fresh emissions from the OG source region and fresh emissions from the Metro Area. The ventilation index indicates that during morning there is limited venting in the NFRMA with

lowest values for the north-eastern NFRMA. In the afternoon (12-18 LT), the source regions are more strongly separated and the ventilation index shows that efficient venting out of the PBL is possible. Similar to what is seen for the morning, the lowest ventilation index is simulated for the north-eastern NFRMA (marginal-good). Transport of NFRMA tracers into the Foothills becomes evident. The highest surface ozone is seen for BAO, which interestingly coincides with the region where strong mixing of $TR^{OG}$ and $TR^{AreaMobile}$ is estimated. One explanation is the mix of airmasses, another possible explanation for this could also be that, independent of the flow regime, the daytime upslope flow towards the foothills is more likely to pass BAO compared to other sites. In the evening (18-24LT), when the PBL faded away limiting the degree of mixing (not shown), the $TR^{AreaMobile}$ and $TR^{OG}$ source regions are more clearly separated and the tracers remain close to their sources. Even though $TR^{AreaMobile}$ and $TR^{OG}$ have sources throughout Colorado, that could potentially impact the NFRMA, we did not find, on average, a significant transport of emissions from any other source regions in Colorado, at least not in the 2-day lifetime the inert tracers represent.

The mixing of aged urban pollution and fresh emissions from OG sources in the morning has interesting implications for chemistry. The early morning buildup of ozone in these mixed air masses warrants further detailed photochemistry studies as it will influence the magnitude of the afternoon ozone maximum. Similarly, follow-up chemical studies are needed to validate whether the most efficient ozone production is happening in air masses with the strongest mixing from the different emission sectors such as suggested by the tracer analysis. Mixing of hydrocarbon-rich air from the oil and gas area around Greeley with $NO_x$ rich air from the Denver urban area could possibly result in more efficient ozone production than in either of the contributing air masses by themselves.

In Figure 9 we calculate statistics for the model tracers for surface sites in Colorado for which ozone measurements during FRAPPÉ/DAQ are available, to provide insight into the range of different regimes that were covered by the surface sampling. As before, we show statistics for the PBL averaged tracer concentrations to omit the impact of diurnal changes in boundary layer height and limit the data to daytime (10-17 LT) to emphasize the influence during the

photochemically most active period of the day. During nighttime (not shown) the statistics are more strongly dominated by the nearby sources due to the shallow PBL.

$TR^{AreaMobile}$ is largest at monitoring sites in and near the Denver metro area the highest being La Casa, CAMP and I-25. This can be expected as this is the region with the largest industrial sources and most transportation. Looking at $TR^{Area}$ and $TR^{Mobile}$ separately (not shown) we find a much broader coverage across sites in the NFRMA for the latter reflecting the wide-spread impact of emissions from transportation ranging from sites close to the Foothills to East of Denver. $TR^{Area}$ has higher values compared to $TR^{Mobile}$ due to the high emission strength of individual point sources (Figure S1), which dominate the spatial pattern.

Maximum mean $TR^{OG}$ impact is experienced at surface sites in the north-eastern NFRMA (WC Tower and Platteville), which have an overall minor impact from $TR^{AreaMobile}$, and also other sites located nearby OG sources such as BAO (Erie) and Longmont. The $TR^{OG}$ influence is decreasing towards the South, but elevated concentrations are found throughout all NFRMA sites. At high elevation sites West of the NFRMA, the concentrations for both $TR^{AreaMobile}$ and $TR^{OG}$ show a general decline with increasing distance from the NFRMA, yet sites like Longs Peak, Squaw Mountain or Niwot Ridge do also show elevated tracers indicating transport from the NFRMA as will be discussed later. It should be noted that pollution from upslope events typically reaches these sites later in the afternoon/evening, which is not fully covered by the chosen time window.

While the average $TR^{AreaMobile}$ and $TR^{OG}$ concentrations overall agree well with the emission source regions, this analysis reveals a large variability likely due to efficient mixing and transport in the NFRMA and hints at the existence of a variety of changing chemical regimes. To show how conditions change over the course of a day, we include in Figures 10 and 11 statistics of the diurnal cycle for tracer and ozone concentrations for the same surface sites that are highlighted in Figure 9. Note that for these graphs, we show the diurnal cycle from 6am to 6am LT, similar to Figure 2. The tracers indicate transport of emissions to the surface sites but given they are only emitted and have no chemical production associated, are not a representation for ozone concentrations.

The selected sites later are used to discuss upslope events and also represent different source regions: The two easternmost NFRMA sites include WC Tower located in the OG and agricultural source region and Aurora East located east of the Denver area. The two other NFRMA sites are located near the Foothills and include RF North at the interface of urban and OG source regions and Golden, West of Denver (Figure 1). It has to be kept in mind that $TR^{AreaMobile}$ has a diurnal cycle with largest emissions during the day (Figure S2), which biases the diurnal cycle in concentrations towards higher daytime values. The OG emissions have no diurnal cycle attached. The average wind direction and speed for these sites have been discussed above (also see Figure 2) except for Mines Peak and Squaw Mountain for which no wind measurements are available.

In line with the overall tracer distribution discussed in Figure 8, WC Tower, located within the region of strong OG and agricultural activities, has the highest OG tracer concentrations of the selected sites. WC Tower is located in Greeley, a town of about 100,000 people and ~20 km east of a major S-N oriented Highway (I-25). Greeley also is surrounded by oil and gas facilities. Hence, we do expect that tracer concentrations are impacted by nearby sources and might reach the site independent of wind direction. While Greeley is in the region of drainage flows from the Denver Area, nighttime winds, on average, are from a Northerly direction. This suggests that mostly sources in the Greeley area contribute to elevated tracer concentrations, but given the localized representativeness of the wind data at surface sites, it is likely that emission transport from the Denver region through the more regional flow, as suggested in Figure 8, adds to elevated tracer levels.

At RF North and NREL Golden, where the average wind directions are similar, both tracers peak around late morning/noontime as easterly upslope flows transport emissions from the NFRMA region to these sites. Enhanced ventilation and a higher PBLH also allow for more efficient mixing and distribution of emissions within the NFRMA as the day progresses. The magnitude of $TR^{OG}$ decreases with distance from the OG source region, i.e. is higher at RF North compared to NREL Golden, while $TR^{AreaMobile}$ is higher at NREL Golden due to the proximity of urban sources. From the four sites considered, Aurora-East shows the lowest tracer concentrations as the dominant flow patterns in the south-eastern NFRMA tend to carry pollutants away from this

site. The enhancement in the tracers in the morning is in line with winds from the Denver area (N-NW). Ozone concentrations, also shown in the graphs, peak generally earlier at the eastern Sites compared to sites closer to the Foothills (around noon versus early afternoon). The average daytime concentrations are in the order of ~60 ppb for all sites, but the rate of the morning buildup and the width of the daytime maximum varies across the sites, indicating that different processes are contributing to the ozone production.

Model tracer concentrations and ozone at mountain sites are shown in Figure 11. From the four sites considered, Mines Peak is the furthest West of the NFRMA (Figure 1). Tracer concentrations are smaller compared to NFRMA sites because there are no nearby sources and the tracers get diluted during the transport from the NFRMA. Ozone, in contrast, which is not emitted and only chemically produced in the atmosphere, can reach higher concentrations at the mountains sites compared to sites in the NFRMA. On average, $TR^{OG}$ is higher at the Northern Sites (Longs Peak and Trail Ridge Road), while $TR^{AreaMobile}$ is higher at the southern sites (Squaw Mountain and Mines Peak). This is, because the urban and OG emissions are often separated during upslope transport with Denver metro area air masses staying further South and OG influenced air masses staying further North. This is indicated in Figure 8 and will be discussed in more detail in the next Section.

The peaks in $TR^{AreaMobile}$ and $TR^{OG}$ occur in the late afternoon/evening; the closer a site to the NFRMA (i.e. the further east) the earlier the peak. The distance between Trail Ridge Road to WC Tower is 95 km, between Longs Peak and Platteville 67 km, between Squaw Mountain and downtown Denver 45 km, and 65 km between Mines Peak and downtown Denver. On average, there is a ~2-3 hours delay between Mines Peak and Squaw Mountain and between Longs Peak and Trail Ridge Road. Trail Ridge and Mines Peak are the furthest from the NFRMA and as a result reach their peak the latest. The peak in the model tracers coincides roughly with an increase in ozone or an increase in the variability in ozone. Mean hourly maximum ozone concentrations are highest for Trail Ridge (58 ppb) and about 54-55ppb for the other sites.

Many of the features shown in the average spatial and temporal patterns of the model tracers and also in wind direction can be explained by mountain-valley winds suggesting this was a

dominant transport pattern during FRAPPÉ/DAQ. General mountain-valley flows and selected cases for these flow patterns will be discussed in greater detail in the following Section.

# 7. Mountain-Valley Transport

Mountain-Valley winds or upslope-downslope winds are a common occurrence in the Colorado Front Range, developing under clear sky conditions and weak synoptic-scale winds. The development of mountain-valley winds is a complex interaction between thermally driven and ambient flow. For more detail the reader is referred to previous studies (e.g., Arritt et al., 1992, Bauman et al., 1997 or Reddy and Pfister, 2016) and to the recent study by Sullivan et al. (2016), who provide a discussion on mountain-valley flows in the NFRMA during FRAPPÉ/DAQ. A brief overview is given here. In the morning, daytime solar heating of higher terrain and sun-facing slopes causes a pressure gradient and generates localized slope winds, which draw air from the valley floor. This results in winds blowing up-valley (from the SE, E and NE in the NFRMA) that are more regional in scale than the slope winds. For the scales we look at here, we will define both flow patterns as “upslope”. Given the limited resolution of the model it will not be able to fully resolve the narrow canyons and related slope winds, which will introduce uncertainties in the simulated development of mountain-valley flows as well as localized wind directions due to channeling effects. The air masses, when reaching the mountain tops during the afternoon, get lifted vertically and mix into the prevailing westerlies. Vertical mixing and re-entrainment into the boundary layer potentially close the loop and might bring part of the pollution back into the Front Range.

How much of the pollution transported to the East in the free troposphere is mixing back down to the surface is poorly understood. The study by Kaser et al. (2017) uses the FRAPPÉ/DAQ data to quantify the effect of ozone entrainment, yet the field measurements do not allow a complete separation of the contribution of recirculation from that of regional and long-range pollution. Efficient recirculation with a high potential of impacting surface concentrations occurs when the winds within the PBL change from easterly at the surface to westerly at the top of the PBL. Subsidence on the east end of the solenoid could introduce re-circulated and free-tropospheric material into the top of the PBL. Understanding the re-circulation patterns and associated

pollution build-up and how well models are able to represent them are important factors in air pollution studies. Here, we use the model tracers together with observations made from different platforms during FRAPPÉ/DAQ to visualize and characterize mountain-valley winds encountered during the campaign.

The implications of mountain-valley transport in regard to air quality are the transport of pollution into the mountains and its impact on pristine regions, the impact of possible recirculation of Front Range pollution, the buildup of ozone and the mixing of pollution into the free troposphere. To establish the frequency and timing of general upslope flows we show in Figure 12 the frequency of upsloping and downsloping winds during FRAPPÉ/DAQ at selected surface sites. The upslope direction has been chosen based on visual analysis of windroses and is defined as a 90 degree wide swath surrounding the most prominent upslope angle for each site. This definition is somewhat arbitrary but necessary because the direction of upslope flows can be highly variable due to the influence of topography and large-scale weather systems. However, the general conclusions hold regardless of the definitions applied.

The analysis shows a dominant upslope flow during daytime at all sites. Upslope flows develop the earliest at the sites closest to the Foothills (RF-North and Golden) and then spread to the East and into the mountains. Daytime upslope winds are also dominant at the sites east of the NFRMA, but these do not show a well-established downslope (or drainage) flow in line with the average wind direction in Figure 2. The model represents the observed patterns well at NFRMA sites as well as mountain sites but predicts daytime upslope flows too frequently at the NFRMA sites as well as at Longs Peak. Note that the timing of upslope flow based on the wind analysis is in line with the diurnal cycle of the tracers shown in Figure 11. For the mountain sites, the model suggests a more pronounced downslope pattern which is due to our definition of downslope as winds from within 270±45 degree and the fact that the model winds are predominantly from the West, while measured winds at Trail Ridge Road and Longs Peak are mostly from the NW and variable across the W-N, respectively (Figure 2).

To assess how important mountain-valley winds are on high ozone days, we show in Figure 13 concentration wind roses for ozone and $TR^{OG}$ for Longs Peak and Trail Ridge Road. The data are

separated into high and low ozone days, which has been defined as the average ozone concentration at RF-North for 12-18LT being > 70 ppb (high) or < 60 ppb (low). The results are similar if other nearby Front Range Foothills sites are used or if we choose a different threshold for high ozone such as 75 ppb. Note that there are more data points for low ozone days compared to high ozone days, which is due to the FRAPPÉ/DAQ time period overall being characterized by few high pollution episodes.

High ozone at the Foothills sites, in general, results in high ozone at the mountain sites. On high ozone days, the measurements show a strong component of upslope flows with elevated ozone concentrations (> 60 ppb) during the afternoon, whereas for low ozone days the dominant wind direction is from the West and North West with ozone concentrations mostly below 60 ppb. This is in line with findings by Reddy and Pfister (2016) who state that high ozone days occur mostly on days with upper level high pressure ridges. In addition to bringing warmer temperatures and fewer clouds, upper level ridges in this region reduce synoptic winds and thus allow cyclic terrain-driven circulations.

The model simulates the measured wind statistics well and on high ozone days suggests significantly enhanced $TR^{OG}$ from the SE sector, which confirms that the high ozone is related to transport of pollution from the NFRMA. Longs Peak shows a higher variability of the measured wind directions compared to Trail Ridge Road. This is explained by the Longs Peak sites being more strongly affected by local influences whereas the site of Trail Ridge Road is more exposed and somewhat better captures the regional flow. Similar conclusions as for Longs Peak and Trail Ridge Road are drawn for Squaw Mountain and Mines Peak if model winds are used to substitute the missing wind measurements (not shown).

## 7.1 Thermally driven upslope and transport over the Divide

On 12 August 2014, the NCAR/NSF C-130 conducted a flight designed to measure the upslope of Front Range pollution into the mountains that was forecast by various model products including the WRF Tracer model. The flight consisted of two parts. The first part was targeted at characterizing daytime pollution and emissions in the Front Range, and the second part (22:41-2:26 UTC or 16:41-20:26 LT) included a set of S-N legs over the city and the Foothills, followed

by two legs over the Continental Divide and a missed approach into Granby Airport (40.09N, -105.94W, 2500 m) located in the Fraser Valley West of the Divide. Upslope transport was evident to the Divide and spillover of high ozone air into the Fraser Valley over Berthoud Pass (where Mines Peak is located) was observed. We use the aircraft data together with the model tracers and surface measurements to investigate in detail the upslope flow and the pollution "spill-over" across the Continental Divide. Here, as well as throughout the rest of the paper when we focus on individual days, we restrict the analysis to a single model cycle to avoid inconsistencies in the model data over the course of a day. We select the 12 UTC (6 LT) forecast cycles as this allows for the shortest forecast lead and the most constrained of the forecast with analysis fields; i.e. for 12 August we select the model forecast cycle 20140812 12UTC.

Figure 14 shows measured ethane and $NO_x$ concentrations together with the modeled $TR^{OG}$ and $TR^{AreaMobile}$ concentrations. The measured and modeled wind data are added to each of the graphs. The model data are interpolated to the time and location of the 1-minute merged observations and all data sets are then averaged over a 0.1 degree x 0.1 degree grid. Only the second part of the NCAR/NSF C-130 flight, which focused on the upslope event, is considered and only data below 2 km agl are used to emphasize the impact on near-surface pollution levels. The 2 km agl upper limit does not guarantee that all the data were within the PBL, but is used here to have sufficient number of data points to demonstrate the spatial variability. Specifically, over the Foothills and the continental Divide, the aircraft often was not able to get close enough to the ground due to the flight restrictions and sampling was done in parts above the PBL in prevailing westerlies more strongly influenced by background tracer concentrations.

The aircraft data demonstrate a strong push of Front Range pollution into the mountains and a clear distinction between airmasses dominated by urban emissions and those dominated by oil and gas sources with the former mostly impacting the southern Foothills, and the latter impacting the Northern Foothills. The highest $NO_x$ concentrations, used here as a tracer for urban emissions, are seen in the southern legs of the aircraft track and it is evident from the data that this pollution has been transported to the Continental Divide and actually also descended into the valleys to the West, which was measured by the aircraft during the missed approach into Granby airport. The highest ethane concentrations are seen in the northernmost legs of the aircraft track.

$TR^{AreaMobile}$ and $TR^{OG}$ give a good representation of the features found in the aircraft data and the model also simulates well the wind field with mostly easterly and south-easterly winds over the region at the lowermost altitudes during the upslope event. The model data interpolated to the flight track do not show the enhanced ethane concentrations measured during the time of the aircraft descent into Granby but, as will be shown later, the model simulates the "spill over" of $TR^{OG}$.

A closer look at the high elevation surface sites is provided in Figure 15. In this graph, the diurnal cycles for ozone, $TR^{OG}$ and $TR^{AreaMobile}$ are shown for 12 August. We also include, for reference, their respective average diurnal cycle. Upslope is more pronounced at the northern mountain sites, but all four mountain sites experience above average influence from $TR^{AreaMobile}$, with Longs Peak and Trail Ridge Road also impacted by transport of enhanced $TR^{OG}$. On this day, the ozone reported at Longs Peak and Trail Ridge Road was amongst the highest of all the sites considered, which can be attributed to the nature of the upslope flow and the highest afternoon surface ozone concentrations being reported at the northern NFRMA sites. Ozone concentrations and model tracers increase starting after noon, when stable upslope winds had established (Figure S7). At Trail Ridge Road, a pronounced second peak in the tracers is modeled at around 22 LT roughly coinciding with a slight increase or leveling-off in ozone and a switch in winds from E to W. Looking at model longitudinal cross sections (not shown here) this likely is related to return flow of NFRMA transported tracers. Similar return flow is also seen at Longs Peak albeit less pronounced for the model tracers.

Ozone concentrations and model tracers at Squaw Mountain and Mines Peak reach their maxima later in the day compared to Longs Peak and Trail Ridge Road with maximum concentrations of ~65-70 ppb. $TR^{AreaMobile}$ is enhanced while $TR^{OG}$ remains fairly low, which is in agreement with the air mass separation discussed earlier. We attempt to establish the start of the upslope flow for northern and southern parts of the Front Range using wind data for WC Tower and Aurora East, respectively (Figure S7). Both observations and model show that upslope winds in the northern part of the Front Range (WC Tower) developed earlier in the morning compared to southern sites (Aurora East), which adds to the difference in the timing of the air masses arriving at the

mountain sites. Different transport pathways will also add to the different timing at the mountain sites.

Figure 16 provides a different view of the transport across the divide by showing a longitude – altitude cross section along 40.09N for $TR^{OG}$. We use $TR^{OG}$ because it has no sources near the Granby area and demonstrates the transport from NFRMA better than $TR^{AreaMobile}$, which has some local sources in the Granby area. As mentioned above, upslope flows developed around mid-morning at the Foothills site and by 22 UTC (16 LT) upslope winds in the PBL covered the entire region from the Plains up to the Continental Divide. On the Western side of the Divide upslope winds (Westerlies) are present. Accordingly, $TR^{OG}$ is enhanced all the way from the Front Range up to the Divide and low on the Western side of the Divide. The model estimates the PBLH at ~2 km agl. We can also see a weak solenoid flow with updraft over the Divide, winds switching to westerlies near the top of the PBL and an area of downdraft over the eastern NFRMA. As stated earlier, such a flow pattern has the potential of recirculating Front Range pollution back to the Front Range and bringing it back to the surface efficiently. A radiosonde launched at the BAO Tower in Erie (Table 1) indicates a switch in the winds from south-easterlies to West at about 3 km, which agrees well with the model for the same time (not shown).

At 2 UTC on 13 August 2014 (20 LT on 12 August 2014), which is around the time of the missed approach of the NCAR/NSF C-130 into Granby airport, upslope flow on the eastern side of the Divide continues, but on the Western side we now see downsloping winds prevailing carrying the air masses from the Front Range down into the Fraser Valley. The model PBL has shrunk to about 500 m, but upsloping winds on the eastern side in the Divide and downsloping winds on the Western side of the Divide also persist above the PBL. Tracer concentrations remain elevated above the PBL in the NFRMA. There are no PBL measurements in the NFRMA for evaluation available for this day and time, but the NCAR/NSF C-130 temperature and water vapor measurements during the descent into Granby indicate that there have been two different mixing regimes with one layer up to about 500 m agl, which is in line with the model PBLH, and another layer up to about 1000 m agl (not shown). Wind measurements at most surface sites as well as model results show a shift to westerly winds at the eastern side of the Divide after ~20

LT accompanied with an increase in ozone concentrations and model tracers (not shown). Until FRAPPÉ/DAQ there was uncertainty whether NFRMA pollution can potentially impact the valleys to the West of the Continental Divide. The aircraft measurements together with the model tracers confirm a "spill-over" of pollution and provide a well-documented case for such an event.

## 7.2 Discussion

The case study for 12 August demonstrates a general separation of OG and urban dominated air masses during upslope events. This leads to the question if air masses are always separated during upslope events given that such dominance would have different implications for air quality impacts on remote mountain areas than if the pollutants were more mixed. A tendency towards a separation of airmasses is indicated by the model showing a dominance of $TR^{OG}$ at Longs Peak and Trail Ridge Road and a dominance of $TR^{AreaMobile}$ at Squaw Mountain and Mines Peak over the entire FRAPPÉ/DAQ period (Figure 11). To demonstrate the variability in upslope events, we show in Figure 17 the spatial distribution of $TR^{OG}$ and $TR^{AreaMobile}$ for different days when upslope was modeled together with the average surface ozone concentrations for all sites where measurements are available. We focus on 14-20 LT as this covers the time period when upslope generally reaches the high mountain sites. In addition to the average over the FRAPPÉ/DAQ period and the 12 August case study discussed above and where air mass separation was observed, we also show results for 22 July, and 2, 4 and 8 August. All these days demonstrate transport of NFRMA pollution to the mountains, but the spatial patterns and strength of the upslope vary considerably. In addition to the graphs, we list in Table 3 for the cases shown the maximum hourly ozone concentrations together with the respective local hour for selected mountain and NFRMA sites.

First, we look at the general tracer distribution on 12 August and compare to the average over the campaign period. On this day, $TR^{OG}$ showed a more widespread distribution compared to the average distribution, but elevated $TR^{OG}$ concentrations stayed mostly North and shows only a small influence on the Denver area. With the onset of upslope around mid-morning (see Figure S6 for wind direction plots for WC-Tower and Aurora East) the flow patterns change and SE flows push the NFRMA tracers into the Foothills at the same time keeping $TR^{OG}$ away from the

Denver Area. As the day progresses, the strong upslope flow continues transporting the tracers all the way to the Continental Divide similar to what was seen from the aircraft data. The high elevation surface ozone monitors report elevated ozone up to ~80 ppb at Longs Peak and Trail Ridge Road at 14 LT and 15 LT and also the Niwot Ridge monitors report hourly ozone concentrations above 70 ppb. In line with this, the highest surface ozone in the NFRMA on this day has been recorded at sites close to the Foothills in the Northern part of the NFRMA, yet none of these sites reach hourly ozone maxima as high as the mountain sites (Table 3). It is interesting to note that the surface ozone monitors along the E-W transect into the mountains report elevated ozone, yet surface ozone in the Denver area, where the air is coming from, is low. This suggests that (1) the airmasses from the Denver area had a great potential for forming ozone and (2) the $NO_x$ and VOC mix in the Denver area has a high ozone forming potential also without significant contributions from OG. The amount of ozone produced during upslope transport is clearly a topic that should be explored further using chemistry observations and modeling.

The highest ozone day experienced during the campaign was on 22 July 2014. Compared to the average conditions and the patterns seen on 12 August, $TR^{OG}$ extended further South in the afternoon mixing with areas of high $TR^{AreaMobile}$, whereas $TR^{AreaMobile}$ had only a small impact on the north-eastern NFRMA. Widespread high ozone comes along with the widespread emission tracers. Clear skies, a lower and slow growing PBLH (Figure 4; evident for NREL Golden) and reduced ventilation (not shown) resulted in less dilution with increased tracer concentrations, which contributed to the high ozone concentrations. During the transport into the Foothills, $TR^{OG}$ and $TR^{AreaMobile}$ stay mostly separate, yet the distribution of both tracers is shifted to the South compared to 12 August. The model also indicates transport across the Divide reaching the Granby area ~ 20 LT on 23 July (not shown).

Hourly ozone concentrations reached 80 ppb and higher on 22 July at most NFRMA sites. Ozone concentrations remained elevated into the late afternoon/evening in and near the Foothills but decreased at surface sites in the southern and eastern NFRMA. This might be explained in that, similar to 12 August, recirculation of NFRMA pollution lead to ozone buildup and the onset of downsloping winds ~18LT at sites near the Foothills likely contributed to keeping ozone values elevated. A potential solenoid flow has been discussed by Sullivan et al. (2016) for the northern

NFRMA on 22 July around 2 UTC (20 LT) when ozone concentrations at Fort Collins West and RF North experienced a small second peak. Similar to what was shown for 12 August, we do see recirculation flows and subsidence over the NFRMA but mostly these are simulated during the day whereas at 2 UTC (20 LT) the model simulations show the establishment of surface downsloping winds. However, we note that the wind and PBL fields for 22 July change notably between the different forecast cycles pointing towards a larger uncertainty in the model transport for this event.

Strongly elevated ozone concentrations are also detected at the mountain sites on 22 July. Hourly ozone concentrations greater than 80 ppb occur at Squaw Mountain and Mines Peak around 16LT and 17LT, respectively, where enhanced $TR^{AreaMobile}$ and slightly enhanced $TR^{OG}$ is modeled. The ozone concentrations at the mountain sites are higher than would be suggested by the tracers, but this is because the tracers are purely emission tracers and have no chemical production, whereas ozone was produced efficiently during the transport to the mountains. $TR^{OG}$ is enhanced at Longs Peak and Trail Ridge Road, but $TR^{AreaMobile}$ remains low in line with the reduced influence of $TR^{AreaMobile}$ in the north-eastern NFRMA on this day. Still, Longs Peak and Trail Ridge Road experience peaks in ozone concentrations of 76 ppb and 82 ppb, respectively, demonstrating the ozone formation potential of air masses originating from the OG area and transported over the northern part of the Front Range urban areas.

On 2 August, upslope is very pronounced in the South with $TR^{AreaMobile}$ being transported well beyond the Continental Divide. Similar to the two cases discussed before, the two tracers are mostly separated during transport into the mountains yet transport of $TR^{OG}$ appears to be weaker. This might have contributed to the lower ozone concentrations at Longs Peak and Trail Ridge Road (72 ppb and 71 ppb, respectively), whereas higher maximum ozone was detected at Squaw Mountain and Mines Peak (77 ppb).

On 3 August, we see that fairly strong upslope transports the tracers to the West but, similar to the day before, is most established at the southern part of the NFRMA with high levels of $TR^{AreaMobile}$ reaching to and beyond the Continental Divide. The model tracers agree well with the emission data measured by the NCAR/NSF C-130 on this day (not shown here), when a similar flight pattern was carried out as on 12 August. Numerous sites in the NFRMA reach

hourly ozone maxima beyond 80 ppb including the northern Foothills sites, yet Longs Peak and Trail Ridge Road hourly ozone concentrations remain in the moderate range. Similar to the day before, Mines Peak and Squaw Mountain reach the highest ozone concentrations of 84 ppb at 19 LT and 79 ppb at 21 LT, respectively.

Our last example is 8 August, when upslope was weakest of the days considered. We chose this day because it reflects elevated ozone along the W-E transect of ozone monitors and where $TR^{OG}$ and $TR^{AreaMobile}$ intersect. The NFRMA monitors near the start of this transect close to the Foothills (RF North and SBCreek) reach > 80 ppb at 16 LT and the two Niwot Ridge sites at the end of this transect reach 78 ppb at 17 LT. From the four main mountain sites, only Longs Peak and Squaw Mountain show enhanced ozone with the former reaching a narrow peak of 75 ppb at 18 LT and the latter a much broader peak of up to 78 ppb at 17 LT, respectively. It is also interesting to note that $TR^{OG}$ shows enhanced concentrations West of the Divide on this day. This is not related to transport from the NFRMA but to eastward transport of OG emissions from the Western Slopes.

The considered cases show that upslope flow conditions can be quite variable. While OG sources are the main contributor to tracer concentrations in the northern mountains and urban sources represent the major contribution to tracer concentrations in the southern mountains, one cannot exclude that either emissions sources can impact any of the remote area. Whether or not air masses remain separated during upslope flows depends on the degree of mixing in the NFRMA and on the direction of the upslope. The tracer analysis also points towards efficient ozone production under conditions when airmasses originating from OG source regions mix with airmasses originating from urban and mobile source sectors. In addition, we find a tendency for highest hourly ozone concentrations occurring at NFRMA sites closest to the Foothills.

The inert model tracers are valuable in the analysis of upslope flows as they do not depend on conditions being conducive to ozone production. Not all upslope days necessarily are also high ozone days and even on low ozone days, other pollutants (e.g. ammonia) still might be transported to the mountain regions affecting the ecosystems when deposited (e.g. Benedict el al., 2011; Benedict et al., 2013; Thompson et al., 2015)

# 8. Conclusions

We have introduced a set of inert emission tracers in the regional Weather Research and Forecasting Model (WRF) to assist in flight planning during the FRAPPÉ and DISCOVER-AQ campaigns in summer 2014 in the Colorado Northern Front Range Metropolitan Area (NFRMA). The tracers represent the emissions from oil and gas activities and from urban sources in Colorado and have shown high value for forecasting during the campaigns and for the analysis of the comprehensive measurement data set. The tracers help to visualize the flow patterns and support chemical analysis with information about mixing of air masses from different emission sources. This paper also serves to provide an overall evaluation of the tracers as they have been used in other studies (Vu at el., 2016).

The NFRMA is a very challenging region to model because of the complex topography but comparison to wind observations from surface sites and ozone sonde launches shows that the model overall simulates well the general wind patterns, which are dominated by mountain-valley flows. However, the model does not necessarily resolve the very localized nature of the surface wind measurements. Statistical analysis of chemical trace gases measured from aircraft with the respective model tracers reveals a high degree of correlation and provides confidence in using the model to support the analysis of transport patterns in the NFRMA.

The tracers provide a means of analyzing the general distribution and mixing of different emission sources. During nighttime, the urban tracer reveals a pooling of emissions from the Denver Metro Area to the NE towards the region of strong oil and gas sources. Flow reversal in the morning transports aged urban emissions together with fresh oil and gas emissions towards the Metro area with important implications for chemistry. Around mid-morning upslope flows frequently develop starting at near-Foothills sites and then spreading to the East and West. These have the potential of carrying NFRMA pollution to the remote mountain areas. During the campaigns, numerous cases of upslope flows have been encountered and these form the focus of this study.

The analysis of model tracers and surface ozone observations together with wind data at NFRMA and mountain sites demonstrates that on days with high ozone values at NFRMA

Foothills sites there is also a high likelihood of strong upslope flows and as a result the mountain sites experience high ozone and high tracer concentrations. On 12 August 2014, the NCAR/NSF C-130 well captured a strong upslope event, which was forecast by the tracer model. The aircraft followed transport of NFRMA pollution towards the Continental Divide and also captured spill-over into the Frasier Valley on the West side of the Continental Divide. Measured chemical tracers and modeled emission tracers both indicate a separation of airmasses from the northern and southern parts of the NFRMA with the former mostly influenced by oil and gas emissions and the latter by urban emissions. While there seems to be a tendency for oil and gas and urban influenced airmasses to be separated during upslope events, this is not necessarily true for all events and the exact nature of the impact of NFRMA pollution on remote mountain areas depends on the degree of mixing in the NFRMA and the general direction of upslope flows which can vary from NE to E or SE.

The presented analysis demonstrates that oil and gas pollutants from sources to the North and Northeast of Denver frequently remain unmixed with Denver-based pollutants as they are both transported to the mountains in upslope flow and potentially spill over the Continental Divide into the valleys to the West. Some of the transported pollution gets lofted and recirculated back to the NFRMA. This implies that mountain sites are not necessarily representative of inflow/background conditions. Even if winds are from the West, the air masses still can carry some influence from sources in the NFRMA given that NFRMA pollution can be transported across the Divide and then brought back via return flows. For this reason, it is important to look at the air mass history and not just actual wind data. The study also demonstrates how complex the flow patterns in the NFRMA can be and their high variability on small scales (in time and space) highlights how crucial it is for models to provide a reasonably accurate simulation of transport when assessing air quality. The NFRMA contains a range of different emission sources with very different chemical signatures and the photochemistry is strongly dependent on their degree of mixing and interaction. The FRAPPÉ and DISCOVER-AQ provide highly valuable data on flow patterns frequently occurring in the Front Range and provide an excellent testbed for evaluating model performance.

**Acknowledgements**

The data for this paper are publicly available at the FRAPPÉ/DISCOVER-AQ data archive (http://www-air.larc.nasa.gov/missions/discover-aq/discover-aq.html) including model output along the aircraft flight tracks. Forecast graphics from the WRF tracer simulation are available from the FRAPPÉ Field Catalog (http://catalog.eol.ucar.edu/frappe). The authors would like to thank the State of Colorado/Colorado Department of Public Health and Environment and the National Science Foundation (NSF) for funding of FRAPPÉ and NASA for funding of DISCOVER-AQ. The authors acknowledge the use of WRF-Chem version 3.3.1 (http://www2.mmm.ucar.edu/wrf/users/download/get_source.html) and Stu McKeen at NOAA for providing the NEI 2011 emissions inventory (ftp://aftp.fsl.noaa.gov/divisions/taq/emissions_data_2011/). We further acknowledge Alpine Geophysics, Ramboll/Environ and the Western Regional Air Partnership (WRAP) for help with sector based emission inventories. We thank Richard Clark (Millersville University), Raymond Hoff (U. Maryland) and Timothy Berkoff (University of Maryland) for providing PBLH data. The Niwot Ridge surface ozone measurements were prepared by Audra McClure (NOAA) and Russel Long (US EPA) provided surface data for NREL Golden. NASA P-3 CO data were carried out by Glen Diskin (NASA Langley), NCAR-C130 CO measurements were carried out by Teresa Campos (NCAR/ACOM) and NCAR TOGA VOC data were carried out by Eric Apel (NCAR/ACOM). Aircraft VOC WAS samples have been collected and analyzed by Don Blake (UC Irvine). Ethane on the NASA P-3 was measured by the Aerodyne Research, Inc. mini-TILDAS and we acknowledge Joseph R. Roscioli and John Nowak for collecting $NH_3$ data using the Aerodyne Research, Inc. dual-TILDAS spectrometer. Dirk Richter, Peter Weibring and James Walega (INSTAAR) contributed to collecting ethane measurements on the NCAR/NSF C-130. PTR-ToF-MS measurements on the NASA P-3 were carried out by P. Eichler, T. Mikoviny, and M. Müller, and were supported by the Austrian Federal Ministry for Transport, Innovation and Technology (bmvit) through the Austrian Space Applications Programme (ASAP) of the Austrian Research Promotion Agency (FFG). We acknowledge the help of Arthur Mizzi (NCAR/ACOM) and NCAR/MMM with conducting the model simulations. G. Pfister's work has

in parts been supported by the NASA AQAST project (grant NNX11AI51G). The National Center for Atmospheric Research is sponsored by the National Science Foundation.

**References**

Angevine, W. M., et al. (2013), Pollutant transport among California regions, J. Geophys. Res. Atmos., 118, 6750–6763, doi:10.1002/jgrd.50490.

Arritt, R.W., J.M. Wilczak, G.S. Young (1992), Observations and Numerical Modeling of an Elevated Mixed Layer, Monthly Weather Review, Volume 20, 2869-2880.

Barth, M. C., Lee, J., Hodzic, A., Pfister, G., Skamarock, W. C., Worden, J., Wong, J., and Noone, D.: Thunderstorms and upper troposphere chemistry during the early stages of the 2006 North American Monsoon, Atmos. Chem. Phys., 12, 11003-11026, doi:10.5194/acp-12-11003-2012, 2012.

Baumann, K., E. J. Williams, J. A. Olson, J. W. Harder, and F. C. Fehsenfeld (1997), Meteorological characteristics and spatial extent of upslope events during the 1993 Tropospheric OH Photochemistry Experiment, J. Geophys. Res., 102(D5), 6199–6213, doi:10.1029/96JD03251.

Benedict, K. B., J. L. Collett, C. M. Carrico, S. Raja, F. M. Schwandner, M. Schurman, E. Levin, D. Day, S. M. Kreidenweis, W. C. Malm, and B. A. Schichtel (2011), Transport and deposition of reactive nitrogen in the Rocky Mountain region. Abstr. Pap. Amer. Chem. Soc., 242, Meeting Abstract: 303-ENVR, Aug. 28, 2011.

Benedict, K. B., Carrico, C. M., Kreidenweis, S. M., Schichtel, B., Malm, W. C. and Collett, J. L. (2013), A seasonal nitrogen deposition budget for Rocky Mountain National Park. Ecological Applications, 23: 1156–1169. doi:10.1890/12-1624.1

Brioude, J., Arnold, D., Stohl, A., Cassiani, M., Morton, D., Seibert, P., Angevine, W., Evan, S., Dingwell, A., Fast, J. D., Easter, R. C., Pisso, I., Burkhart, J., and Wotawa, G.: The Lagrangian particle dispersion model FLEXPART-WRF version 3.1, Geosci. Model Dev., 6, 1889-1904, https://doi.org/10.5194/gmd-6-1889-2013, 2013.

Brodin, M., D. Helmig, S. Oltmans (2010), Seasonal ozone behavior along an elevation gradient in the Colorado Front Range Mountains. Atmospheric Environment 44 :5305-5315

Brodin, M., D. Helmig, B. Johnson, and S. Oltmans (2011), Comparison of ozone concentrations on a surface elevation gradient with balloon-borne ozonesonde measurements. Atmos. Environ., 45, 5431- 5439.

Compton, J.C., R. Delgado, T.A. Berkoff, and R.M. Hoff (2013): Determination of Planetary Boundary Layer Height on Short Spatial and Temporal Scales: A Demonstration of the Covariance Wavelet Transform in Ground-Based Wind Profiler and Lidar Measurements. J. Atmos. Oceanic Technol., 30, 1566–1575, https://doi.org/10.1175/JTECH-D-12-00116.1

Darrouzet-Nardi, A., J. Erbland, W. D. Bowman, J. Savarino, and M. W. Williams (2012), Landscapelevel nitrogen import and export in an ecosystem with complex terrain, Colorado Front Range. Biogeochemistry, 109, 271-285.

Doran, J.C. (1996), The influence of Canyon Winds on flow fields near Colorado's Front Range, J. Appl. Meteorology, Volume 35, 587-600.

Greenland, D. (1980), The Climate of Niwot Ridge, Front Range, Colorado, U.S.A., Arctic and Alpine Research, vol. 21, no. 4, 1989, pp. 380–391., www.jstor.org/stable/1551647.

Haagenson, P. L., (1979), Meteorological and climatological factors affecting Denver air quality, Atmos. Environ., 13, 79–85.

Halliday, H. S., A. M. Thompson, A. Wisthaler, D. Blake, R. S. Hornbrook, T. Mikoviny, M. Müller, P. Eichler, E. C. Apel, and A. J. Hills, Atmospheric benzene observations from oil and gas production in the Denver Julesburg basin in July and August 2014, J. Geophys. Res. Atmos., 121, doi:10.1002/2016JD025327, 2016.

Hegarty, J., R. R. Draxler, A. F. Stein, J. Brioude, M. Mountain, J. Eluszkiewicz, T. Nehrkorn, F. Ngan, and A. Andrews (2013), Evaluation of Lagrangian particle dispersion models with measurements from controlled tracer releases, J. Appl. Meteorol. Climatol., 52, 2623–2637.

Herndon, S.C., et al., Characterization of urban pollutant emission fluxes and ambient concentration distributions using a mobile laboratory with rapid response instrumentation,

Faraday Discuss. 2005, 130, 327-329. Jimenez, R., et al,. In Atmospheric trace gas measurements using a dual quantum-cascade laser mid-infrared absorption spectrometer, Proc. of SPIE, 2005; Mermelstein, C.; Bour, D., Eds. 2005. McManus, J.B., et al., Application of quantum cascade lasers to high-precision atmospheric trace gas measurements., Opt. Eng., 2010, 39, (11), 111124-111124-11.

Hong, S. Y. Noh, and J. Dudhia, 2006: A new vertical diffusion package with an explicit treatment of entrainment processes. Mon. Wea. Rev., 134, 2318–2341, doi:10.1175/MWR3199.1

Hong, S. Y. (2010), A new stable boundary layer mixing scheme and its impact on the simulated East Asian summer monsoon, Quart. J. Roy. Meteor. Soc., 136(651), 1481–1496, doi:10.1002/Qj.665.

Hu, X.-M., P. M. Klein, and M. Xue (2013), Evaluation of the updated YSU planetary boundary layer scheme within WRF for wind resource and air quality assessments, J. Geophys. Res. Atmos., 118, 10,490–10,505, doi:10.1002/jgrd.50823.

Iacono, M. J., J. S. Delamere, E. J. Mlawer, M. W. Shephard, S. A. Clough, and W. D. Collins, 2008: Radiative forcing by long–lived greenhouse gases: Calculations with the AER radiative transfer models. *J. Geophys. Res.*,113, D13103.

Johnson, R.H.  and J.J. Toth (1982), Topographic effects and weather forecasting in the Colorado PROFS mesonetwork area, Preprint Volume: 9th Conference on Weather Forecasting and Analysis, June 28 - July 1, 1982; Seattle, WA, 440-445.

Kaser, L., E. G. Patton, G. G. Pfister, A. J. Weinheimer, D. D. Montzka, F. Flocke, A. M. Thompson, R. M. Stauffer, and H. S. Halliday (2017), The effect of entrainment through atmospheric boundary layer growth on observed and modeled surface ozone in the Colorado Front Range, J. Geophys. Res. Atmos., 122, 6075–6093, doi:10.1002/2016JD026245.

Kain, John S., 2004: The Kain–Fritsch convective parameterization: An update. *J. Appl. Meteor.*, 43, 170–181.

Janjic, Z. I., 1994: The step-mountain Eta coordinate model: further developments of the convection, viscous sublayer and turbulence closure schemes. Mon. Wea. Rev., 122, 927–945.

Olson, J. A., K. Baumann, C. J. Volpe, J. W. Harder, E. J. Williams, and G. H. Mount (1997), Meteorological overview of the 1993 OH Photochemistry Experiment, J. Geophys. Res., 102(D5), 6187–6197, doi:10.1029/96JD00402.

Parrish, D.D., D.W. Fahey, E.J. Williams, S.C. Liu, M. Trainer, P.C. Murphy, D. L. Albritton, F.C. Fehsenfeld, F.C., (1986) Background ozone and anthropogenic ozone enhancement at Niwot Ridge, Colorado. *Journal of Atmospheric Chemistry 4 :63-80*

Reddy, P. J., and G. G. Pfister (2016), Meteorological factors contributing to the interannual variability of midsummer surface ozone in Colorado, Utah, and other western U.S. states, J. Geophys. Res. Atmos., 121, 2434–2456, doi:10.1002/2015JD023840.

Richter, D., P. Weibring, J. Walega, A. Fried, S.M. Spuler, M.S. Taubman (2015), Compact highly sensitive multi-species airborne mid-IR spectrometer. Applied Physics B: Lasers and Optics, 119(1 SI): 119-131. DOI: 10.1007/s00340-015-6038-8-9071

Stohl, A., Forster, C., Frank, A., Seibert, P., and Wotawa, G.: Technical note: The Lagrangian particle dispersion model FLEXPART version 6.2, Atmos. Chem. Phys., 5, 2461-2474, https://doi.org/10.5194/acp-5-2461-2005, 2005.

Sullivan, J. T., et al. (2016), Quantifying the contribution of thermally driven recirculation to a high-ozone event along the Colorado Front Range using lidar, J. Geophys. Res. Atmos., 121,10,377–10,390, doi:10.1002 /2016JD025229.

Sun, K., K. Cady-Pereira, D.J. Miller, L. Tao, M.A. Zondlo, J.B. Nowak, J.A. Neuman, T. Mikoviny, M. Müller, A. Wisthaler, A.J. Scarino, C.A. Hostetler (2014), Validation of TES ammonia observations at the single pixel scale in the San Joaquin Valley during DISCOVER-AQ, J. Geophys. Res. Atmos., 120 (10) (2015), pp. 5140–5154, http://dx.doi.org/10.1002/2014JD022846

Tewari, M., F. Chen, W. Wang, J. Dudhia, M. A. LeMone, K. Mitchell, M. Ek, G. Gayno, J. Wegiel, and R. H. Cuenca, 2004: Implementation and verification of the unified NOAH land surface model in the WRF model. 20th conference on weather analysis and forecasting/16th conference on numerical weather prediction, pp. 11–15.

Thompson, Gregory, Paul R. Field, Roy M. Rasmussen, William D. Hall, 2008: Explicit Forecasts of Winter Precipitation Using an Improved Bulk Microphysics Scheme. Part II: Implementation of a New Snow Parameterization. *Mon. Wea. Rev.*, **136**, 5095–5115.

Thompson, T. M., M. A. Rodriguez, M. G. Barna, K. A. Gebhart, J. L. Hand, D. E. Day, W. C. Malm, K. B. Benedict, J. L. Collett Jr., *and* B. A. Schichtel *(*2015*)*, Rocky Mountain National Park reduced nitrogen source apportionment, J. Geophys. Res. Atmos., 120, 4370–4384. *doi:*10.1002/2014JD022675.

Toth, J. J., and R. H. Johnson (1985), Summer surface flow characteristics over northeast Colorado, Mon. Weather Rev., 113(9), 1458–1469.

Vu, K. T., Dingle, J. H., Bahreini, R., Reddy, P. J., Campos, T. L., Diskin, G. S., Fried, A., Herndon, S. C., Hornbrook, R. S., Huey, G., Kaser, L., Montzka, D. D., Nowak, J. B., Richter, D., Roscioli, J. R., Shertz, S., Stell, M., Tanner, D., Tyndall, G., Walega, J., Weibring, P., Weinheimer, A. J., Pfister, G., and Flocke, F.: Impacts of the Denver Cyclone on Regional Air Quality and Aerosol Formation in the Colorado Front Range during FRAPPÉ 2014, Atmos. Chem. Phys., 16, 12039-12058, doi:10.5194/acp-16-12039-2016, 2016.

Weinheimer, A.J., J.G. Walega, B.A. Ridley, B.L. Gary, D.R. Blake, N.J. Blake, F.S. Rowland, G.W. Sachse, B.E. Anderson, J.E. Collins, Meridional distributions of NOx, NOy, and other species in the lower stratosphere and upper troposphere during AASE II, *Geophys. Res. Lett., 21*, 2583-2586, 1994.

Yacovitch TI, Herndon SC, Roscioli JR, Floerchinger C, McGovern RM, et al. (2014), Demonstration of an Ethane Spectrometer for Methane Source Identification. Environ Sci Technol 48(14): 8028-8034. doi:10.1021/es501475q.

Zhang, Y., Wang, Y., Chen, G., Smeltzer, C., Crawford, J., Olson, J., Szykman, J., Weinheimer, A., Knapp, D., Montzka, D. D., Wisthaler, A, Mikoviny, T., Fried, A., and G. Diskin (2016), Large vertical gradient of reactive nitrogen oxides in the boundary layer: Modeling analysis of DISCOVER-AQ 2011 observations, J. Geophys. Res. Atmos., 121, 1922-1934, doi:10.1002/2015JD024203.

Table 1: Location information for surface sites mentioned in this study ordered by longitude. Sites focused at in the analysis are indicated by “A”, NASA P-3 spiraling sites by “S”, non-spiral Front Range sites by “F” and mountain sites by “M”. The Continental Divide stretches along the highest elevation points.

Table 2: Spatial correlations of aircraft measurements of $NO_x$, $C_2H_6$ and $NH_3$ with model tracers for (top row) 0-3km and (second row) 0-2km, 0-1km and all altitudes. See text for details on the calculation of spatial correlation. R values larger than 0.7 are marked in bold characters.

Table 3: Maximum hourly surface ozone concentrations and hour of occurrence for the five days shown in Figure 17. Only monitoring sites as part of the CDPHE network are included together with the four mountain sites used before and two additional high altitude sites at Niwot Ridge. Sites are ordered from West to East and only values equal or larger than 70 ppb are shown for NFRMA sites. Values above 75 ppb are highlighted in bold. The start time of the hourly averaging period is listed. NA indicate days with missing observations. Sites close to the Foothills on the western edge of the NFRMA are shown in Italic.

Figure 1: Topography of the study region. Light grey dots indicate the four mountain sites used in this study, dark grey dots the 4 sites in the NFRMA used in the analysis of upslope events. White dots indicate other NFRMA spiral sites for the NASA P-3. Site characteristics are listed in Table 1. Additional sites used later in the analysis are indicated by triangles. County lines are shown as solid lines.

Figure 2: Measured (black) and modeled (red) diurnal cycle for 6am – 6am LT in wind direction (vector average for wind speed > 0.3 m/s ; left) and wind speed (right) for selected surface sites. Shown are mean, median, standard deviation and, for wind speed only, minimum and maximum over the FRAPPÉ time period (15 July – 20 August).

Figure 3: Measured (black) and modeled (red) average wind direction, wind speed, relative humidity and temperature for sonde launches in (a) Platteville (40 sonde launches) and (b) Fort Collins West (40.59N and -105.14W; 12 sonde launches) and (c) windroses for Platteville from surface measurements for 8-12LT and 14-20LT. For averaging the sonde wind direction data only observations with wind speed > 0.3 m/s were considered.

Figure 4: Observed and modeled PBL height for (from top to bottom): Fort Collins West, Platteville and Golden for 19 July – 11 August.

Figure 5: Observed NCAR/NSF C-130 $NO_x$ and ethane concentrations and model tracers $TR^{AreaMobile}$ and $TR^{OG}$ averaged over 0.1 deg x 0.1 deg for altitudes < 3km agl. Averages of observed and model tracer concentrations are calculated for grids with at least 3 data points. The spatial correlation is listed here, as well as in Table 2. Areas above 2500m a.s.l. are shaded in grey.

Figure 6: Observed NASA P-3 $NO_x$ and ethane concentrations and model tracers averaged over 0.05 deg x 0.05 deg for altitudes < 3km agl. Averages of observed and model tracer concentrations are calculated for grids with at least 3 data points. The spatial correlation is listed here, as well as in Table 2. Areas above 2500m a.s.l. are shaded in grey.

Figure 7: Spatial correlations between measured species and ratios and model tracers for the area/mobile (blue) and OG (red) sources. Big circles represent the average over all flights, small circles represent results for individual flights. Top: NCAR/NSF C130 flights (same spatial coverage as Figure 5); Bottom: NASA P-3 flights. Statistics are derived for data points below 3 km a.g.l. See text for details on the calculation of spatial correlation.

Figure 8: Average spatial tracer distribution (average concentrations within the PBL) for 0-6LT, 6-12LT, 12-18LT and 18-24 LT for the FRAPPÉ time period (14 July to 21 August). Contour lines show the PBL average for $TR^{AreaMobile}$, filled contours show the PBL average $TR^{OG}$ concentrations. Colored points denote the mean ozone measured at surface sites. The tracers are scaled by a common factor and then by their mean ratio ($TR^{AreaMobile} = 60.\bullet TR^{OG}$) to appear on the same scale.

Figure 9: Tracer Statistics for surface sites employed during FRAPPÉ/DAQ for $TR^{AreaMobile}$ (top) and $TR^{OG}$ (bottom). Sites are arranged from West to East and averaged over 10-17 LT (though an average over all times would not look vastly different). Sites focused on in the analysis of upslope events are colored in red. Shown are mean (dot), median (triangle), standard deviation (horizontal bars), $10^{th}$ and $90^{th}$ percentiles (thick line), minima and maxima (thin lines). In addition to sites shown in Figure 1 we also added sites in the Global Ozone (GO3) project (Black Hawk, Lyons, East Boulder and Longmont) as well as additional sites from the CDPHE network (I-25 Denver, CAMP).

Figure 10: Average diurnal observed surface ozone (black) and PBLH average $TR^{OG}$ (red) and $TR^{AreaMobile}$ (blue) for selected surface sites in the Front Range for 6am – 6am LT. Shown are mean, median, standard deviation, minimum and maximum. A line is drawn though the mean values.

Figure 11: As Figure 10 but for selected surface sites in the mountains. Note the y-scale is reduced to half of the one used in Figure 10.

Figure 12: Upslope (red) and Downslope (black) statistics from observations (solid lines) and WRF (dotted lined). Flow is defined when winds are from within a defined wind sector at least $2/3^{rd}$ of the time within a given hour (Note that wind data for Trail Ridge Road are available

hourly only and that model data are also only available on an hourly basis). Upslope: Upslope Angle ±45deg; Downslope: 270±45deg; only data with wind speeds > 0.3 m/s (i.e. data that are not defined calm based on Beaufort scale). The upslope angle has been defined based on windrose analysis. The frequency is given as percentage of upslope or downslope of all valid measurements.

Figure 13: Ozone and Tracer roses for (a) Longs Peak (1-minute data) and (b) Trail Ridge road (hourly data) on days when RF North 12-18LT average ozone was > 70 ppb ("RF North HIGH") or < 60 ppb ("RF North LOW"). Only data for 12-20LT are shown.

Figure 14: NCAR/NSF C-130 measured ethane and NOx (top row) and modeled $TR^{OG}$ and $TR^{AreaMobile}$ (bottom row) for the the upslope part of the 12 August flight (after refueling). All data averaged over 0-2km ag and a 0.1 deg x 01 deg grid. The vector averaged measured and modeled winds for each grid point are shown by the windbarbs and the monitoring sites RF North, NREL Golden, WC Tower, Aurora East and Golden are indicated by diamond symbols. Areas above 2500m a.s.l. are shaded in grey.

Figure 15: as Figure 10 but for 12 August 2014 and for mountain sites only. Lines show the average diurnal cycle from Figure 11.

Figure 16: Longitude-Altitude Cross Section of $TR^{OG}$ at 40.09N (single grid box in latitude) for 12 August 22 UTC (16 LT, top) and 13 August 2 UTC (12 August 20 LT, bottom); The location of the Granby airport is indicated by the black dot. Horizontal winds are indicated by black arrows, vertical winds are shown as white arrows. For clarity, only vertical winds > 0.2m/s are included. The height of the PBLH is plotted as a black line.

Figure 17: as Figure 8 but for 14-20 LT. Top row: average over FRAPPÉ period and 12 August; middle row: 22 July and 2 August; bottom row: 3 and 8 August.

Table 1: Location information for surface sites mentioned in this study ordered by longitude. Sites focused at in the analysis are indicated by "A", NASA P-3 spiraling sites by "S", non-spiral Front Range sites by "F" and mountain sites by "M".

| Site | Latitude (N) | Longitude (W) | Elevation (m asl) | Type |
|---|---|---|---|---|
| Aurora East (AUREAST) | 39.639 | -104.569 | 1552 | AF |
| Platteville | 40.182 | -104.727 | 1516 | S |
| Weld County (WC) Tower | 40.386 | -104.737 | 1484 | AF |
| LaCasa | 39.779 | -105.005 | 1602 | S |
| BAO | 40.043 | -105.006 | 1579 | S |
| Chatfield Park (CHATPARK) | 39.534 | -105.070 | 1676 | S |
| Fort Collins (FTC) CSU | 40.571 | -105.080 | 1524 | S |
| NREL Golden | 39.744 | -105.178 | 1832 | AFS |
| RF North | 39.913 | -105.189 | 1802 | AF |
| Squaw Mountain | 39.681 | -105.496 | 3420 | AM |
| Longs Peak | 40.278 | -105.545 | 2743 | AM |
| Trail Ridge Road | 40.39 | -105.686 | 3498 | AM |
| Mines Peak | 39.794 | -105.764 | 3805 | AM |

Table 2: Spatial correlations of aircraft measurements of $NO_x$, $C_2H_6$ and $NH_3$ with model tracers for (top row) 0-3km and (second row) 0-2km, 0-1km and all altitudes. See text for details on the calculation of spatial correlation. R values larger than 0.7 are marked in bold characters.

| | $TR^{AreaMobile}$ | | $TR^{OG}$ | | $TR^{Agr}$ | |
|---|---|---|---|---|---|---|
| | *C-130* | *P-3* | *C-130* | *P-3* | *C-130* | *P-3* |
| $NO_x$ | **0.82**<br>**0.81,0.79,0.82** | **0.72**<br>0.69,0.67,**0.79** | 0.23<br>0.18,0.07,0.23 | 0.20<br>0.10,-0.04,0.37 | 0.21<br>0.16,0.02,0.21 | 0.12<br>0.06,-0.05,0.26 |
| $C_2H_6$ | 0.38<br>0.35,0.20,0.39 | -0.02<br>-0.14,-0.27,0.25 | **0.80**<br>**0.79,0.76,0.80** | **0.86**<br>**0.85,0.84,0.90** | **0.76**<br>**0.75,0.70,0.76** | **0.80**<br>**0.80,0.78,0.84** |
| $NH_3$ | 0.06<br>0.04,-0.07,0.08 | -0.03<br>-0.14,-0.36,0.11 | **0.73**<br>**0.73**,0.68,**0.74** | **0.73**<br>**0.70**,0.65,**0.77** | **0.70**<br>0.69,0.66,**0.70** | **0.81**<br>**0.81,0.79,0.82** |

Table 3: Maximum hourly surface ozone concentrations and hour of occurrence for the five days shown in Figure 17. Only monitoring sites as part of the CDPHE network are included together with the four mountain sites used before and two additional high altitude sites at Niwot Ridge. Sites are ordered from West to East and only values equal or larger than 70 ppb are shown for NFRMA sites. Values above 75 ppb are highlighted in bold. The start time of the hourly averaging period is listed. NA indicate days with missing observations. Sites close to the Foothills on the western edge of the NFRMA are shown in Italic.

| | 12 Aug | 22 July | 2 Aug | 3 Aug | 8 Aug |
|---|---|---|---|---|---|
| Mines Peak | 71 ppb (19 LT) | **88 ppb (17 LT)** | **77 ppb (20LT)** | **79 ppb (21 LT)** | 54 ppb (5 LT) |
| Trail Ridge | **80 ppb (17 LT)** | **82 ppb (21 LT)** | 71 ppb (21 LT) | 69 ppb (24 LT) | 59 ppb (20 LT) |
| Longs Peak | **78 ppb (16 LT)** | **76 ppb (20 LT)** | 72 ppb (18 LT) | 62 ppb (13 LT) | **75 ppb (18 LT)** |
| Squaw Mtn. | 66 ppb (18 LT) | **86 ppb (16 LT)** | **77 ppb (20 LT)** | **84 ppb (19 LT)** | **78 ppb (17 LT)** |
| Niwot C1 | 73 ppb (16LT) | **80 ppb(18LT)** | 65 ppb (17LT) | 65 ppb (18 LT) | **78 ppb (17 LT)** |
| Niwot TL | **77 ppb (17 LT)** | **NA** | 68 ppb (21 LT) | 72 ppb (21 LT) | **78 ppb (17 LT)** |
| Aspen Park | | **85 ppb (15 LT)** | | | 72 ppb (19 LT) |
| *SBCreek* | | ***89 ppb (18 LT)*** | *73 ppb (16 LT)* | ***75 ppb (15 lT)*** | ***83 ppb (16 LT)*** |
| *Table Mtn* | | ***92 ppb (16 LT)*** | ***77 ppb (17 LT)*** | ***85 ppb (15 LT)*** | ***78 ppb (15 LT)*** |
| Welch | | **87 ppb (15 LT)** | | **76 ppb (14 LT)** | |
| *RF North* | *72 ppb (16LT)* | ***94 ppb (17 LT)*** | ***77 ppb (16 LT)*** | ***83 ppb (14 LT)*** | ***86 ppb (16 LT)*** |
| *FTC West* | ***75 ppb (16LT)*** | ***88 ppb (18 LT)*** | ***77 ppb (16LT)*** | ***81 ppb (15 LT)*** | |
| FTC CSU | 70 ppb (13LT) | **86 ppb (16 LT)** | **77 ppb (15 LT)** | **83 ppb (16 LT)** | |
| *Chatfield* | | ***92 ppb (14 LT)*** | | ***80 ppb (14 LT)*** | |
| LaCasa | | 74 ppb (15 LT) | 70 ppb (16 LT) | **80 ppb (14 LT)** | |
| CAMP | | 71 ppb (14 LT) | | 74 ppb (14 LT) | |
| Welby | | **76 ppb (15 LT)** | | 72 ppb (14 LT) | |
| WC Tower | | | 71 ppb (12 LT) | **84 ppb (14 LT)** | 71 ppb (13 LT) |
| AurEast | | | | | |

Location information for sites not included in Table 1: Niwot C1 40.04N and -105.54W; Niwot TL 40.06N and -105.62W; Aspen Park 39.54N and -105.3W; South Boulder Creek (SBCreek) 39.96N and -105.24W; Table Mtn 40.12N and -105.24W; Welch 39.64N and -105.14W; FTC West 40.59N and -105.14W; Welby 39.84N and -104.95W

Figure 1: Topography of the study region. Light grey dots indicate the four mountain sites used in this study, dark grey dots the 4 sites in the NFRMA used in the analysis of upslope events. White dots indicate other NFRMA spiral sites for the NASA P-3. Site characteristics are listed in Table 1. Additional sites used later in the analysis are indicated by triangles. County lines are shown as solid lines. The Continental Divide stretches along the highest elevation points.

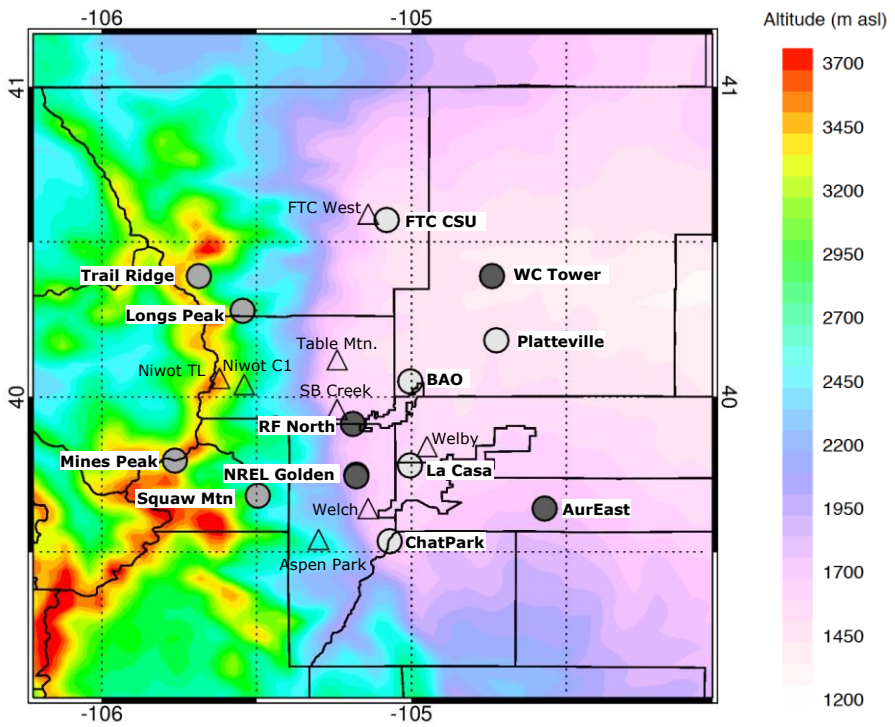

Figure 2: Measured (black) and modeled (red) diurnal cycle for 6am – 6am LT in wind direction (vector average for wind speed > 0.3 m/s ; left) and wind speed (right) for selected surface sites. Shown are mean, median, standard deviation and, for wind speed only, minimum and maximum over the FRAPPÉ time period (15 July – 20 August).

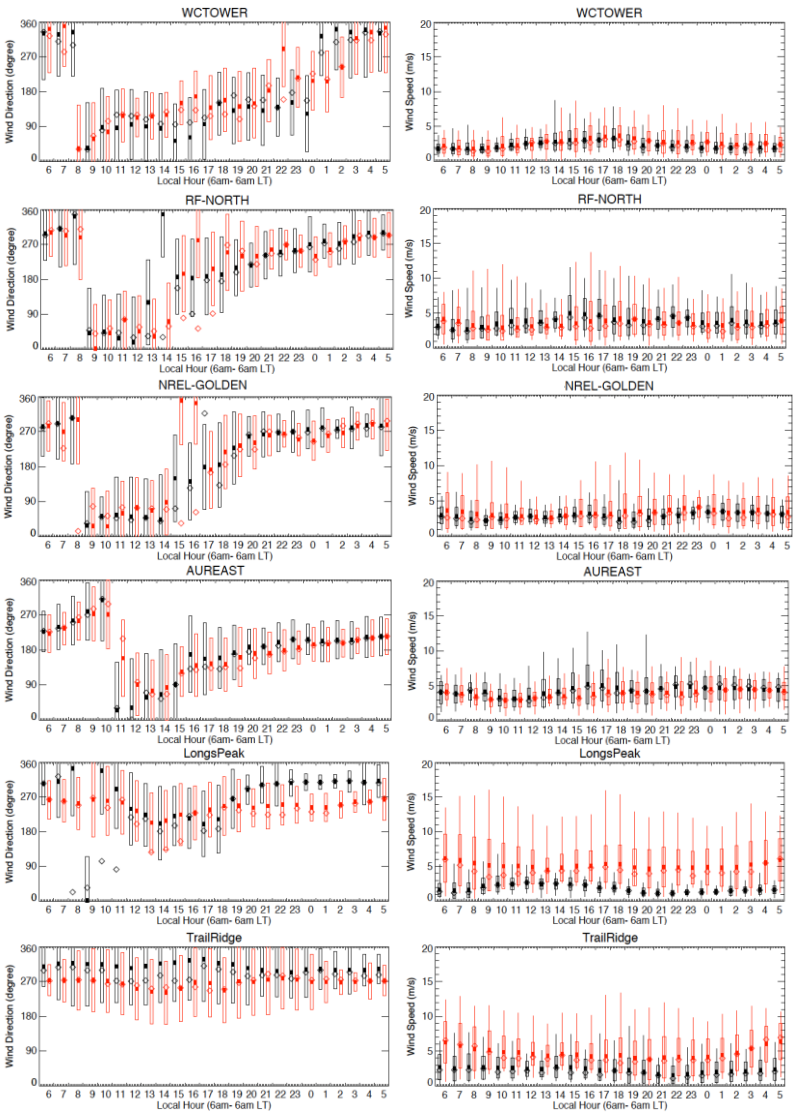

Figure 3: Measured (black) and modeled (red) average wind direction, wind speed, relative humidity and temperature for sonde launches in (a) Platteville (40 sonde launches) and (b) Fort Collins West (40.59N and -105.14W; 12 sonde launches) and (c) windroses for Platteville from surface measurements for 8-12LT and 14-20LT. For averaging the sonde wind direction data only observations with wind speed > 0.3 m/s were considered.

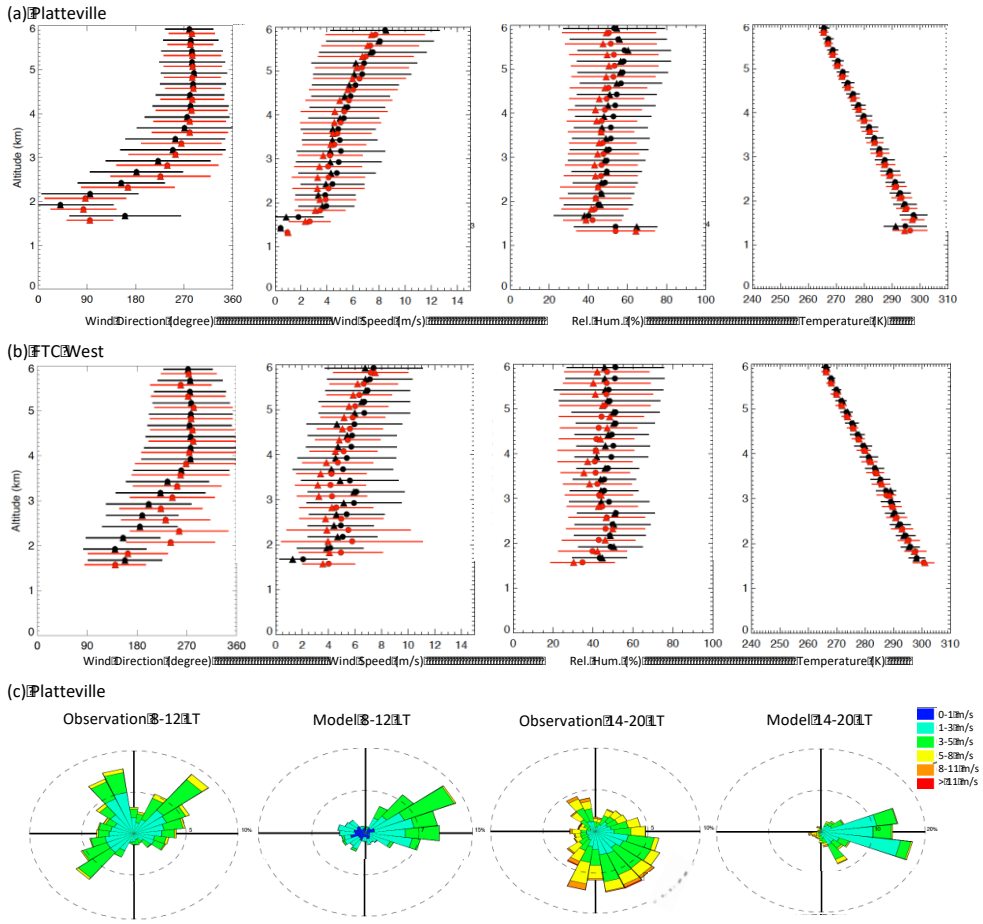

Figure 4: Observed and modeled PBL height for (from top to bottom): Fort Collins West, Platteville and Golden for 19 July – 11 August.

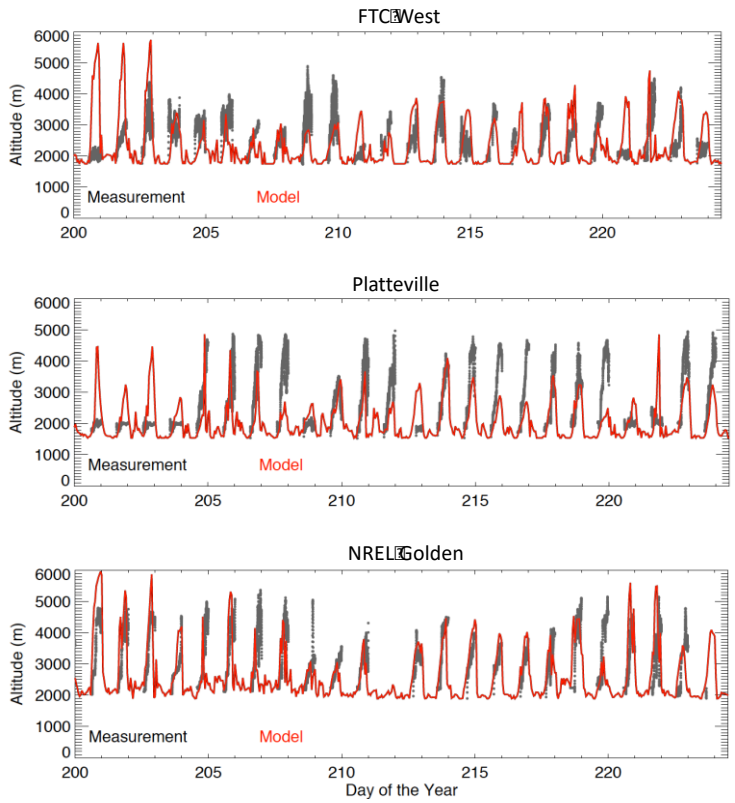


**Formatted:** Font: Times, 12 pt, Font color: Red

Figure 5: Observed NCAR/NSF C-130 $NO_x$ and ethane concentrations and model tracers $TR^{AreaMobile}$ and $TR^{OG}$ averaged over 0.1 deg x 0.1 deg for altitudes < 3 km agl. Averages of observed and model tracer concentrations are calculated for grids with at least 3 data points. The spatial correlation is listed here, as well as in Table 2. Areas above 2500m a.s.l. are shaded in grey.

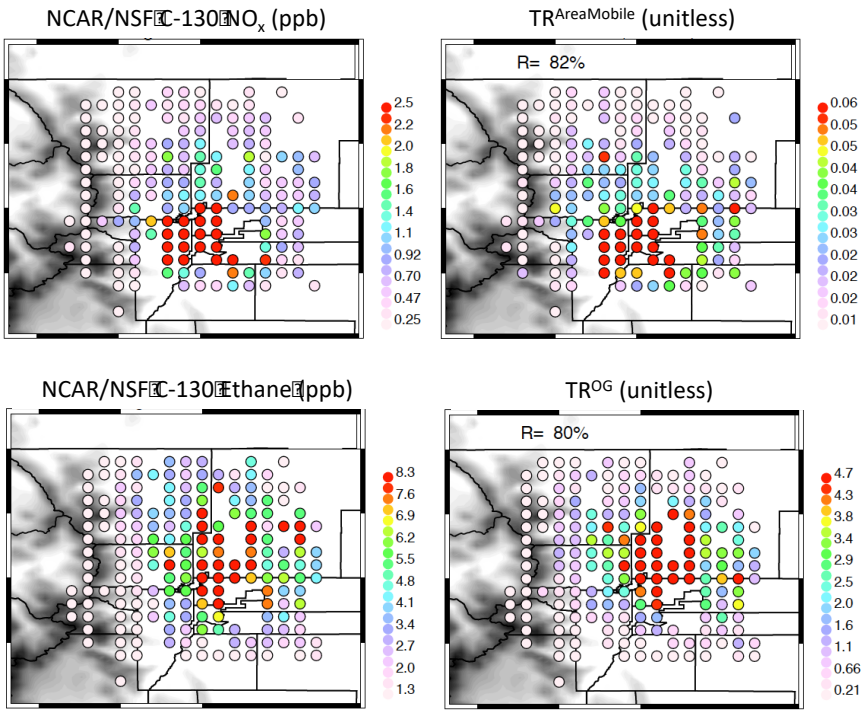

Figure 6: Observed NASA P-3 $NO_x$ and ethane concentrations and model tracers averaged over 0.05 deg x 0.05 deg for altitudes < 3 km agl. Averages of observed and model tracer concentrations are calculated for grids with at least 3 data points. The spatial correlation is listed here, as well as in Table 2. Areas above 2500m a.s.l. are shaded in grey.

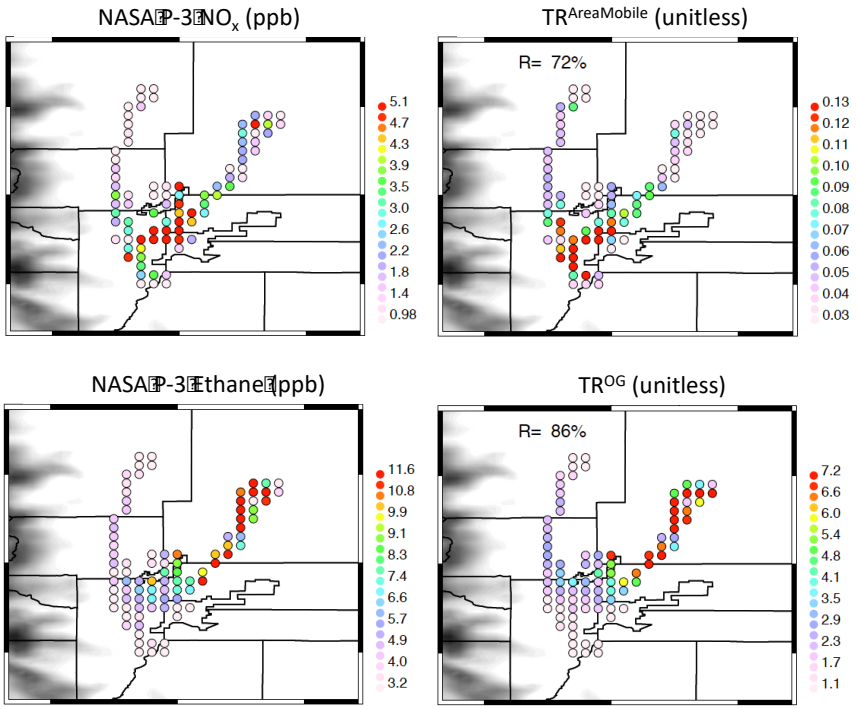

Figure 7: Spatial correlations between measured species and ratios and model tracers for the area/mobile (blue) and OG (red) sources. Big circles represent the average over all flights, small circles represent results for individual flights. Top: NCAR/NSF C130 flights (same spatial coverage as Figure 5); Bottom: NASA P-3 flights. Statistics are derived for data points below 3 km a.g.l. See text for details on the calculation of spatial correlation.

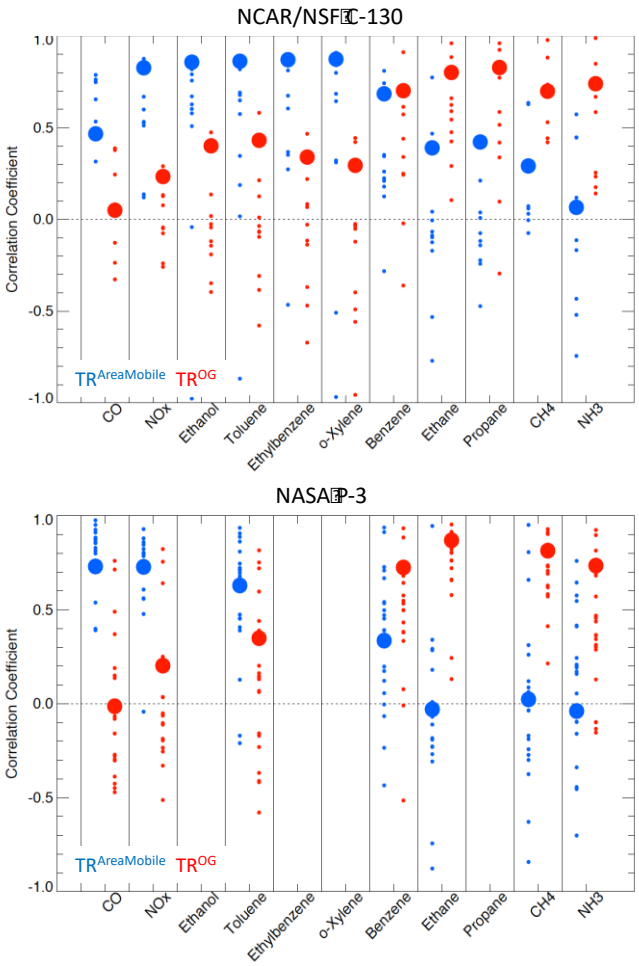

Figure 8: Average spatial tracer distribution (average concentrations within the PBL) for 0-6LT, 6-12LT, 12-18LT and 18-24 LT for the FRAPPÉ time period (14 July to 21 August). Contour lines show the PBL average for $TR^{AreaMobile}$, filled contours show the PBL average $TR^{OG}$ concentrations. Colored points denote the mean ozone measured at surface sites. The tracers are scaled by a common factor and then by their mean ratio ($TR^{AreaMobile} = 60.\bullet TR^{OG}$) to appear on the same scale.

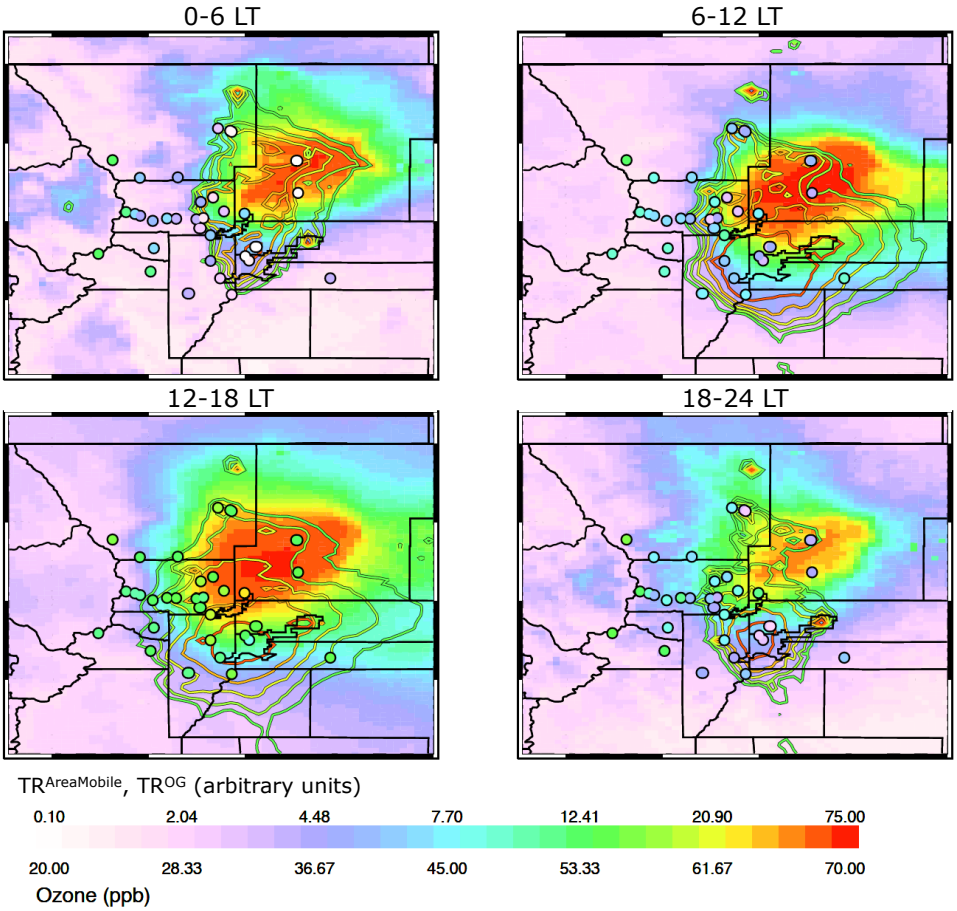

Figure 9: Tracer Statistics for surface sites employed during FRAPPÉ/DAQ for $TR^{AreaMobile}$ (top) and $TR^{OG}$ (bottom). Sites are arranged from West to East and averaged over 10-17 LT (though an average over all times would not look vastly different). Sites focused on in the analysis of upslope events are colored in red. Shown are mean (dot), median (triangle), standard deviation (horizontal bars), 10th and 90th percentiles (thick line), minima and maxima (thin lines). In addition to sites shown in Figure 1 we also added sites in the Global Ozone (GO3) project (Black Hawk, Lyons, East Boulder and Longmont) as well as additional sites from the CDPHE network (I-25 Denver, CAMP).

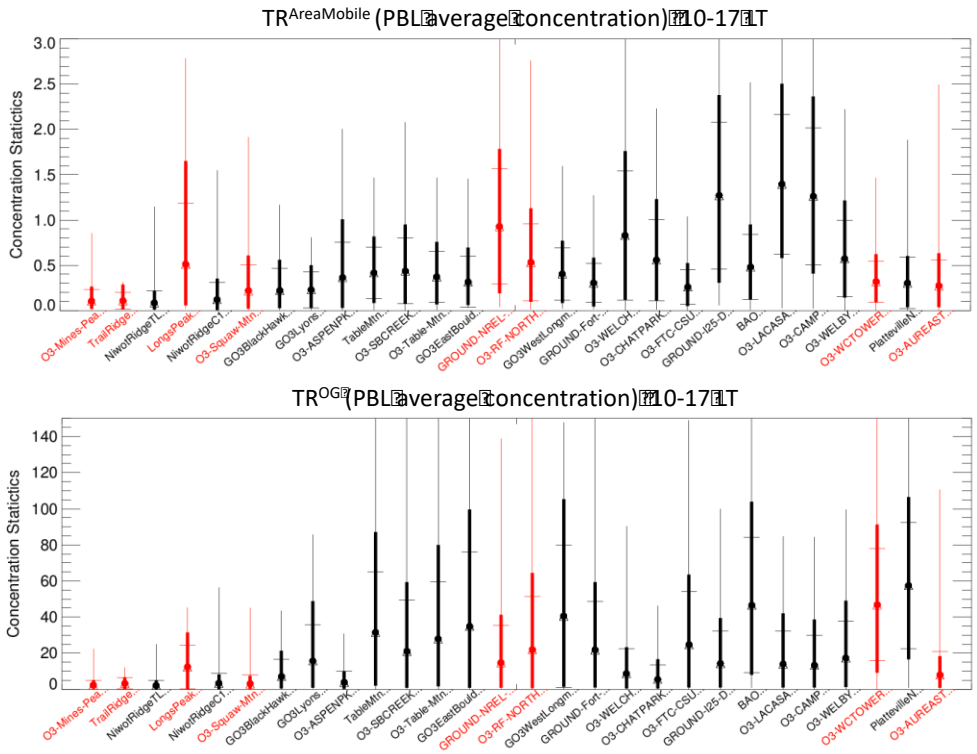

Figure 10: Average diurnal observed surface ozone (black) and PBLH average $TR^{OG}$ (red) and $TR^{AreaMobile}$ (blue) for selected surface sites in the Front Range for 6am – 6am LT. Shown are mean, median, standard deviation, minimum and maximum. A line is drawn though the mean values.

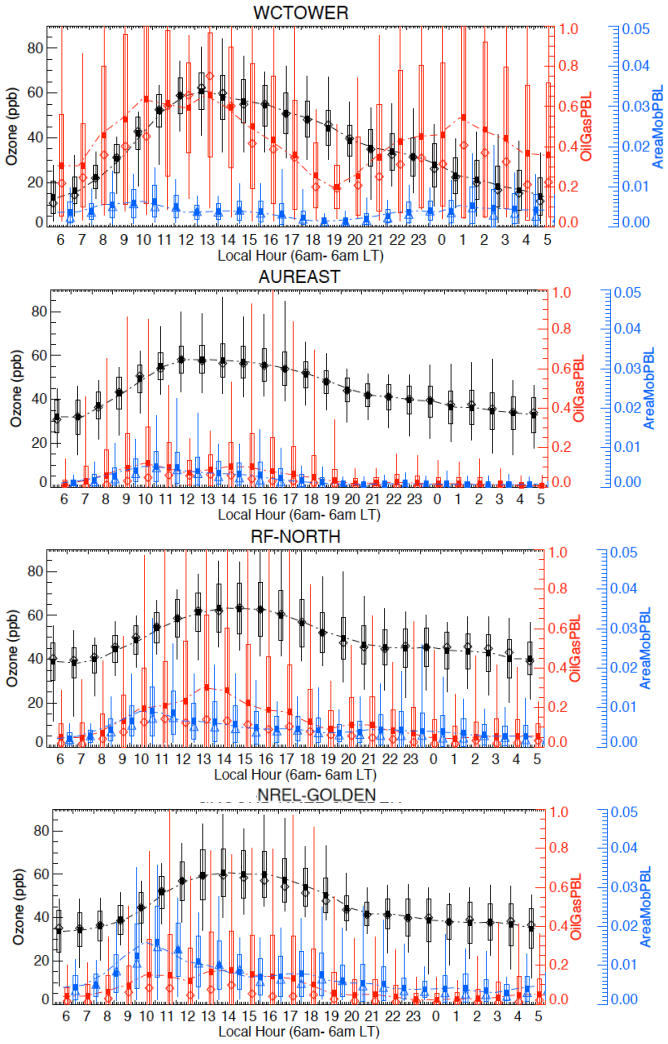

Figure 11: As Figure 10 but for selected surface sites in the mountains. Note the y-scale is reduced to half of the one used in Figure 10.

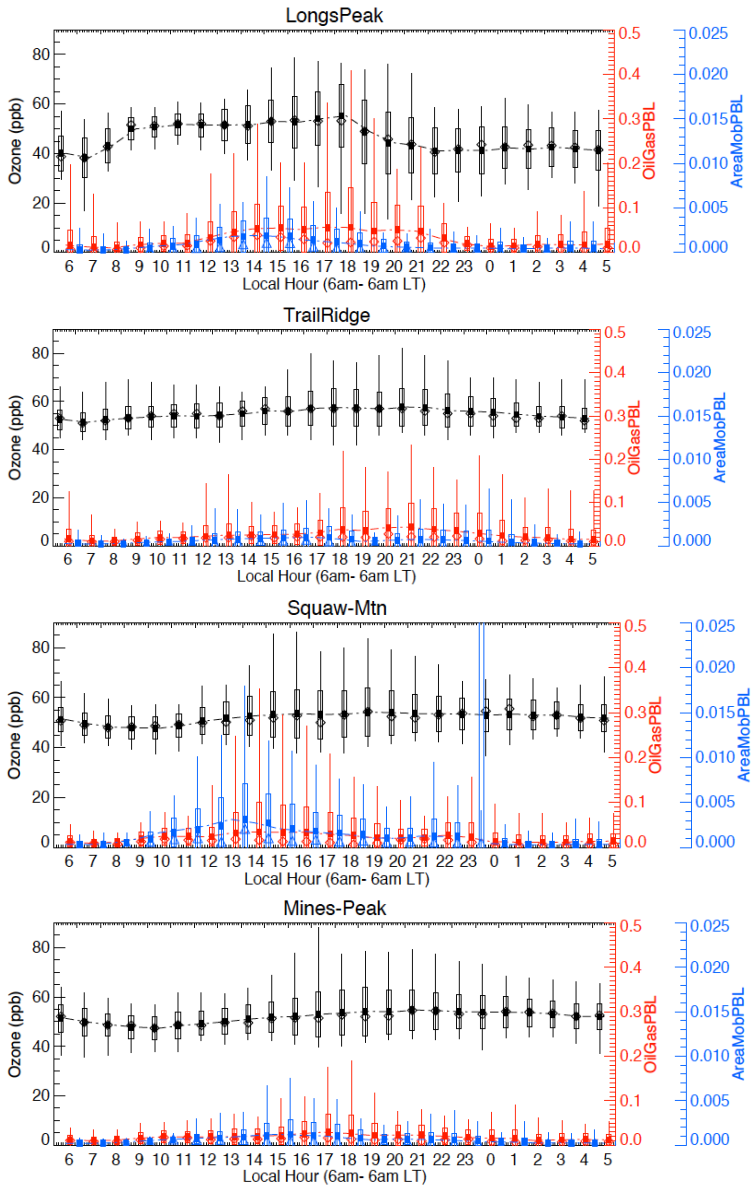

Figure 12: Upslope (red) and Downslope (black) statistics from observations (solid lines) and WRF (dotted lined). Flow is defined when winds are from within a defined wind sector at least 2/3rd of the time within a given hour (Note that wind data for Trail Ridge Road are available hourly only and that model data are also only available on an hourly basis). Upslope: Upslope Angle ±45deg; Downslope: 270±45deg; only data with wind speeds > 0.3 m/s (i.e. data that are not defined calm based on Beaufort scale). The upslope angle has been defined based on windrose analysis. The frequency is given as percentage of upslope or downslope of all valid measurements.

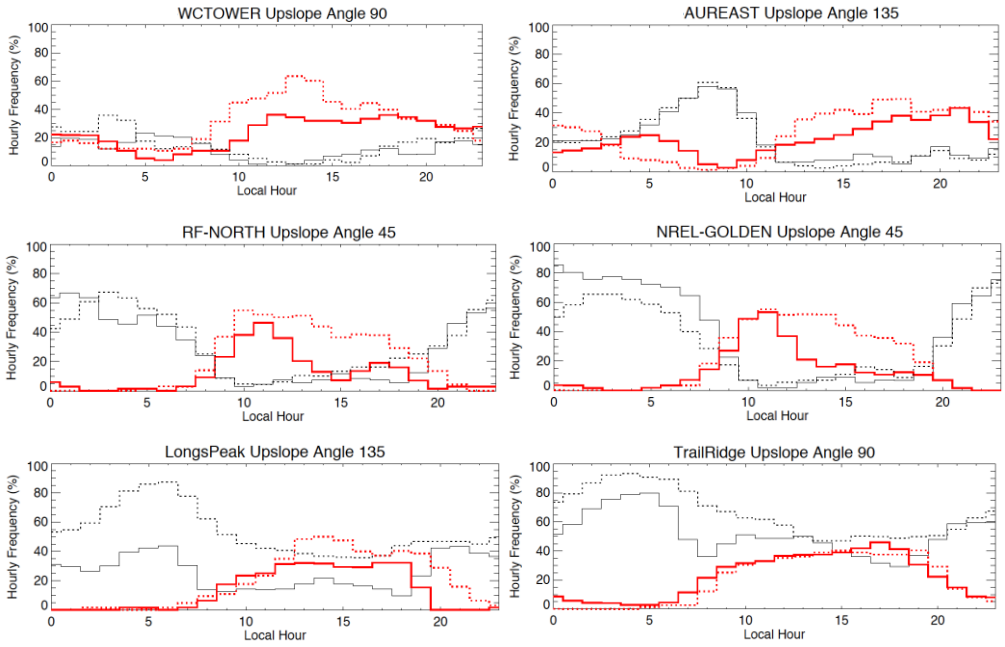

Figure 13: Ozone and Tracer roses for (a) Longs Peak (1-minute data) and (b) Trail Ridge road (hourly data) on days when RF North 12-18LT average ozone was > 70 ppb ("RF North HIGH") or < 60 ppb ("RF North LOW"). Only data for 12-20LT are shown.

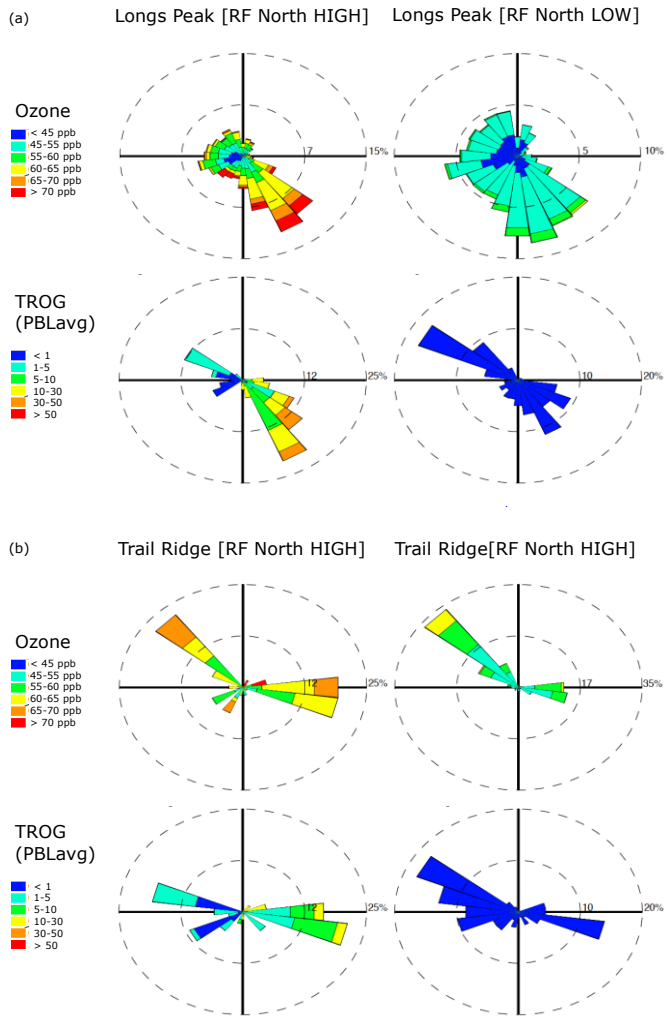

Figure 14: NCAR/NSF C-130 measured ethane and NOx (top row) and modeled TROG and TRAreaMobile (bottom row) for the the upslope part of the 12 August flight (after refueling). All data averaged over 0-2km ag and a 0.1 deg x 01 deg grid. The vector averaged measured and modeled winds for each grid point are shown by the windbarbs and the monitoring sites RF North, NREL Golden, WC Tower, Aurora East and Golden are indicated by diamond symbols. Areas above 2500m a.s.l. are shaded in grey.

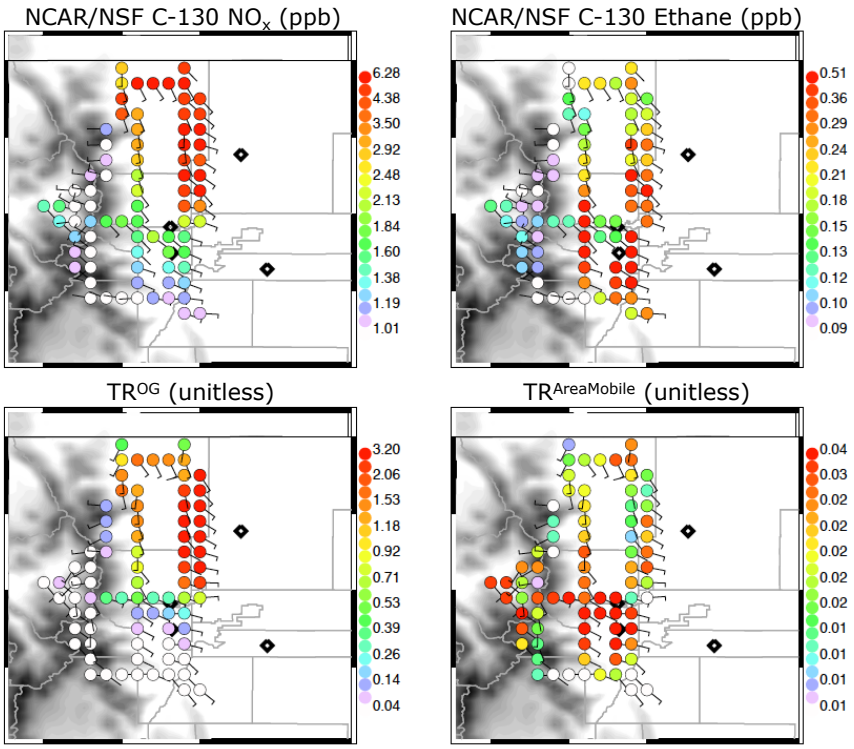

Figure 15: as Figure 10 but for 12 August 2014 and for mountain sites only. Lines show the average diurnal cycle from Figure 11.

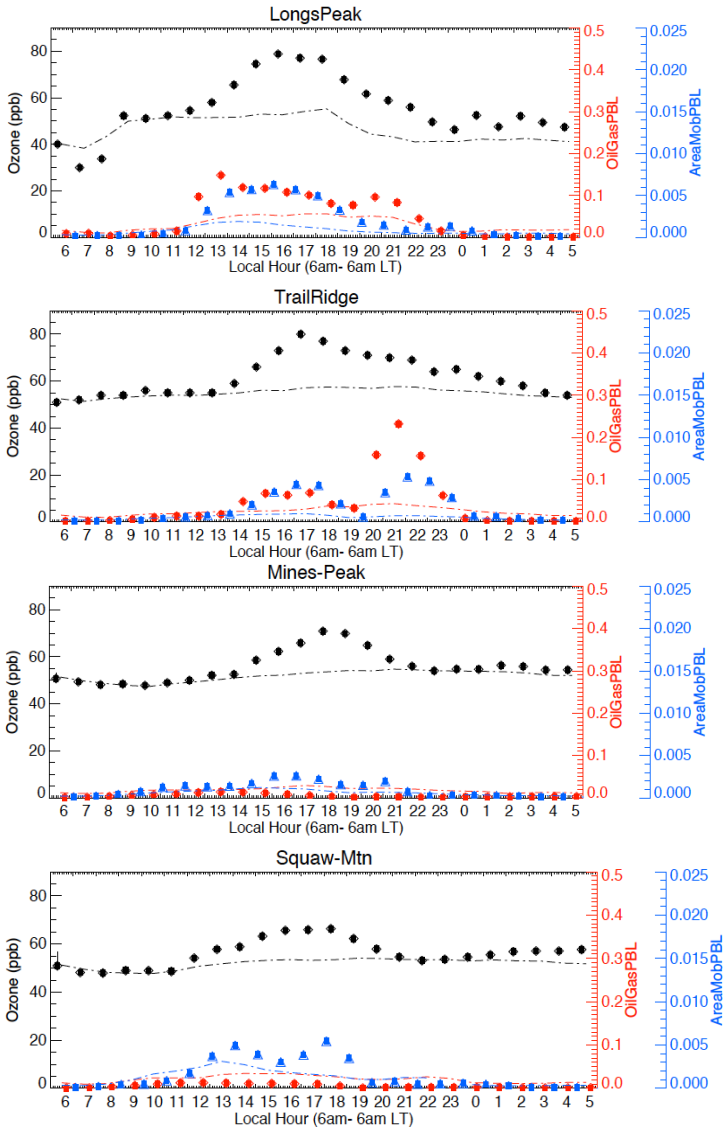

Figure 16: Longitude-Altitude Cross Section of $TR^{OG}$ at 40.09N (single grid box in latitude) for 12 August 22 UTC (16 LT, top) and 13 August 2 UTC (12 August 20 LT, bottom); The location of the Granby airport is indicated by the black dot. Horizontal winds are indicated by black arrows, vertical winds are shown as white arrows. For clarity, only vertical winds > 0.2m/s are included. The height of the PBLH is plotted as a black line.

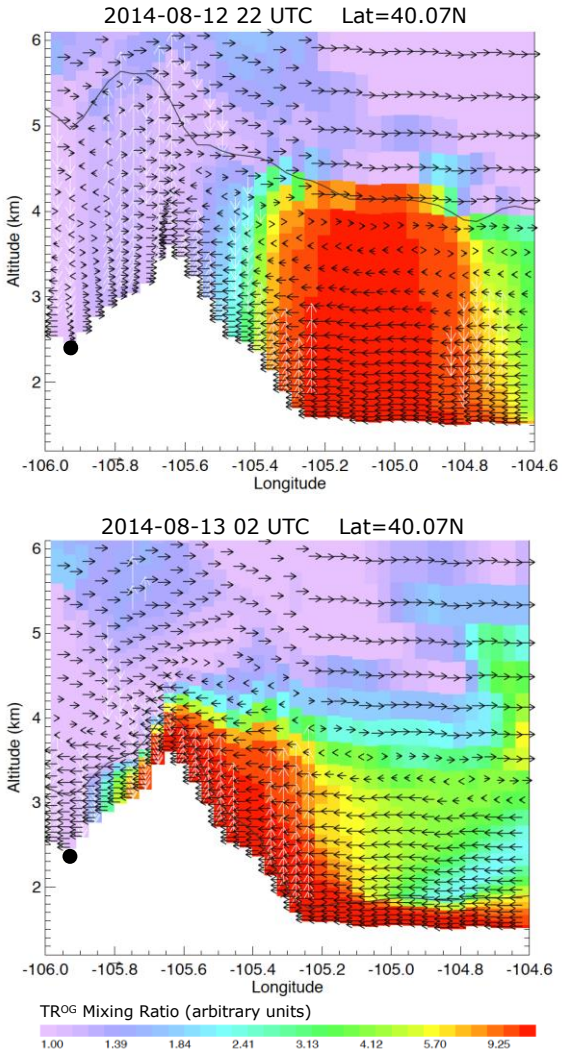

Figure 17: as Figure 8 but for 14-20 LT. Top row: average over FRAPPÉ period and 12 August; middle row: 22 July and 2 August; bottom row: 3 and 8 August.

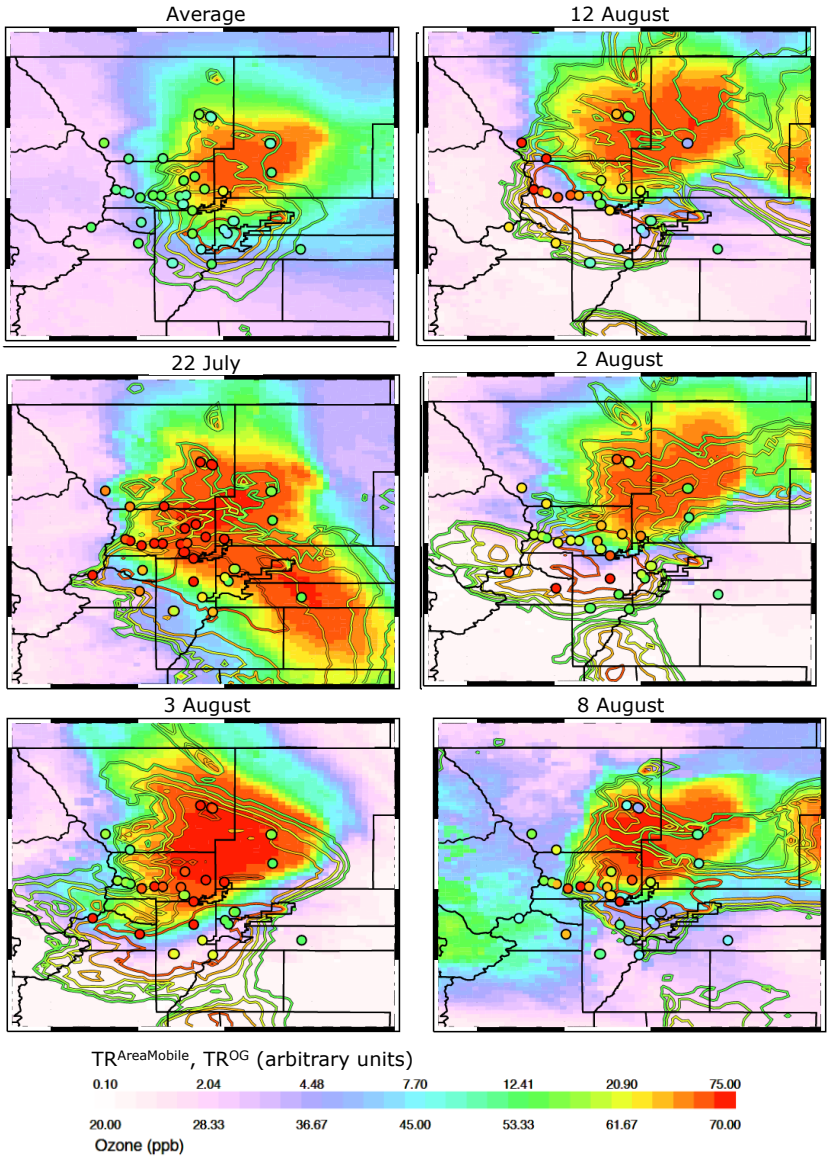

**Figure 1.**

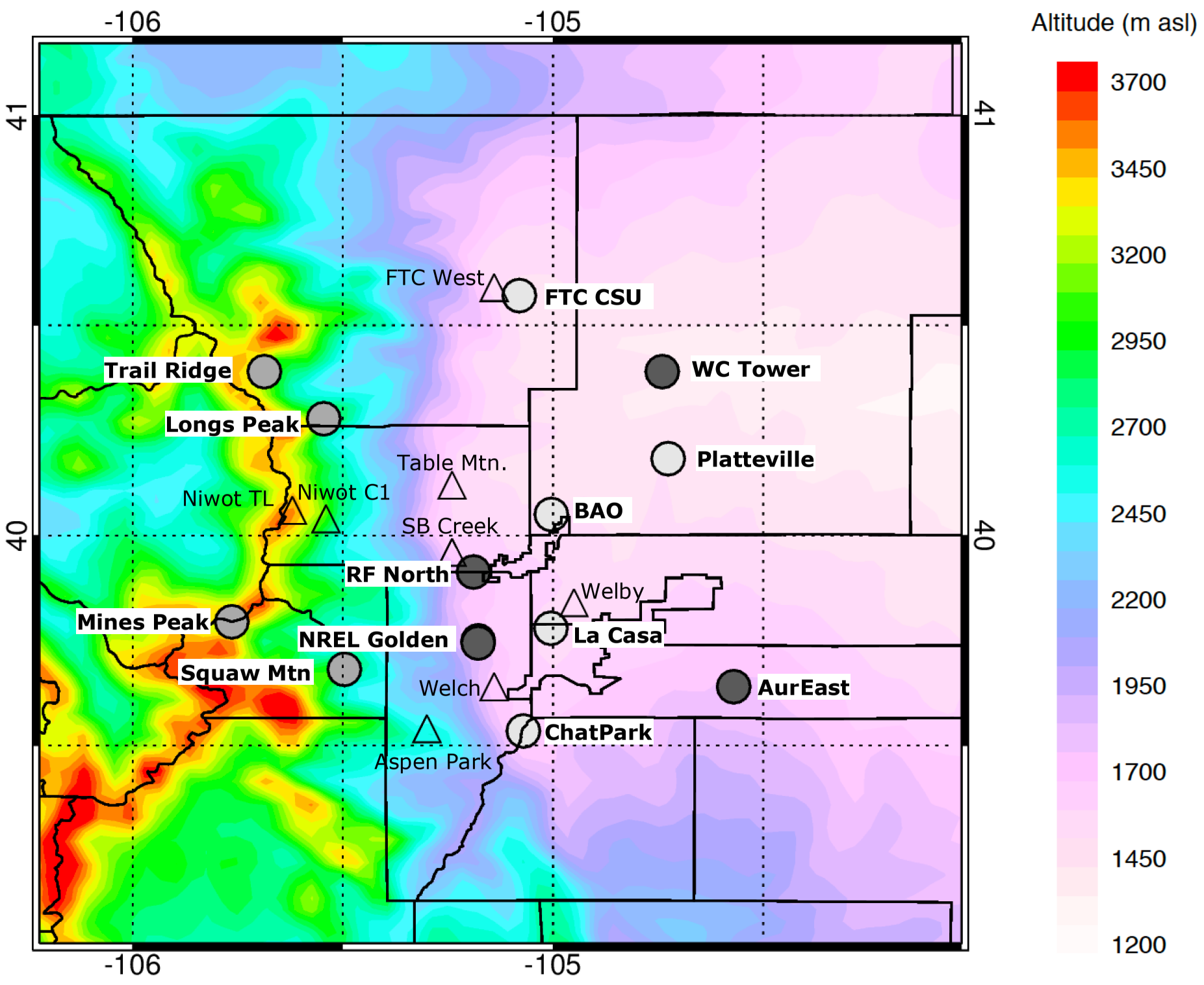
-106
-105
41
40
Altitude (m asl)
3700
3450
3200
2950
2700
2450
2200
1950
1700
1450
1200
FTC West
FTC CSU
Trail Ridge
WC Tower
Longs Peak
Platteville
Table Mtn.
Niwot TL
Niwot C1
BAO
SB Creek
RF North
Welby
Mines Peak
NREL Golden
La Casa
Squaw Mtn
Welch
AurEast
ChatPark
Aspen Park

**Figure 2.**

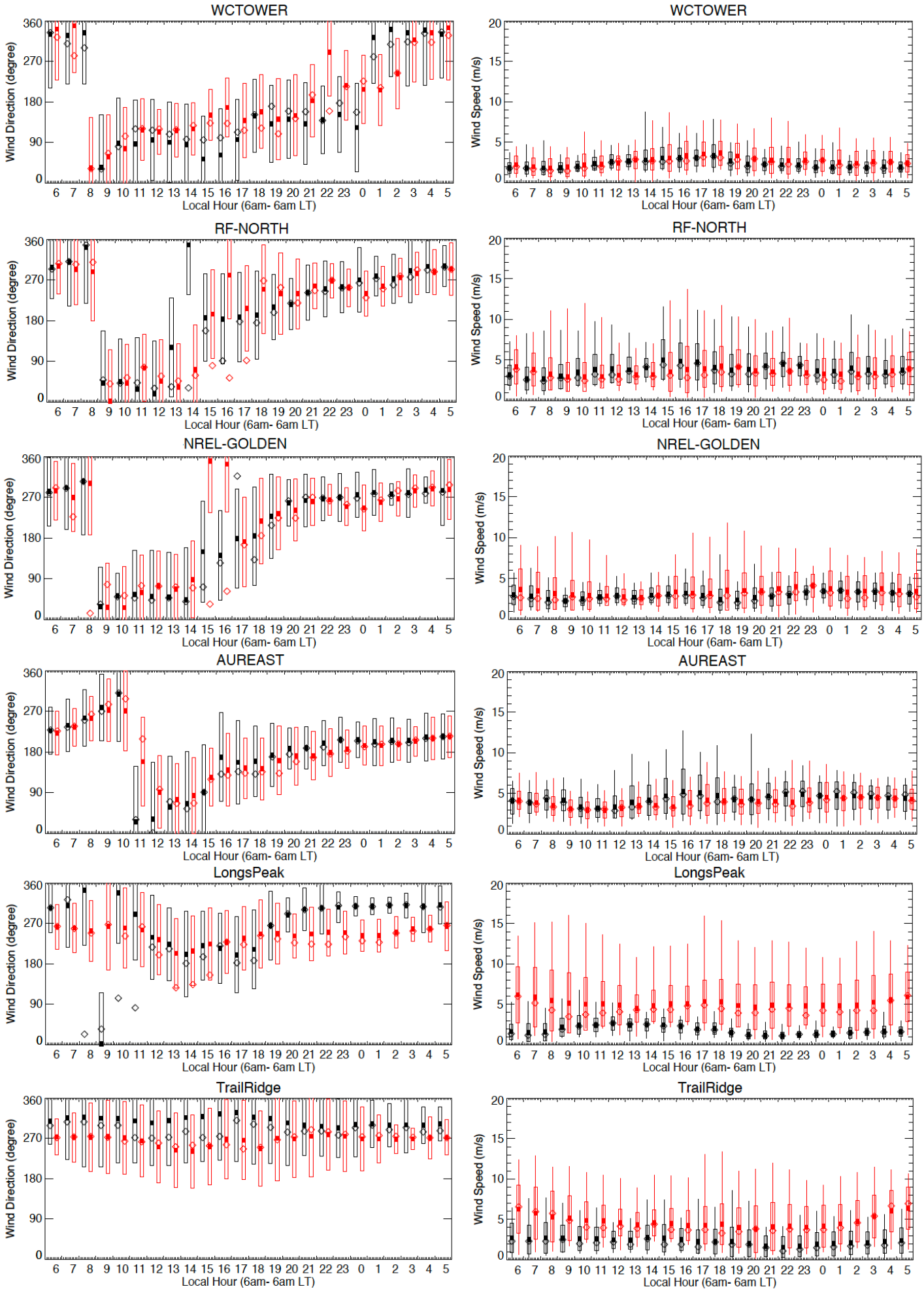
WCTOWER
Wind Direction (degree)
Wind Speed (m/s)
RF-NORTH
NREL-GOLDEN
AUREAST
LongsPeak
TrailRidge
Local Hour (6am- 6am LT)

**Figure 3.**

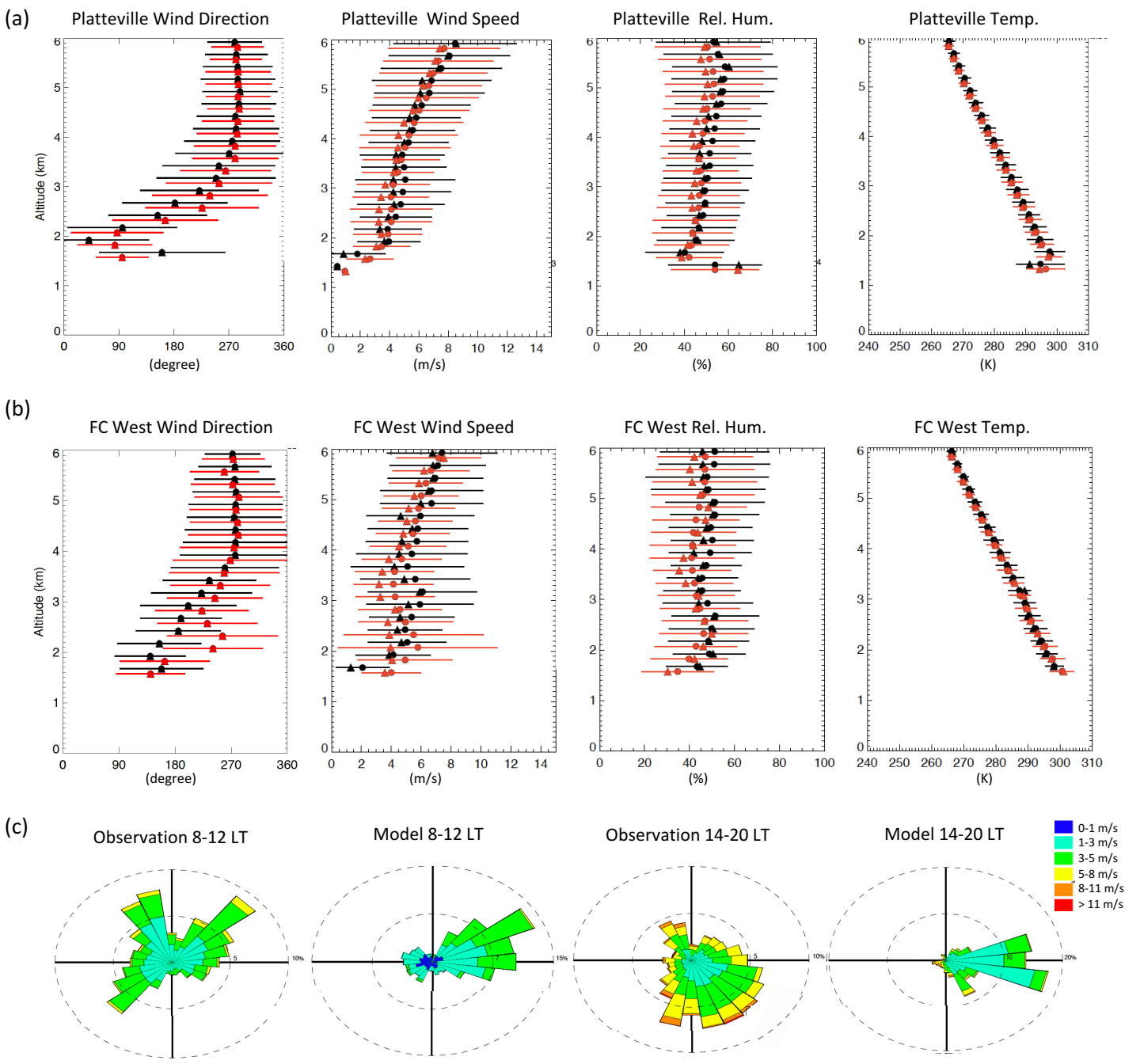
(a)
Platteville Wind Direction
Platteville Wind Speed
Platteville Rel. Hum.
Platteville Temp.
Altitude (km)
(degree)
(m/s)
(%)
(K)
(b)
FC West Wind Direction
FC West Wind Speed
FC West Rel. Hum.
FC West Temp.
Altitude (km)
(degree)
(m/s)
(%)
(K)
(c)
Observation 8-12 LT
Model 8-12 LT
Observation 14-20 LT
Model 14-20 LT
0-1 m/s
1-3 m/s
3-5 m/s
5-8 m/s
8-11 m/s
> 11 m/s

**Figure 4.**

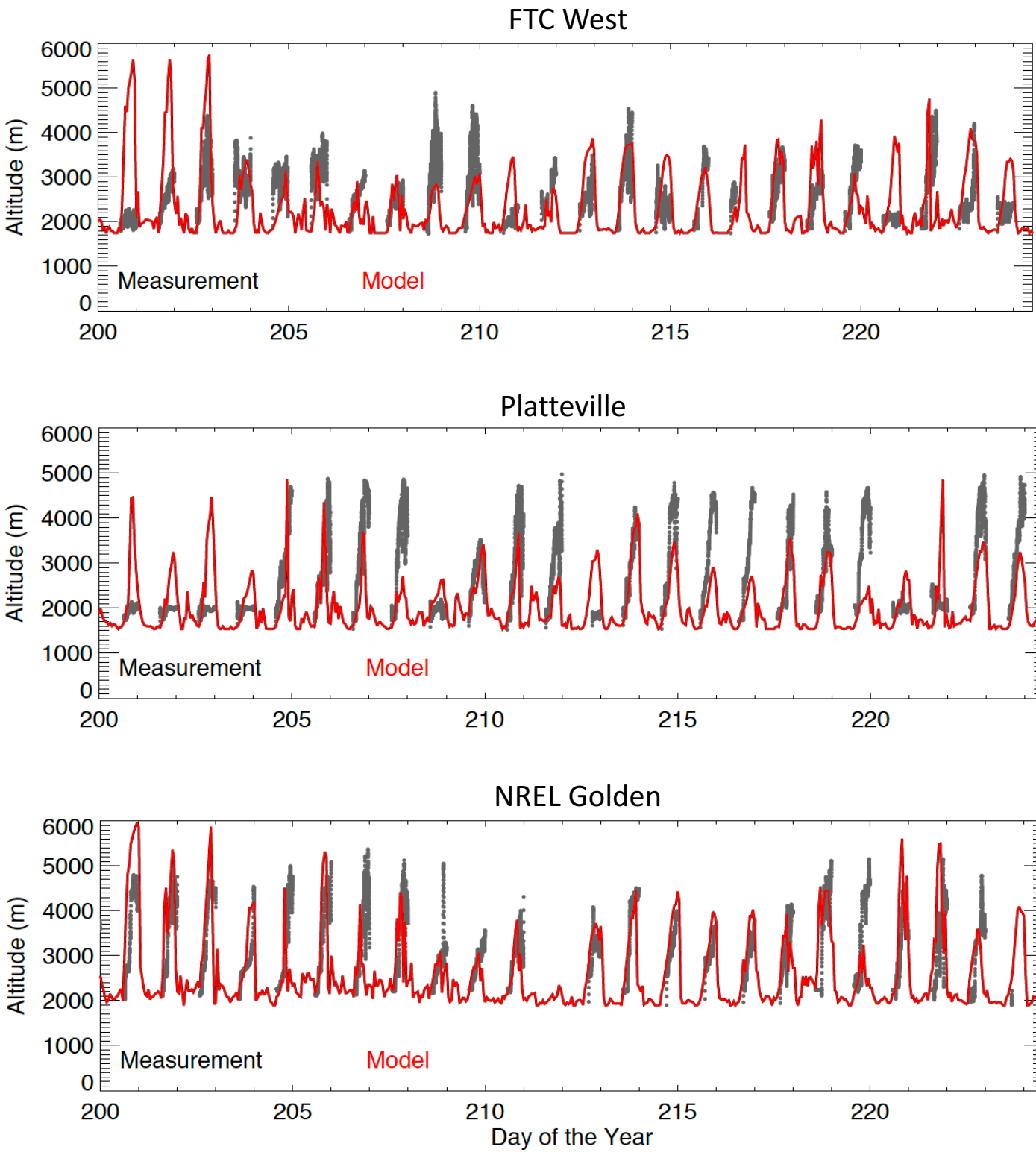
FTC West
Platteville
NREL Golden
Altitude (m)
6000
5000
4000
3000
2000
1000
0
Measurement
Model
200
205
210
215
220
Day of the Year

**Figure 5.**

NCAR/NSF C-130 $NO_x$ (ppb)

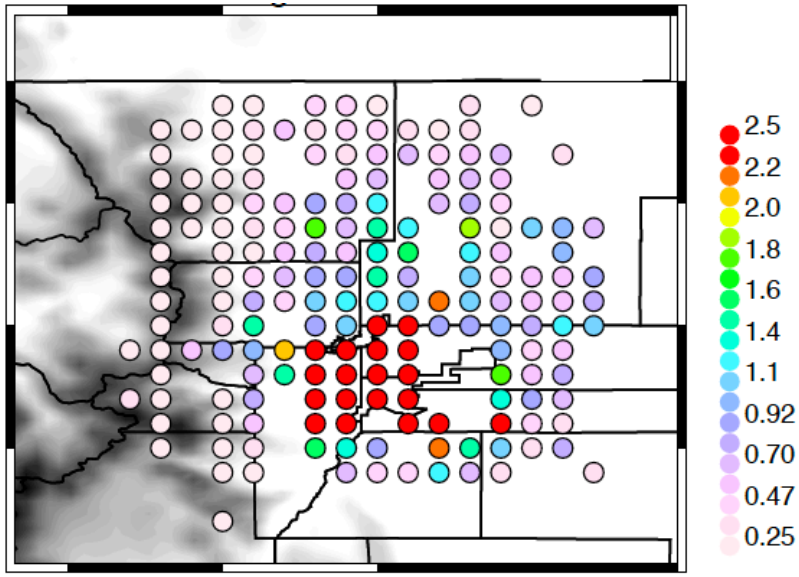


$TR^{AreaMobile}$ (unitless)

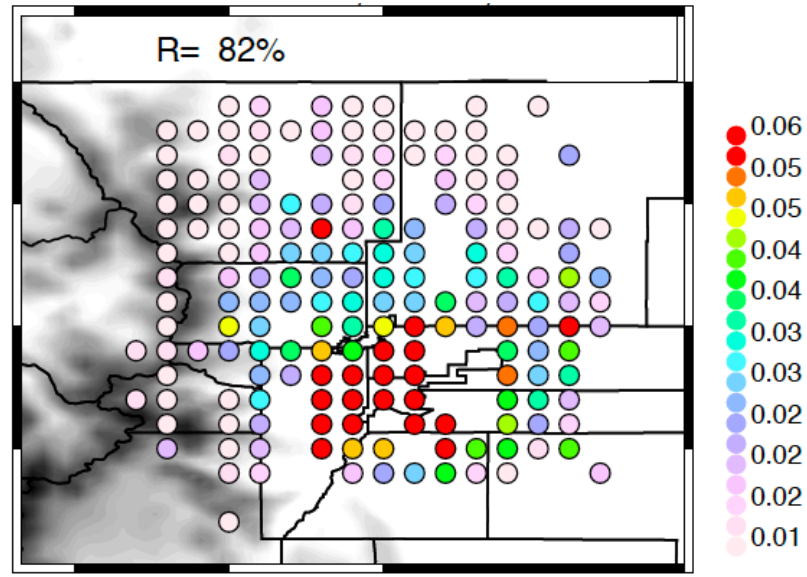


NCAR/NSF C-130 Ethane (ppb)

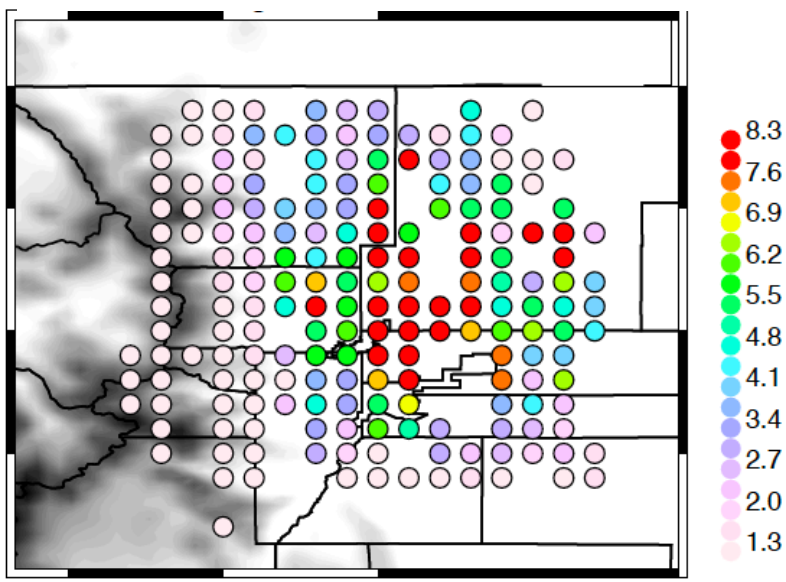


$TR^{OG}$ (unitless)

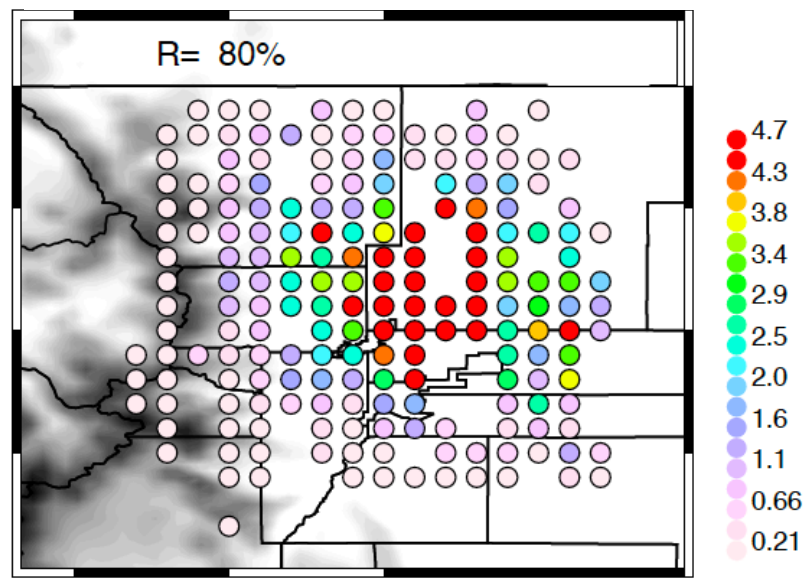

**Figure 6.**

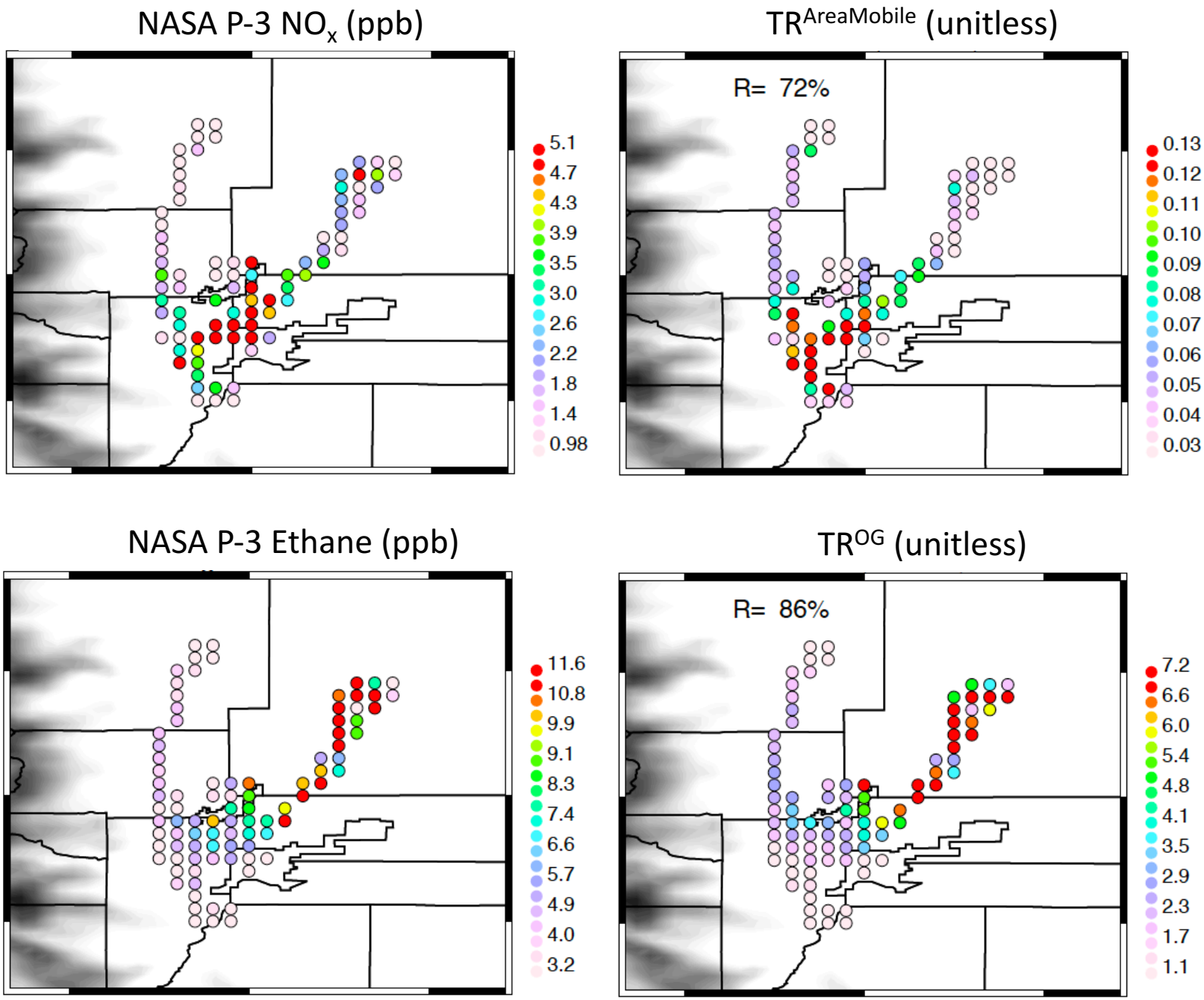
NASA P-3 $NO_x$ (ppb)
5.1
4.7
4.3
3.9
3.5
3.0
2.6
2.2
1.8
1.4
0.98
$TR^{AreaMobile}$ (unitless)
R= 72%
0.13
0.12
0.11
0.10
0.09
0.08
0.07
0.06
0.05
0.04
0.03
NASA P-3 Ethane (ppb)
11.6
10.8
9.9
9.1
8.3
7.4
6.6
5.7
4.9
4.0
3.2
$TR^{OG}$ (unitless)
R= 86%
7.2
6.6
6.0
5.4
4.8
4.1
3.5
2.9
2.3
1.7
1.1

**Figure 7.**

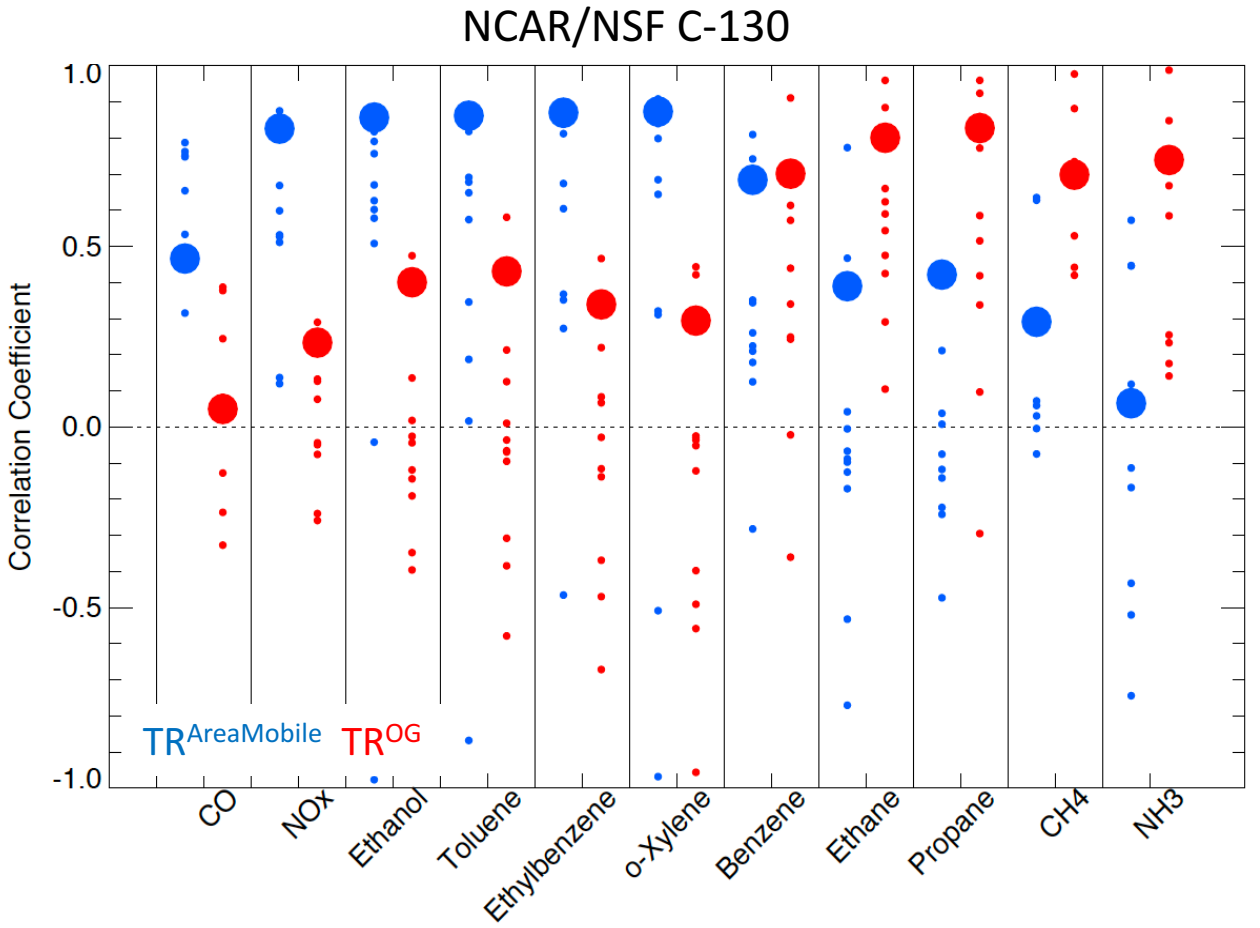
NCAR/NSF C-130
Correlation Coefficient
1.0
0.5
0.0
-0.5
-1.0
TR^AreaMobile
TR^OG
CO
NOx
Ethanol
Toluene
Ethylbenzene
o-Xylene
Benzene
Ethane
Propane
CH4
NH3

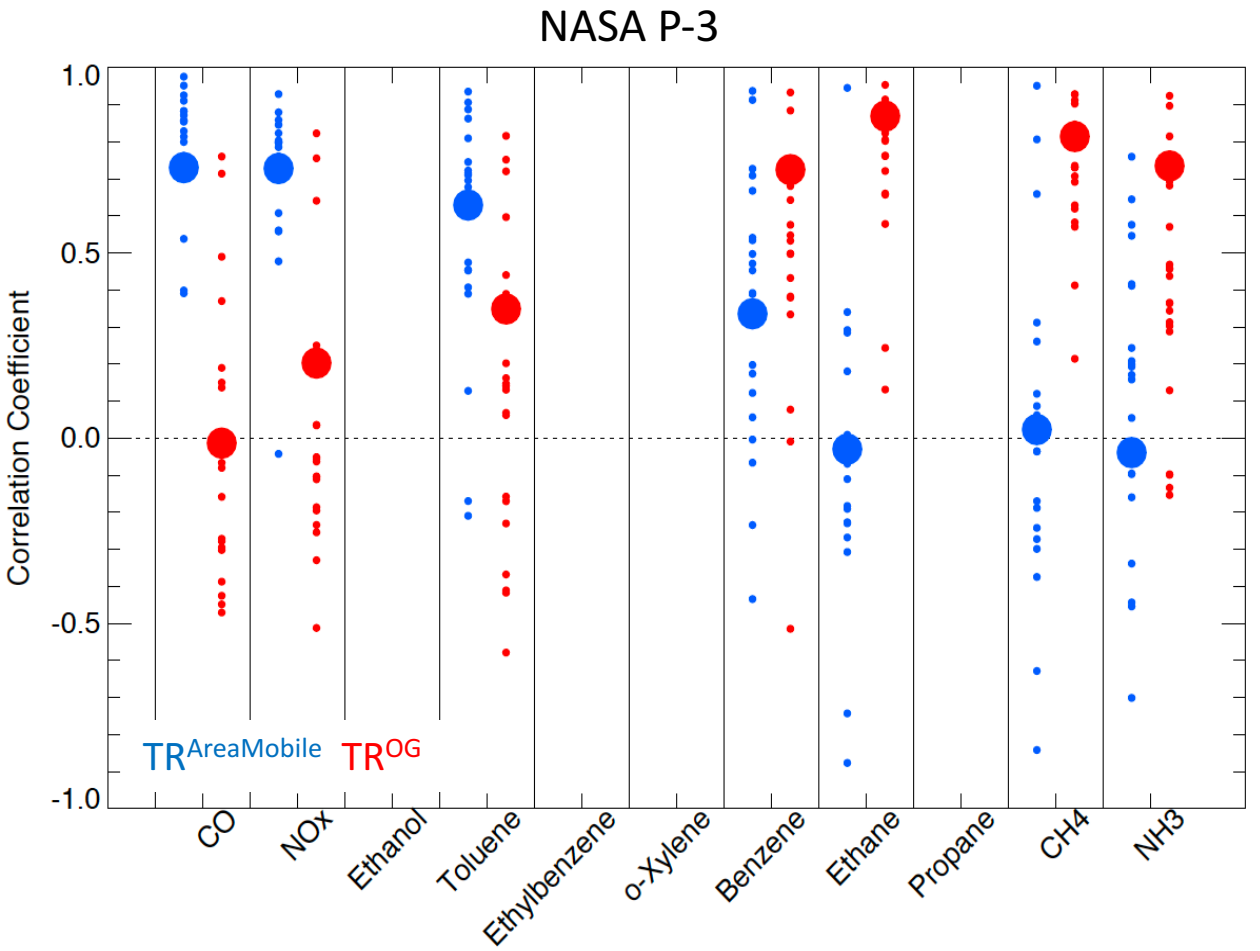
NASA P-3
Correlation Coefficient
1.0
0.5
0.0
-0.5
-1.0
TR^AreaMobile
TR^OG
CO
NOx
Ethanol
Toluene
Ethylbenzene
o-Xylene
Benzene
Ethane
Propane
CH4
NH3

**Figure 8.**

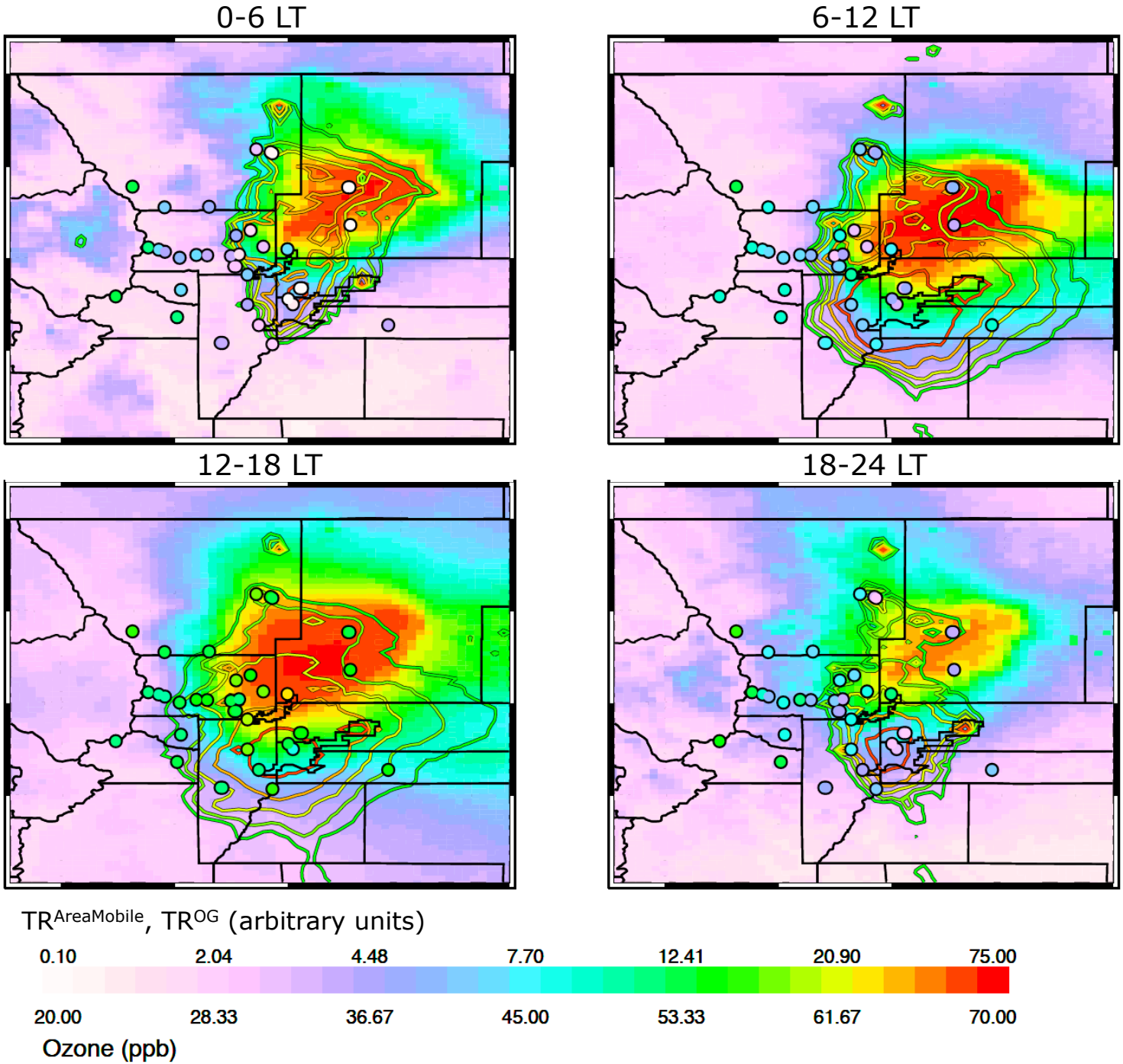
0-6 LT
6-12 LT
12-18 LT
18-24 LT
TR^AreaMobile, TR^OG (arbitrary units)
0.10
2.04
4.48
7.70
12.41
20.90
75.00
20.00
28.33
36.67
45.00
53.33
61.67
70.00
Ozone (ppb)

**Figure 9.**

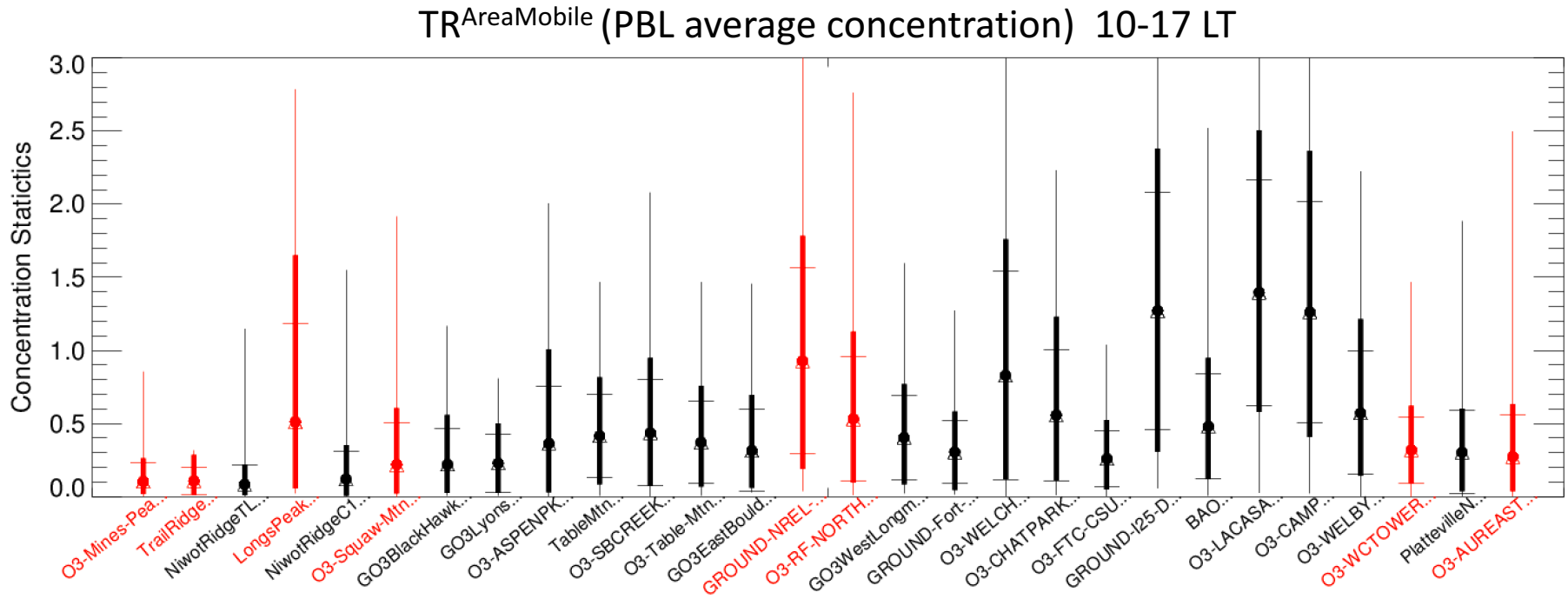
TR^AreaMobile (PBL average concentration) 10-17 LT
Concentration Statictics
3.0
2.5
2.0
1.5
1.0
0.5
0.0
O3-Mines-Pea...
TrailRidge...
NiwotRidgeTL...
LongsPeak...
NiwotRidgeC1...
O3-Squaw-Mtn...
GO3BlackHawk...
GO3Lyons...
O3-ASPENPK...
TableMtn...
O3-SBCREEK...
O3-Table-Mtn...
GO3EastBould...
GROUND-NREL-...
O3-RF-NORTH...
GO3WestLongm...
GROUND-Fort-...
O3-WELCH...
O3-CHATPARK...
O3-FTC-CSU...
GROUND-I25-D...
BAO...
O3-LACASA...
O3-CAMP...
O3-WELBY...
O3-WCTOWER...
PlattevilleN...
O3-AUREAST...

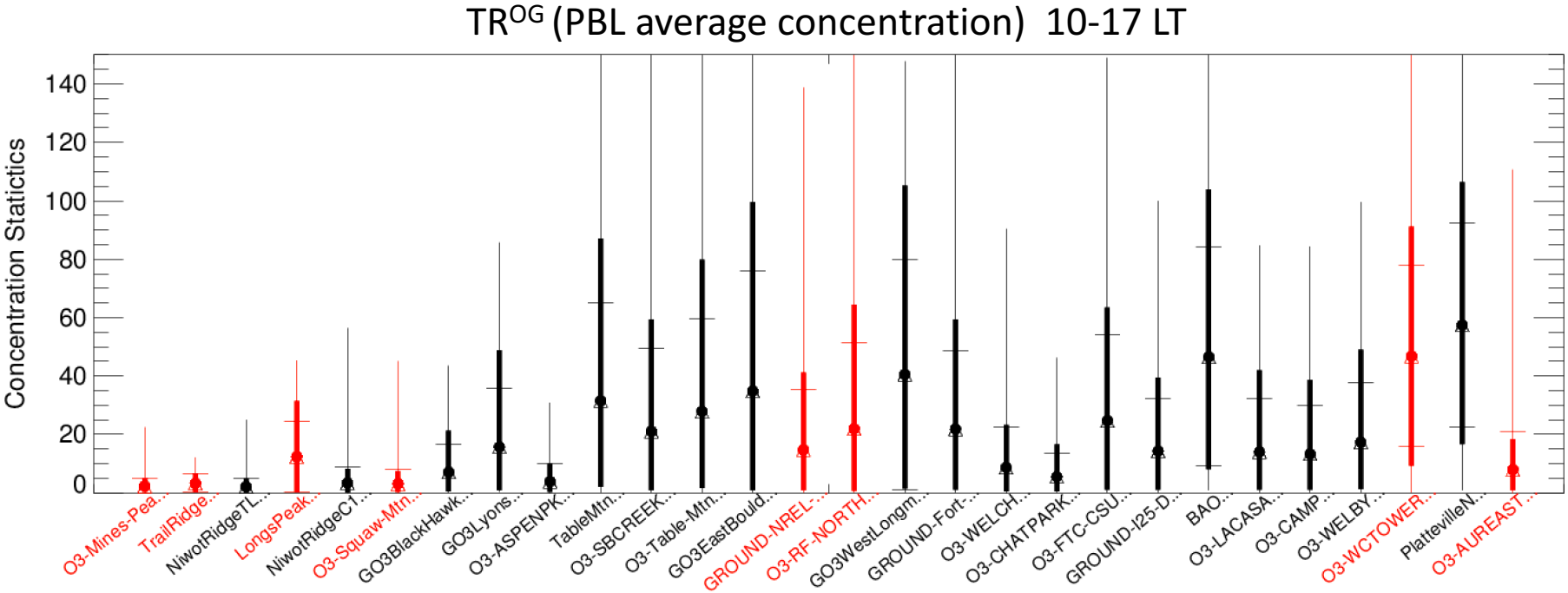
TR^OG (PBL average concentration) 10-17 LT
Concentration Statictics
140
120
100
80
60
40
20
0
O3-Mines-Pea...
TrailRidge...
NiwotRidgeTL...
LongsPeak...
NiwotRidgeC1...
O3-Squaw-Mtn...
GO3BlackHawk...
GO3Lyons...
O3-ASPENPK...
TableMtn...
O3-SBCREEK...
O3-Table-Mtn...
GO3EastBould...
GROUND-NREL-...
O3-RF-NORTH...
GO3WestLongm...
GROUND-Fort-...
O3-WELCH...
O3-CHATPARK...
O3-FTC-CSU...
GROUND-I25-D...
BAO...
O3-LACASA...
O3-CAMP...
O3-WELBY...
O3-WCTOWER...
PlattevilleN...
O3-AUREAST...

**Figure 10.**

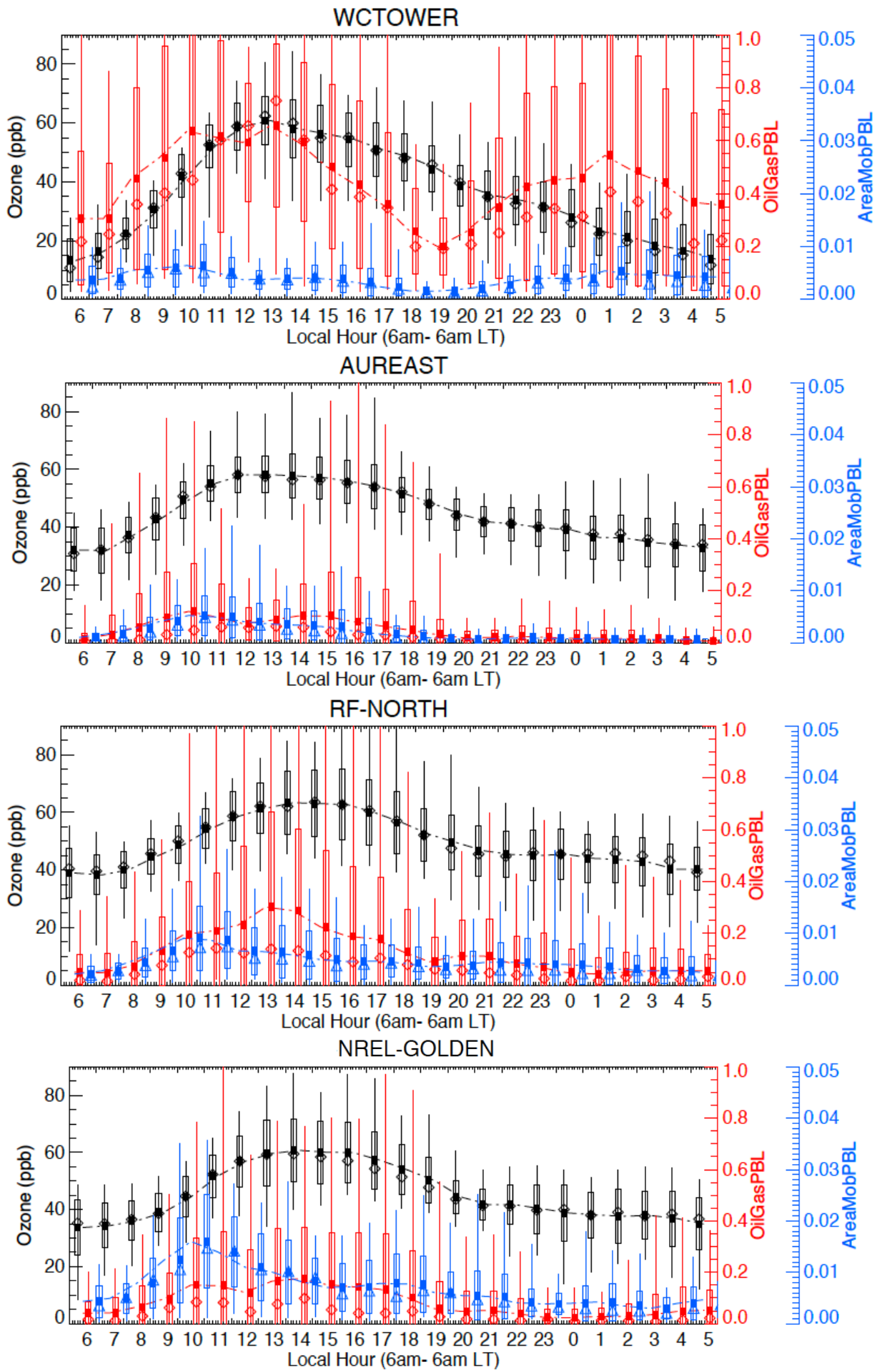
WCTOWER
AUREAST
RF-NORTH
NREL-GOLDEN
Ozone (ppb)
OilGasPBL
AreaMobPBL
Local Hour (6am- 6am LT)
0
20
40
60
80
0.0
0.2
0.4
0.6
0.8
1.0
0.00
0.01
0.02
0.03
0.04
0.05
6 7 8 9 10 11 12 13 14 15 16 17 18 19 20 21 22 23 0 1 2 3 4 5

**Figure 11.**

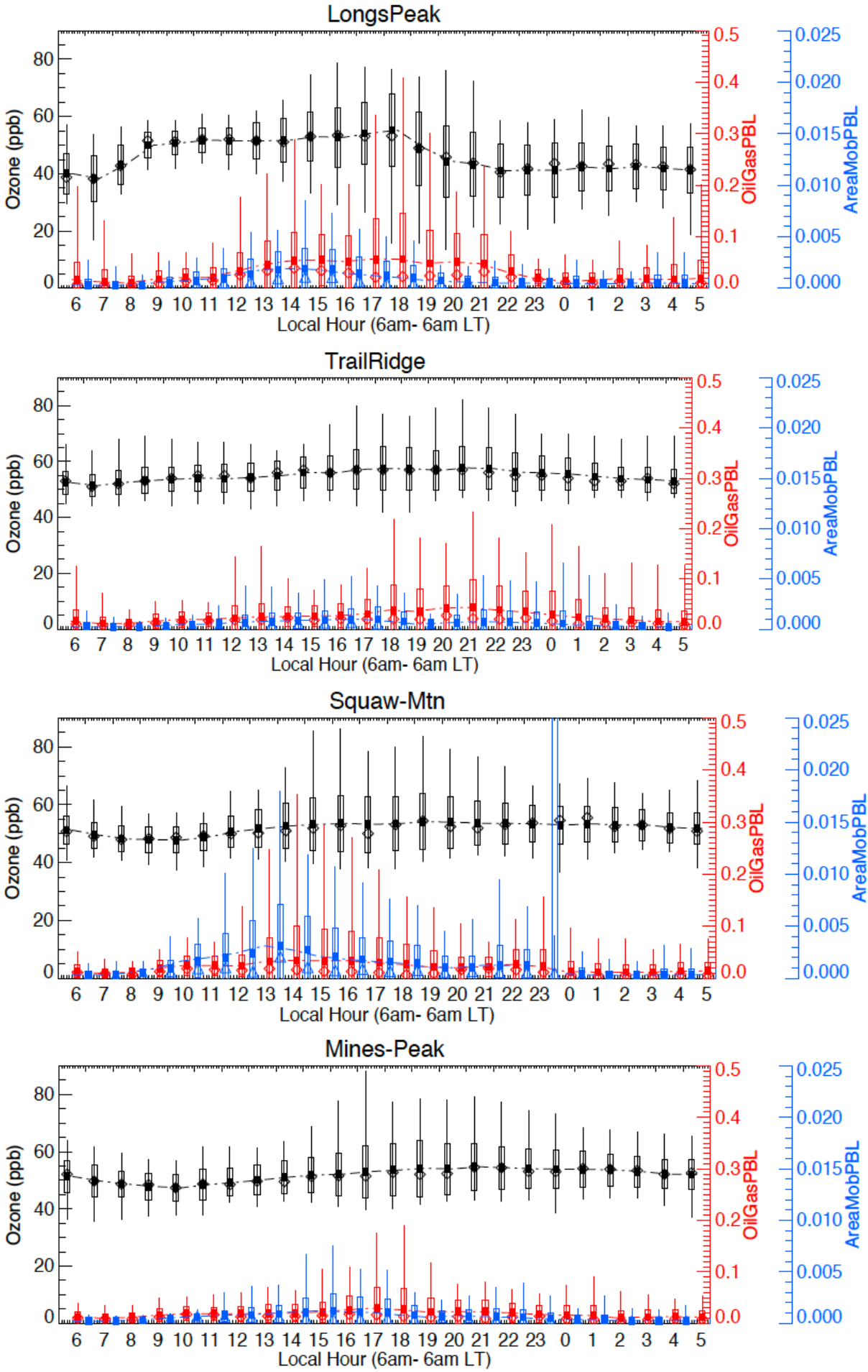
LongsPeak
TrailRidge
Squaw-Mtn
Mines-Peak
Ozone (ppb)
OilGasPBL
AreaMobPBL
Local Hour (6am- 6am LT)
0
20
40
60
80
0.0
0.1
0.2
0.3
0.4
0.5
0.000
0.005
0.010
0.015
0.020
0.025
6 7 8 9 10 11 12 13 14 15 16 17 18 19 20 21 22 23 0 1 2 3 4 5

**Figure 12.**

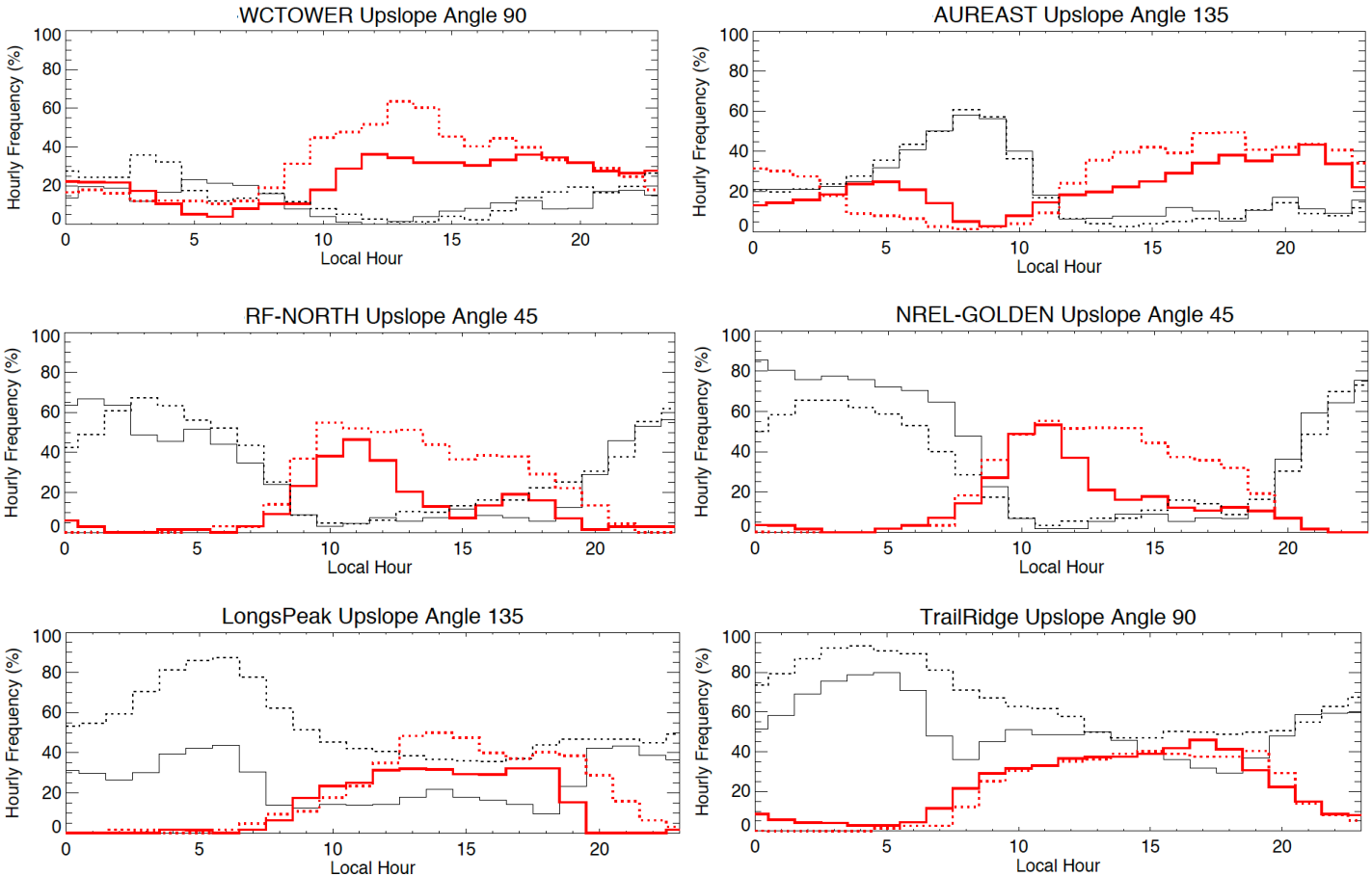
WCTOWER Upslope Angle 90
AUREAST Upslope Angle 135
RF-NORTH Upslope Angle 45
NREL-GOLDEN Upslope Angle 45
LongsPeak Upslope Angle 135
TrailRidge Upslope Angle 90
Hourly Frequency (%)
Local Hour
0
20
40
60
80
100
5
10
15
20

**Figure 13.**

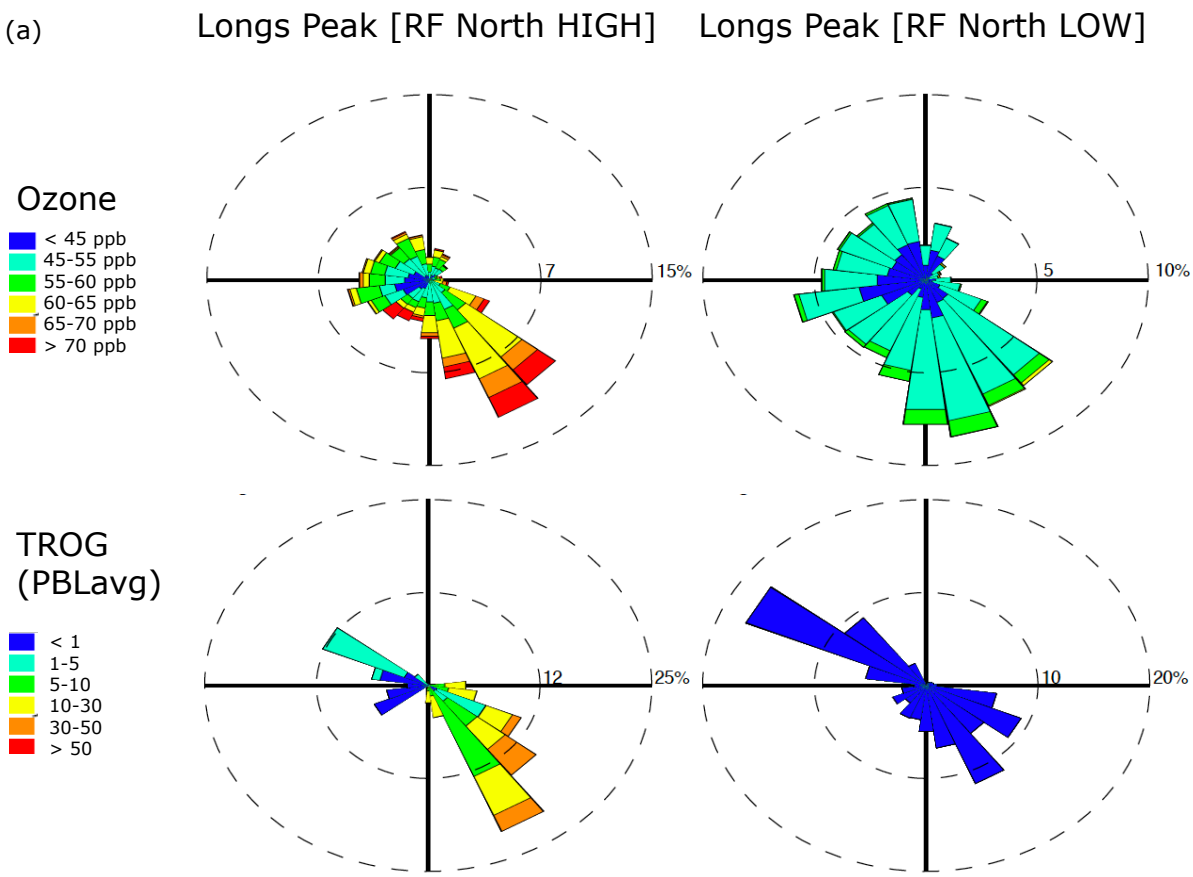
(a)
Longs Peak [RF North HIGH]
Longs Peak [RF North LOW]
Ozone
< 45 ppb
45-55 ppb
55-60 ppb
60-65 ppb
65-70 ppb
> 70 ppb
7
15%
5
10%
TROG
(PBLavg)
< 1
1-5
5-10
10-30
30-50
> 50
12
25%
10
20%

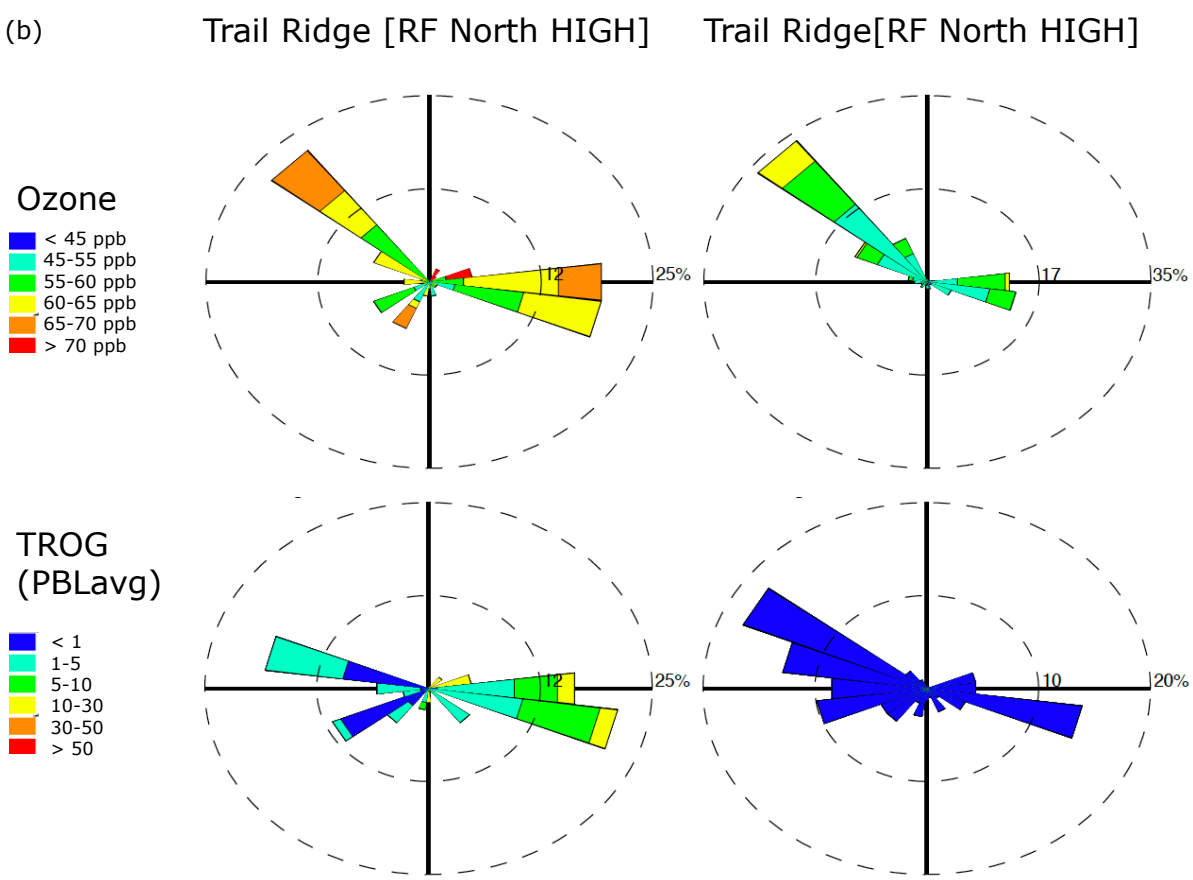
(b)
Trail Ridge [RF North HIGH]
Trail Ridge[RF North HIGH]
Ozone
< 45 ppb
45-55 ppb
55-60 ppb
60-65 ppb
65-70 ppb
> 70 ppb
12
25%
17
35%
TROG
(PBLavg)
< 1
1-5
5-10
10-30
30-50
> 50
12
25%
10
20%

**Figure 14.**

NCAR/NSF C-130 $NO_x$ (ppb)

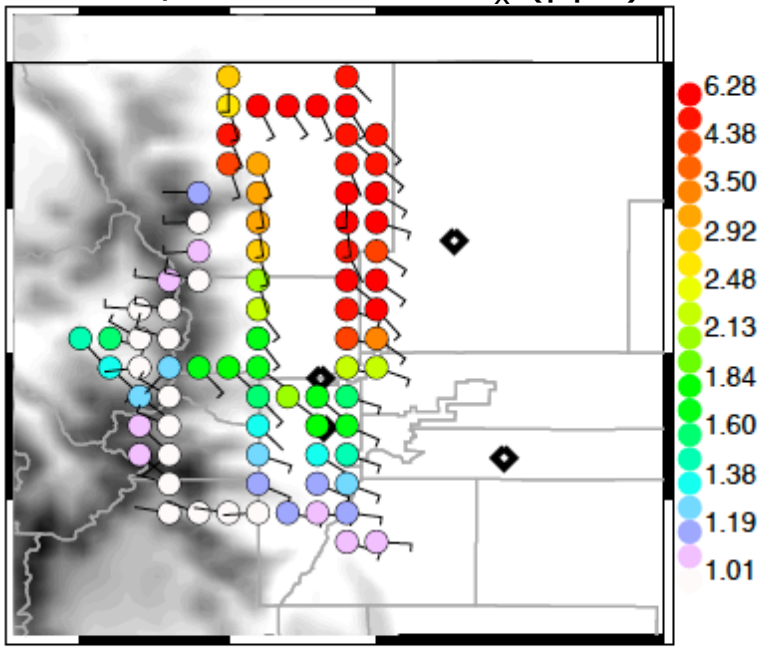


NCAR/NSF C-130 Ethane (ppb)

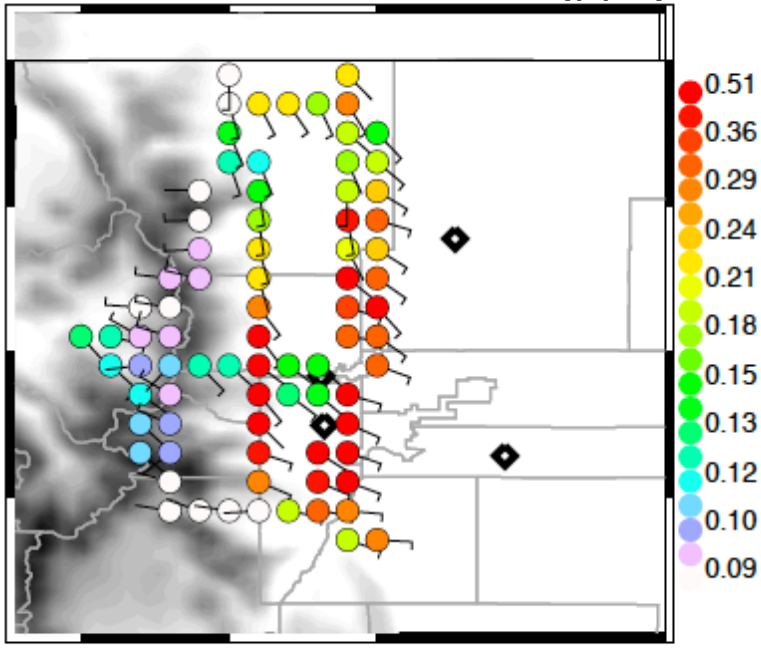


$TR^{OG}$ (unitless)

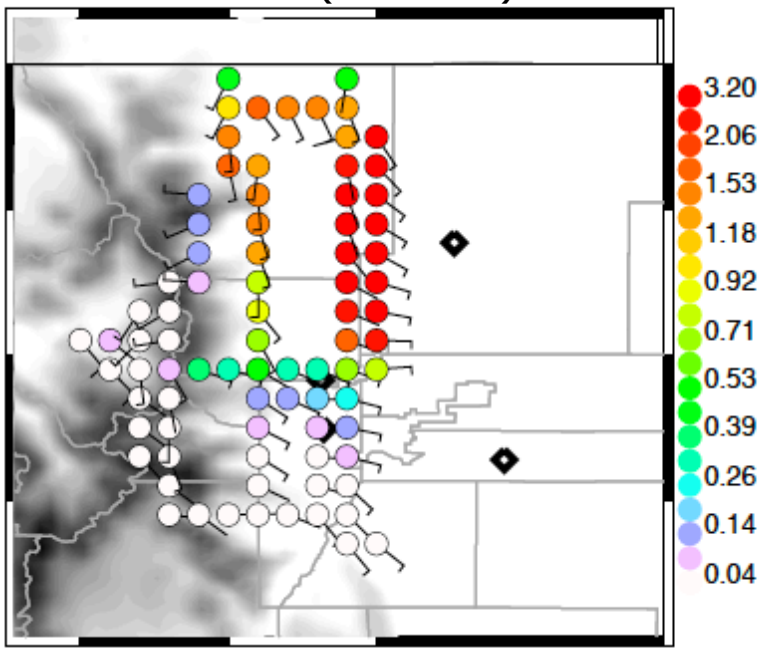


$TR^{AreaMobile}$ (unitless)

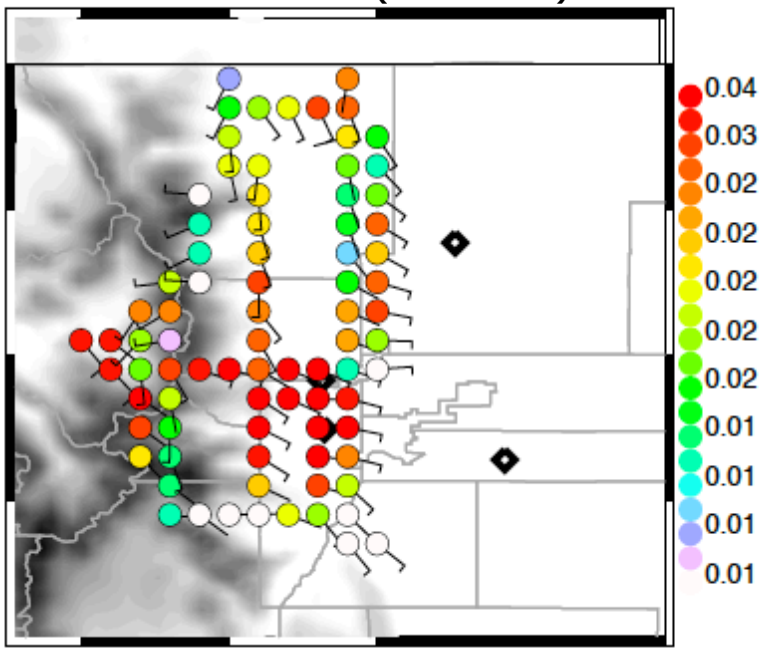

**Figure 15.**

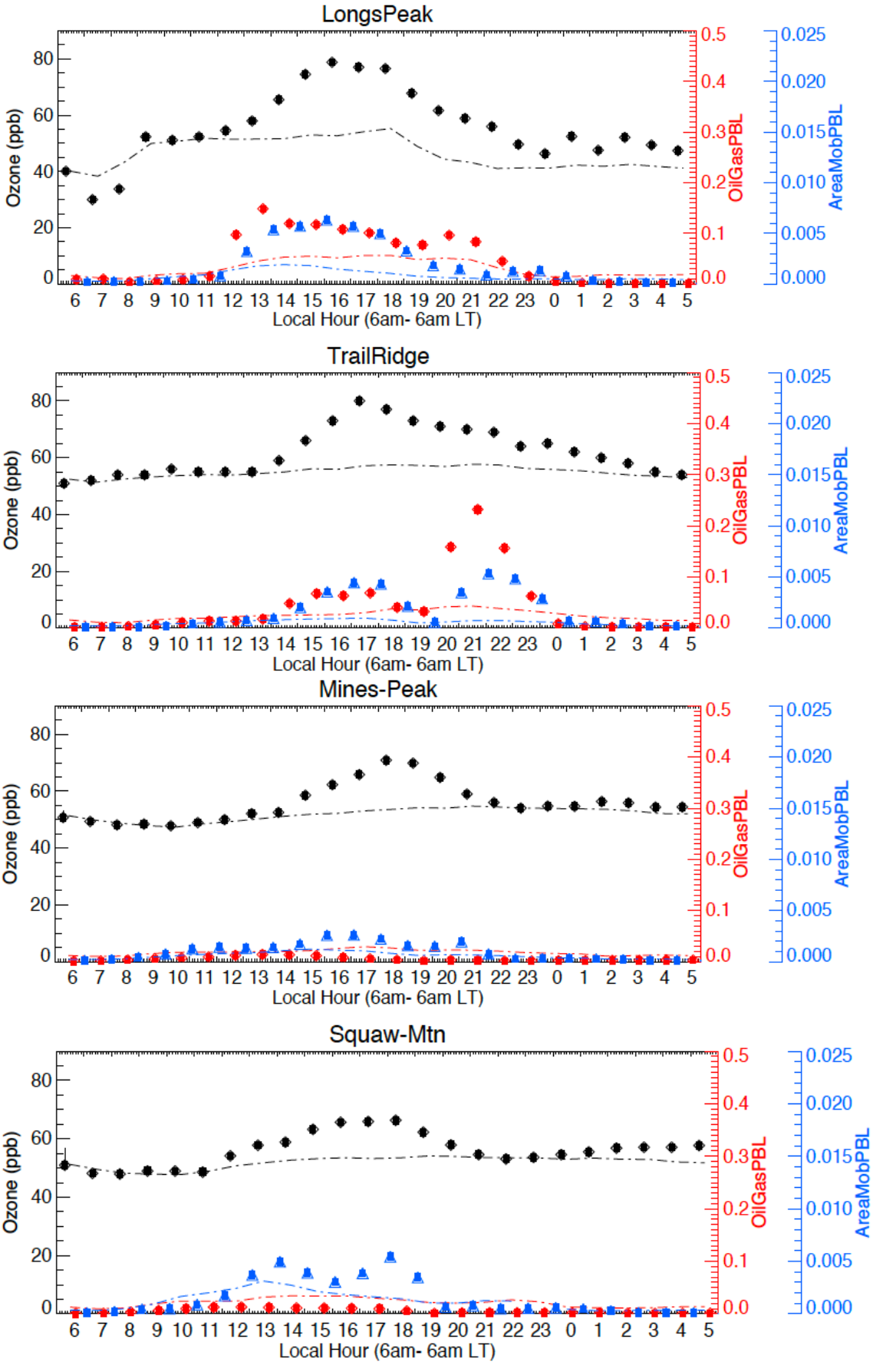
LongsPeak
TrailRidge
Mines-Peak
Squaw-Mtn
Ozone (ppb)
OilGasPBL
AreaMobPBL
Local Hour (6am- 6am LT)
0
20
40
60
80
0.0
0.1
0.2
0.3
0.4
0.5
0.000
0.005
0.010
0.015
0.020
0.025
6 7 8 9 10 11 12 13 14 15 16 17 18 19 20 21 22 23 0 1 2 3 4 5

**Figure 16.**

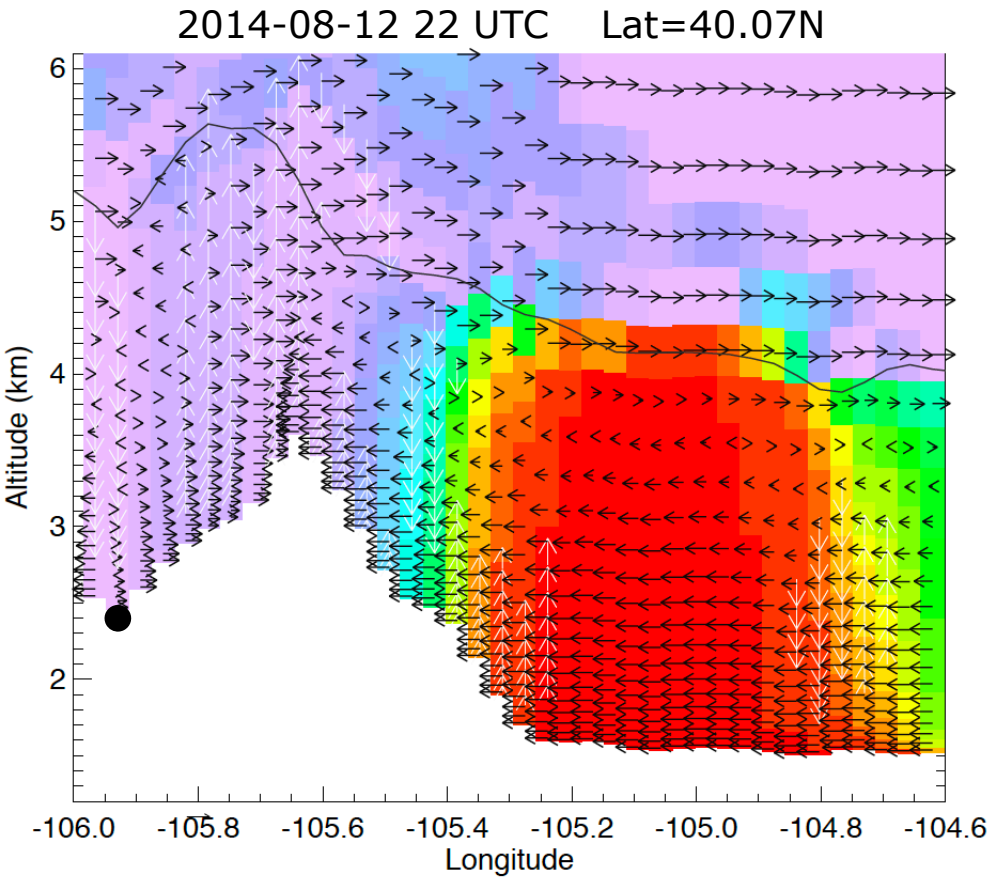
2014-08-12 22 UTC Lat=40.07N
Altitude (km)
6
5
4
3
2
-106.0
-105.8
-105.6
-105.4
-105.2
-105.0
-104.8
-104.6
Longitude

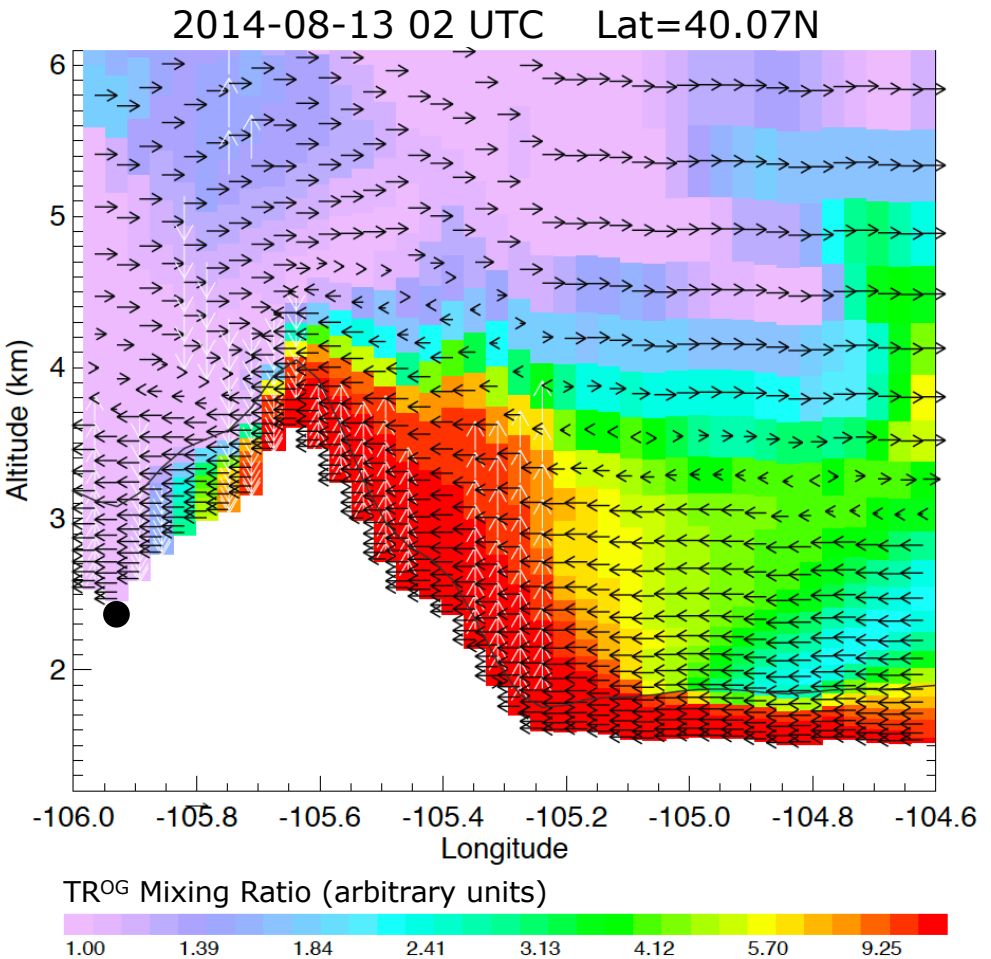
2014-08-13 02 UTC Lat=40.07N
Altitude (km)
6
5
4
3
2
-106.0
-105.8
-105.6
-105.4
-105.2
-105.0
-104.8
-104.6
Longitude
TR^OG Mixing Ratio (arbitrary units)
1.00
1.39
1.84
2.41
3.13
4.12
5.70
9.25

**Figure 17.**

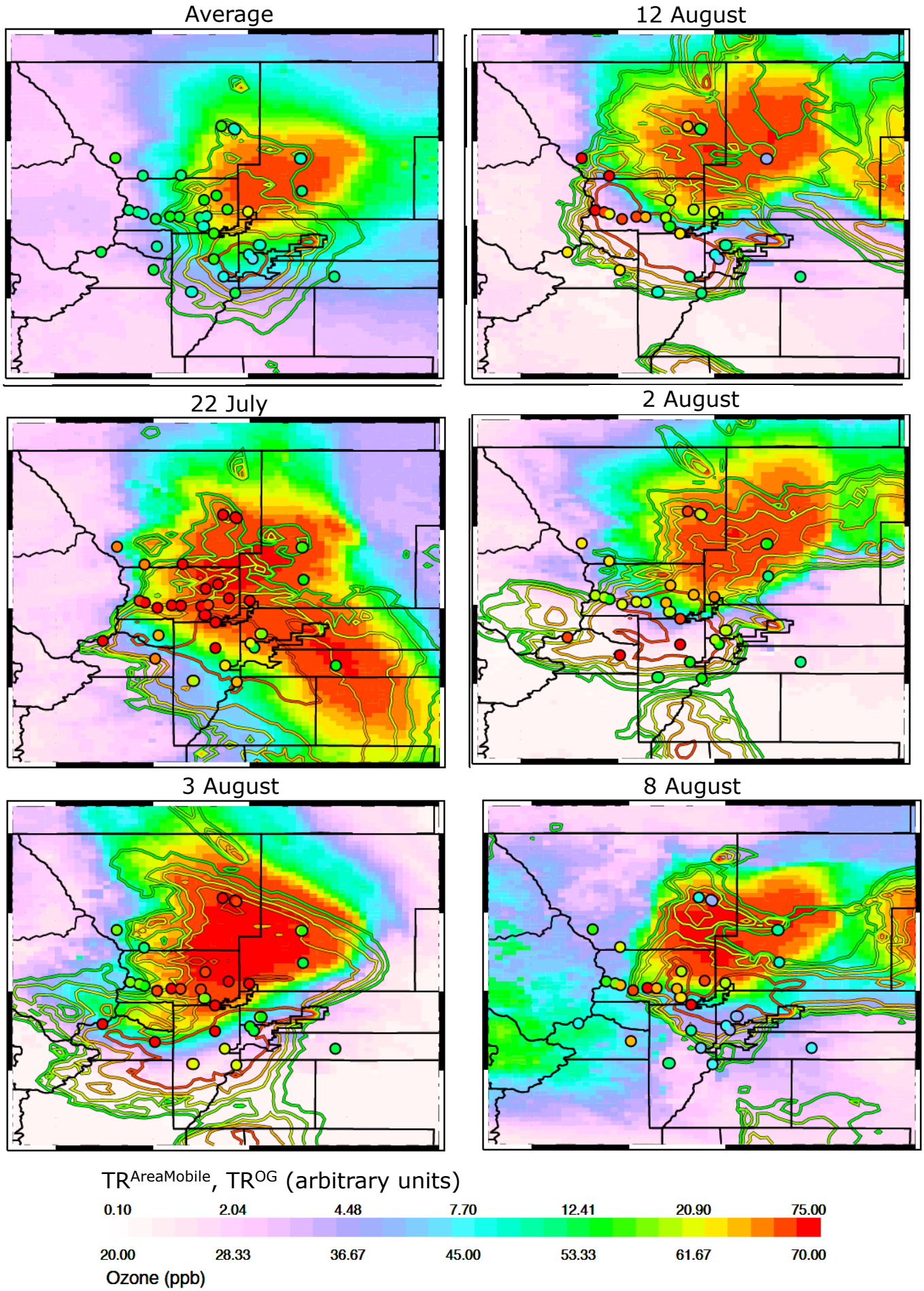
Average
12 August
22 July
2 August
3 August
8 August
TR^AreaMobile, TR^OG (arbitrary units)
0.10
2.04
4.48
7.70
12.41
20.90
75.00
20.00
28.33
36.67
45.00
53.33
61.67
70.00
Ozone (ppb)